CIVIL ENGINEERING STUDIES
Hydraulic Engineering Series No 106

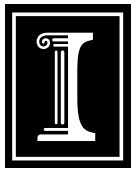

ISSN: 0442-1744

Laboratory Tests of Oil-Particle Interactions in a Freshwater Riverine Environment with Cold Lake Blend Weathered Bitumen

David M. Waterman[1]
Marcelo H. García[2]

[1]Graduate Research Assistant
[2]Professor and Director, Ven Te Chow Hydrosystems Laboratory

Prepared for:
U.S. Environmental Protection Agency, Region 5
Chicago, IL 60604-3590

Ven Te Chow Hydrosystems Laboratory
Dept. of Civil and Envir. Engineering
University of Illinois
Urbana, Illinois

August 2015

Laboratory Tests of Oil-Particle Interactions in a Freshwater Riverine Environment with Cold Lake Blend Weathered Bitumen

David M. Waterman[1]
Marcelo H. García[2]

[1]Graduate Research Assistant
[2]Professor and Director, Ven Te Chow Hydrosystems Laboratory

August 2015

EXECUTIVE SUMMARY

Laboratory tests were conducted on Cold Lake Blend diluted bitumen (dilbit) obtained in July 2013. The objectives of the tests were to quantify important parameters regarding the resuspension, transport, and deposition of oil-particle aggregates (OPAs) deposited on the bed of the Kalamazoo River following a pipeline burst of Enbridge Line 6B in July 2010.

The Cold Lake Blend was weathered by bubbling pressurized air through the fluid. Characteristic states of weathering used in the bench scale mixing tests included unweathered (0% mass loss), intermediately weathered (9.9% mass loss) and heavily weathered (17.4% mass loss) dilbit; the maximum mass loss achieved was 17.4%. The bench scale mixing tests were performed at room temperature where the air, water, and oil temperatures were between 21°C and 22°C. At this temperature, the unweathered dilbit had a density of 0.932 g/cm^3; the heavily weathered dilbit had a density of 0.993 g/cm^3. Thus the dilbit maintained positive buoyancy when added to a freshwater medium under all experimental conditions. At room temperature, the dynamic viscosity of the unweathered dilbit was 4.0x10^2 mPa·s.; the dynamic viscosity of heavily weathered dilbit was 5.4x10^4 mPa·s. Across the full range of temperatures and weathered states tested, the dynamic viscosity varied across five orders of magnitude.

Formation of OPA was achieved using Kalamazoo River sediment obtained from a depositional environment upstream of the spill-affected reach. The grain size distribution had a D_{16} of 7.6 µm, a D_{50} of 29 µm, and a D_{84} of 84 µm (where D_{XX} indicates the grain diameter such that XX percent of the cumulative distribution is finer-grained). The specific conductance of the freshwater medium was 640 µS/cm, which is within the range of conductance observed in the Kalamazoo River. Mixing was achieved using an orbital shaker with baffled flasks where the turbulent kinetic energy dissipation rates (ε) had characteristic values on the order of 10^{-1} to 10^{-3} m^2/s^3 based on previously reported values (Kaku et al., 2006a,b) from measurements using identical equipment. Dilbit was added to the surface of a dilute mixture of suspended sediment and freshwater within the baffled flasks and mixed for specified time periods. Experimentally controlled variables included the weathered state of the oil and the mixing energy. Deposits of sediment were removed for analysis using ultraviolet (UV) epifluorescent microscopy.

The predominant form of OPA observed in the experimental deposits was the droplet-type per Stoffyn-Egli and Lee (2002); the fundamental unit of the droplet-type OPA consists of a spherical oil globule with grains of particulate matter attached to the surface. Aggregates containing one to four oil droplets

(globules) were the most common in the deposits. When loose sediment deposits were consolidated into smaller containers, larger more complex OPA were commonly observed. Although large droplets well in excess of 1 mm diameter were prevalent during mixing, such large droplets did not achieve sufficient sediment attachment during mixing under any of the experimental conditions to appear in the experimental deposits. The most common globule sizes observed in the deposits had diameters between 5 µm and 100 µm; when evaluated on the basis of volume of oil in the deposit, the larger-sized droplets greater than 60 µm dominated the distributions. Very few spherical droplets were identified in the OPA having diameter greater than 200 µm; the largest spherical droplet observed using constant mixing rates was 336 µm.

Abundant solid-type OPA (Stoffyn-Egli and Lee, 2002) were generated when implementing unconventional mixing techniques that involved varying the mixing rates to achieve repeated sequences of oil entrainment, resurfacing, and re-coalescence. The solid-type OPA have been found by Stoffyn-Egli and Lee (2002) to incorporate sediment inside the body of the oil mass. The solid-type OPA were observed to consist of irregularly shaped oil masses that are considerably larger than the spherical droplets observed in the droplet-type OPA; solid-type OPA commonly had a maximum length dimension exceeding 1 mm. Although droplet-type OPA were abundant in the deposits formed using the unconventional mixing techniques, the volume of oil in the deposits formed using the unconventional mixing technique was dominated by the few large irregular-shaped solid-type OPA.

Settling velocity tests were performed on a number of OPA that had been photomicrographed using the UV epifluorescence microscope. The OPA consisted of both solid-type and droplet-type OPA, predominantly in the size range of 100 µm to 1000 µm. The OPA had settling velocities between 1.0 and 11.2 mm/s, with the majority being in the range between 1.0 and 3.0 mm/s.

Annular flume tests were conducted on a sample of the solid-type OPA. When deposited on a uniform fixed granular bed, the critical shear stress to initiate motion was found to vary from a value less than 0.0057 Pa up to 0.14 Pa. Mobilized material was transported both as bedload and in full suspension. Heterogeneity in the size and submerged specific gravity of OPA formed under controlled experimental conditions suggest that critical shear stress can be expected to vary over several orders of magnitude in the absence of macroscopic roughness elements that may shelter deposited material and exert a dominant effect on resuspension in a natural environment.

Table of Contents

Chapter 1: INTRODUCTION

The July 2010 spill of diluted bitumen (dilbit) into the Kalamazoo River was the largest documented release of bituminous oil into an inland water-body in U.S. history. A portion of the oil submerged; the most likely mechanism for submergence involves the attachment of suspended particulate matter in the water column to oil droplets, resulting in oil-particle aggregates (OPAs) that were denser than the ambient water (e.g., Delvigne et al., 1987; Lee et al., 2001; Lee, 2002). An approximately 38-mile long reach of the river shorelines and bed between Marshall and Kalamazoo, MI was affected by the spill. One of the needs of the U.S. Environmental Protection Agency (EPA) has been to understand the conditions under which the remaining submerged oil and oiled sediment in the Kalamazoo River becomes resuspended, transported, and potentially deposited further downstream (Dollhopf et al., 2014).

The Ven Te Chow Hydrosystems Laboratory (VTCHL) at the University of Illinois at Urbana-Champaign (UIUC) assisted in the development of OPA transport models that helped to guide submerged oil recovery and containment operations. Existing data was intended to be used to the maximum extent practicable to guide the inputs to the numerical models. However, existing data regarding the characteristics and behavior of OPA whose oil component is comprised of bituminous material is quite limited; notable exceptions include the studies of Lee et al. (2012), Environment Canada (2013), and King et al. (2014). More extensive OPA data exists pertaining to standard density crude oils dispersed in sea-water (e.g., Khelifa et al, 2008), although the relevance of such studies to the case of dilbit spilled in a freshwater river environment is uncertain. Data pertaining specifically to mixtures of dilbit and Kalamazoo River sediment was identified as a project need to inform the modeling efforts.

The goal of the current laboratory study was to obtain data that would provide useful inputs to numerical models regarding the resuspension, transport, and deposition of residual oiled sediment specific to the Kalamazoo River cleanup. The work plan for the laboratory analysis involved the following objectives: to obtain critical shear stresses for re-entrainment of deposited material, to obtain erosion rates, and to obtain settling velocities of oiled sediment. The data associated with these specific objectives were obtained using an annular flume to generate unidirectional flows for the entrainment tests and using a standard settling column for the settling velocity tests.

To obtain meaningful data that satisfy the objectives outlined, a reasonable representation of the oiled sediment on which to perform the entrainment and settling velocity tests was required. Although much

field data has been acquired that indicates the location of oiled sediment in the river system, and a moderate amount of data exists that indicates petroleum hydrocarbon concentrations, very little is known about the actual configuration of oil in the sediment. Lee et al. (2012) referenced information obtained from early site responders that "bulk oil" could be identified in split sediment cores when illuminated by ultraviolet (UV) light and photographed. However, the samples that Lee et al. (2012) evaluated reveal limited identifiable oil using UV epifluorescence micrsoscopy; these samples were obtained after much bed reworking had occurred as part of site remediation activities. The general sparse presence of identifiable oil was noted even in those sediment samples identified as being from areas classified as heavily oiled. The oil evident in the photomicrographs was in the form of small droplets (size order of 10 μm) in various configurations. Lee et al. (2012) noted that the lack of readily evident oil under the UV epifluorescence microscopy technique does not suggest a lack of oil in the samples, but rather that other factors may be involved that prevent the fluorescent oil from being visible. These findings highlight the issue that limited information is available regarding the configuration of oil amongst mineral and organic particulates in the bed. The extensive agitation and reworking of the sediment bed during site response made it increasingly difficult to accurately characterize the state of oil in the sediment bed soon after the spill and submergence in the fall of 2010.

Due to the lack of specific knowledge regarding the configuration of OPA on the Kalamazoo River bed, a secondary objective beyond the scope of the initial work plan was deemed necessary for the current laboratory analysis; namely, to obtain data regarding oil-particle aggregation processes in the water column so that OPA could be formed that would be reasonably representative of actual oiled sediment. This required the majority of the effort devoted to the laboratory analysis. To satisfy the secondary objective, both conventional and unconventional techniques were implemented to form OPA and analyze the deposits. Mixing of oil and sediment to generate OPA was performed using bench-scale facilities (e.g., Ma et al., 2008; Khelifa et al., 2008), with the dominant variables in the aggregation process being controlled and varied. Conventional mixing techniques readily generated droplet-type OPA as defined in Stoffyn-Egli and Lee (2002). Non-conventional mixing techniques were implemented to generate the larger-sized solid-type OPA as defined in Stoffyn-Egli and Lee (2002). Generating the larger sized OPA was deemed important to match descriptions of OPA observed by field personnel both during the initial response and subsequent cleanup efforts. Deposits were analyzed using UV epifluorescence microscopy techniques (Lee et al., 1985; Ma et al., 2008).

Chapter 2: OIL PREPARATION/WEATHERING

Five-gallon containers of Cold Lake Blend dilbit were provided by the Canadian Association of Petroleum Producers (CAPP) to VTCHL for testing. Prior to transport in the pipelines, the amount of diluent mixed with bitumen is frequently adjusted based on prevailing temperatures. The Cold Lake Blend samples were obtained in late July 2013 such that the specific mixture of diluent and bitumen in the samples was as representative as possible of Enbridge Line 6B pipeline dilbit spilled in July 2010. When exposed to the atmosphere, the lighter-end hydrocarbon groups (primarily associated with the diluent) volatilizes, with the dilbit becoming denser and more viscous in a process commonly known as weathering. The rate at which this occurs and the ultimate asymptotic state of mass loss to volatilization is a function of many factors including the wind speed, ambient temperature, thickness of the slick, and roughness of the surface (e.g., due to surface waves), among other factors. Therefore oil-particle aggregates in the Kalamazoo River system may have formed when the dilbit was in various states of weathering. The goal of preparing the oil to various states of weathering was not to characterize the weathering process (i.e., the change of physical properties as a function of time and environmental variables); rather the goal was to obtain an end product on which to conduct tests involving the aggregation of oil and suspended particulate matter that may best represents OPA on the bed of the Kalamazoo River. The means of weathering the oil was not intended to represent natural environmental conditions occurring at the time of the spill.

Oil was weathered by bubbling pressurized air through open containers of Cold Lake Blend in a fume hood at room temperature (21°C to 23°C). The weathering was performed in two steps. The first step was to determine the maximum percentage of initial mass that could be volatilized within a reasonable time period under the existing conditions and procedure. A 12-quart porcelain-lined steel stock pot was used as the container. An air discharge manifold constructed of ½-inch diameter CPVC pipe was placed in the oil and the vertically oriented member was strapped to the pot with cable ties through holes drilled through the side walls near the top of the stock pot; the holes were in several positions around the perimeter of the stock pot so that the manifold could be occasionally reoriented. The air discharge portion of the assembly was H-shaped and lay flat in the bottom of the pot; each tip of the “H” was an open pipe end, yielding 4 air outputs at equal distance from the input line that entered at the midpoint of the cross-member of the “H”. The air input system was connected via a hose barb fitting to the pressurized air-line. Two National Semiconductor LM35-CAZ temperature sensors input to an Arduino control board connected to a laptop computer were utilized to record temperatures at one-minute

intervals; one sensor was taped inside the stock pot to measure the oil temperature and the other was hung inside the fume hood to measure air temperature. The fully setup system prior to oil being added was then weighed using an ADAM LBK 12a scale (accuracy 1 g). 4712 g of dilbit from a previously unopened 5-gallon container was then transferred into the stock pot using a hand pump; the full system was immediately weighed to establish the initial oil mass. Air inflow was manually adjusted at a valve in the wall to maintain an approximately constant air inflow rate; no attempt was made to measure the flow rate or ensure that the inflow rate was maintained at a precise constant value. Mass readings from the scale were recorded manually at an interval that was initially small (approximately 15 minutes), but which increased over time as the mass loss slowed. After approximately 24 hours, when mass loss had slowed considerably, each time the mass was checked the manifold was unstrapped and used to mix the oil through a slow up-and-down motion; it was then re-oriented such that the outlets were in a different position to ensure no regions of the container were permanently sheltered from contact with the bubbling air. Bubbling proceeded for 5.9 days, when it was observed that no additional mass loss had occurred over a 24-hour period. The final mass of oil remaining was 3892 g, yielding a total mass loss of 17.4%. The remaining oil was poured into 64-oz glass containers for future use in the experiments. A view of the viscous oil during this first step of the weathering process is illustrated in Figure 1.

Figure 1: A frame captured from video recorded approximately 4 days into the initial oil weathering; the rigid vertical member is the CPVC air input line; the flexible line to the right of it is the temperature sensor.

The volatilization is an endothermic process during the initial rapid mass loss, as the oil temperature discernibly drops and then gradually rises back to ambient room temperature. This is illustrated in Figure 2.

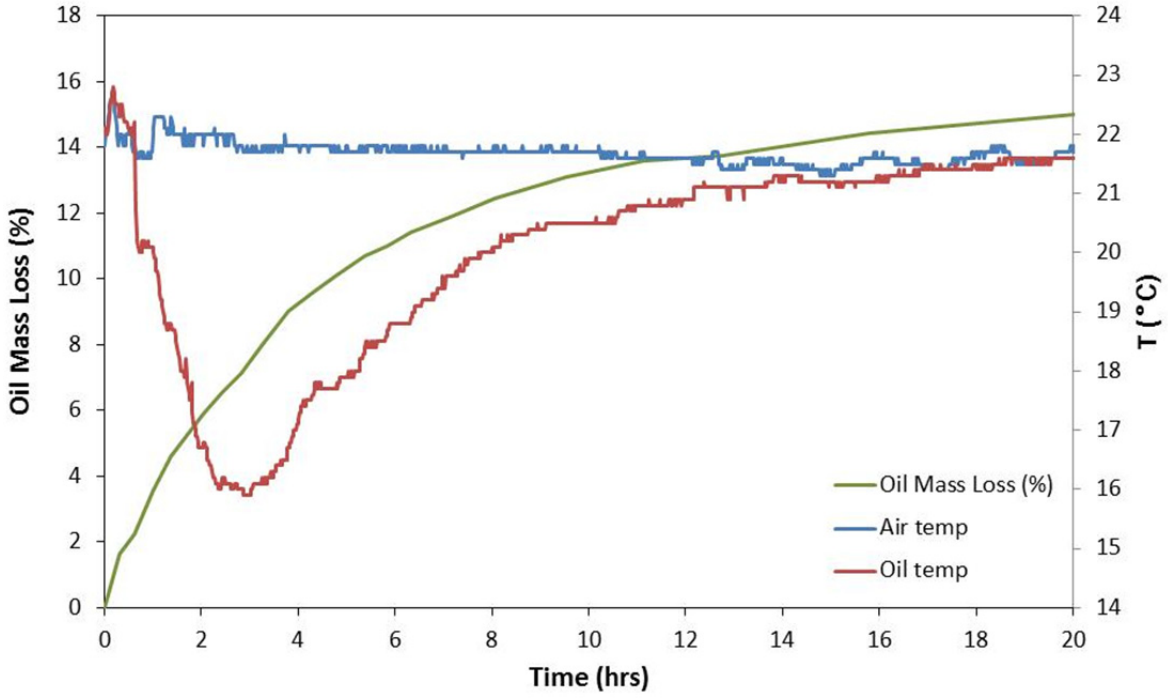

Figure 2a: Measurements taken during the first 20 hours of the oil weathering. Note that no attempt was made to keep the air flux at a specified constant rate or to otherwise represent actual environmental conditions.

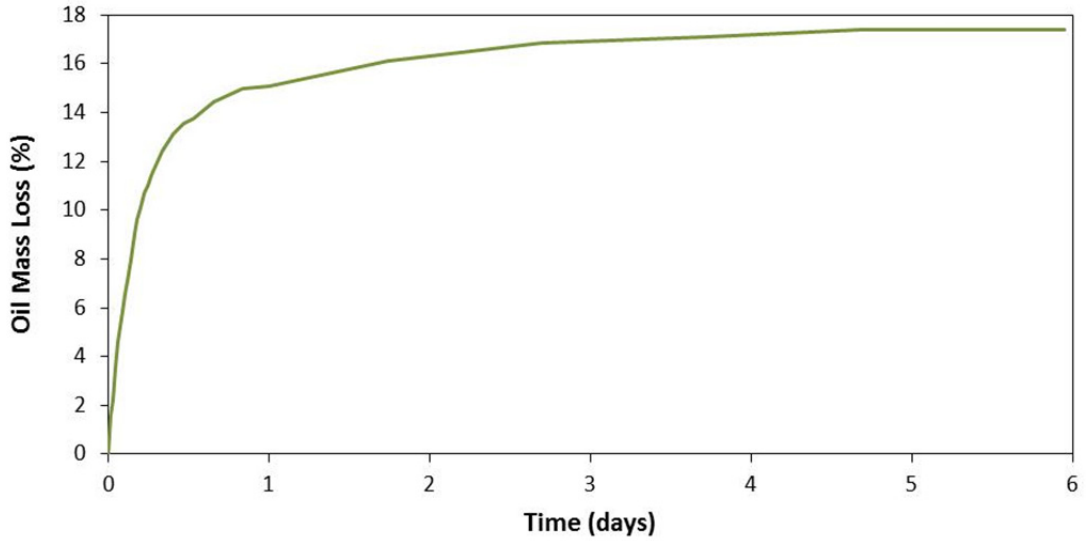

Figure 2b: The full time series of oil mass loss during weathering to the asymptotic condition of 17.4% mass loss achieved at approximately 5 days.

Following the initial test whose purpose was to determine the maximum mass that could be volatilized, additional samples were prepared in separate containers at specified intermediate degrees of mass loss. The containers used for the intermediate-weathered sample preparation were 64-oz. wide-mouth glass jars. A complex manifold was not necessary to distribute air in these smaller containers; a single outlet

from 1/2-inch CPVC piping configured to outlet horizontally at the base of the container was sufficient. Fresh oil from the same 5-gallon container was used to prepare these samples. The glass jar with air piping attached was weighed prior to oil being added; after transferring fresh oil into the container, the full setup was weighed again to establish the initial oil mass. Intermediate samples were desired at approximately 6% mass loss, 10% mass loss, and 13% mass loss. Air was bubbled through until the desired mass was achieved. The air delivery system was detached, and the sample was capped, labeled and stored in a temperature-controlled room. Each sample prepared was started from fresh oil transferred directly from the 5-gallon container.

Chapter 3: LABORATORY TESTS / EXPERIMENTS

3.1 Physical Properties of Cold Lake Blend

While the physical properties of Cold Lake Blend dilbit are reported elsewhere in the literature, for example, Belore (2010) and Environment Canada (2013), it was important to ensure that the properties of the specific samples provided for the current analysis were verified.

3.1.1 Viscosity

Viscosity of the Cold Lake Blend was tested using a Brookfield viscometer (model DV-II+) with a Thermosel temperature controller. The cylindrical container in which the viscosity is measured is seated inside the temperature control unit. This type of temperature controller is able to raise the oil temperature above room temperature to a specified value, but has no capability to cool the sample. A freezer and temperature sensor (National Semiconductor LM35-CAZ) were used to set the temperature values below 20°C. The method used for reducing temperature was to place the test volume of oil in the cylindrical viscosity measurement container with the small temperature sensor immersed in the oil; the spindle was placed separately in the freezer. When the temperature sensor indicating the desired temperature, the sensor was gently moved up and down within the oil to check for uniform temperature conditions; this also served to mix the oil to eliminate temperature gradients from the cylinder wall to the center of the sample. This was repeated until the desired uniform temperature was reached.

Small diameter spindles (SP28 and SP29) were used for the 17.4% mass loss oil sample, the 13.2% mass loss oil, and the 9.9% mass loss oil. A larger diameter spindle (SP21) was used for the 6.2% mass loss oil and the 0% mass loss oil. Spindles were chosen to keep the load on the viscometer within the accurate range of the instrument. A typical practice is to maintain the strain rate at a constant value when measuring viscoelastic fluids that show non-Newtonian behavior. The specific experimental conditions warranted relaxing this requirement, described as follows. During initial testing on cooled samples, an apparent thixotropic behavior was observed whereby the stress required to maintain a constant strain rate decreased with time, indicating a time-dependent reduction of fluid viscosity. Upon further evaluation, it was found that even when running at very low strain rates for short periods of time (<1 minute), the temperature of the viscous oil rapidly increased due to the energy input being dissipated as frictional heat. Thus, while thixotropic behavior cannot be discounted, the more dominant factor in the time-variation in the measured

viscosity was fluid temperature variation (as the viscosity is strongly dependent on temperature). The decision was made to run at the lowest possible strain rate within the accurate range of instrument loading rather than trying to maintain a constant strain rate for all experimental conditions. This also eliminated the need to frequently change spindles as temperature was increased between measurement points using the same oil sample. The measured viscosity values are illustrated in Figure 3. Note that the deviation from the fit lines at the low end of the temperature range is very likely due to the inability to completely eliminate the fluid temperature effect under the experimental conditions used.

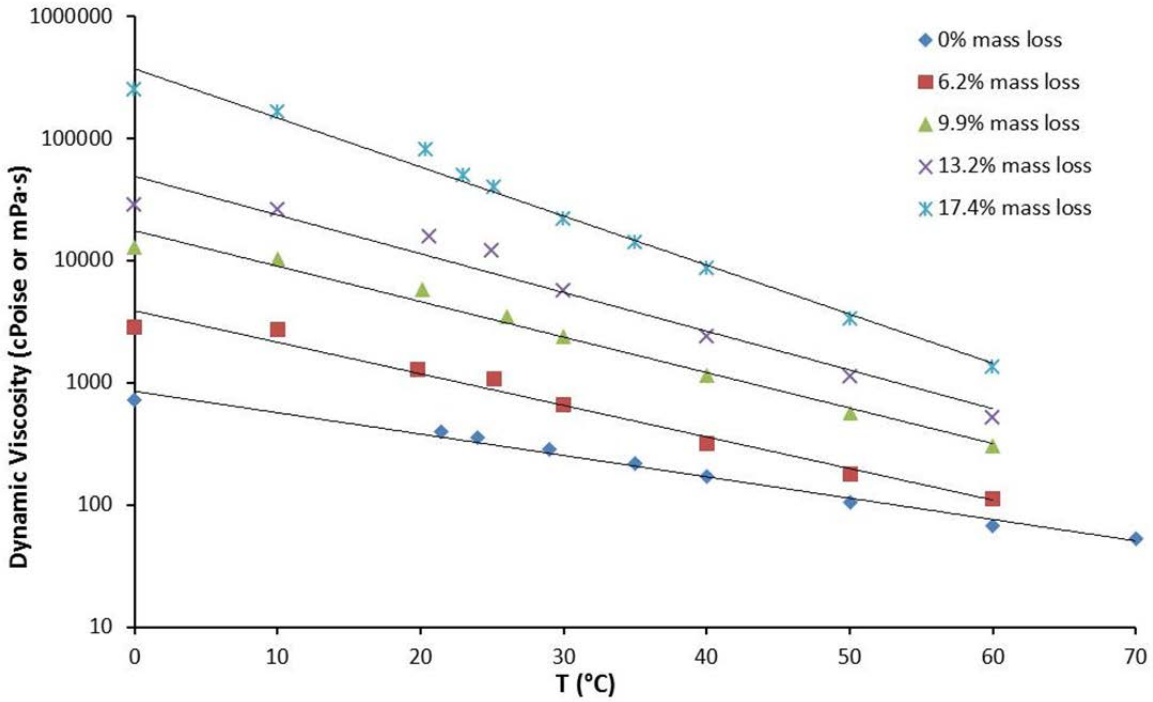

Figure 3: Cold Lake Blend viscosity measurement results

Curves of the form $\mu = Ae^{b_0 T}$ are fit to the data on Figure 3; where μ is dynamic viscosity in mPa·s; A is the interpolated viscosity at 0°C in mPa·s; b_0 specifies the slope of the lines; and T is temperature in °C. The values for the fitting parameters are provided in Table 1.

% mass loss	Intercept (A)	Exponent (b_0)
0	850.9	-0.0403
6.2	3892	-0.0595
9.9	17620	-0.0669
13.2	49180	-0.0731
17.4	372500	-0.0925

Table 1: Parameters for the best fit curves for the viscosity data

3.1.2 Density

Density of the Cold Lake Blend was measured with a Mettler-Toledo Densito 30PX. Large diameter disposable syringes were loaded with oil samples at various states of weathering and placed in a freezer several hours before the evaluation. The fluid temperature increased during evacuation of oil from the syringe and passage through the tubing of the instrument into the measurement cell; the lowest temperature capable of being measured was therefore limited under this experimental method. Note that the Mettler-Toledo Densito 30PX reports the temperature of the sample in the measurement cell, but it does not have an internal temperature controller. Samples warmer than room temperature (21.1 °C) were heated by placing oil in a beaker under a fume hood and heating and stirring at low temperature on a heating plate before loading the syringes. The density results are illustrated on Figure 4.

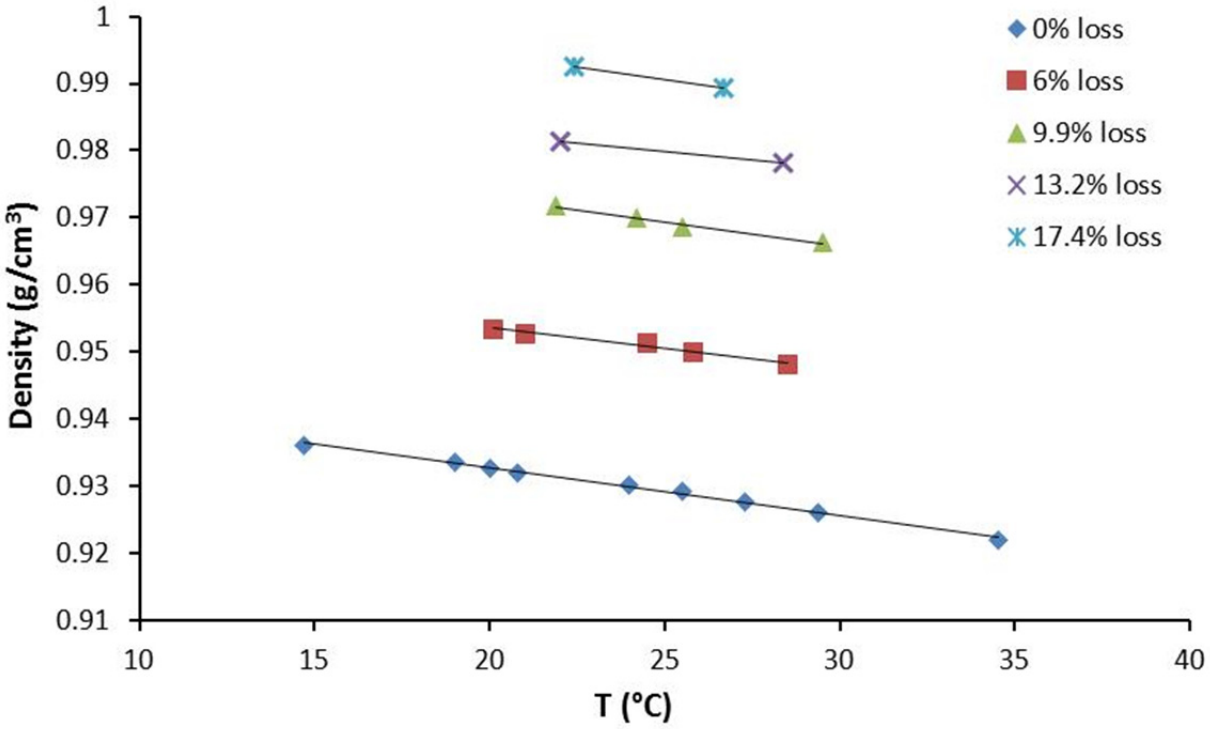

Figure 4: Cold Lake Blend density measurement results

Curves of the form $\rho_{oil} = m_1 T + b_1$ are fit to the data illustrated in Figure 4; where ρ_{oil} is density; m_1 is the slope in g/(cm^3·°C); b_1 is the intercept in g/cm^3; and T is temperature in °C. The fitting parameters are reported in Table 2.

% mass loss	Slope (m_1)	Intercept (b_1)
0	$-7.13 \cdot 10^{-4}$	0.9470
6.2	$-6.04 \cdot 10^{-4}$	0.9656
9.9	$-7.02 \cdot 10^{-4}$	0.9869
13.2	$-4.84 \cdot 10^{-4}$	0.9920
17.4	$-7.44 \cdot 10^{-4}$	1.0093

Table2: Parameters for the best fit curves for the density data

The slope fit is most accurate on the lines containing the most data points. Because the slopes are very similar, and the amount of data points on each curve varies considerably, it is justifiable to use a single slope value for all the lines, using a weighted average:

$$m_2 = \frac{1}{N} \sum_{i=1}^{5} n_i m_{1,i} \quad (1)$$

Where i represents each curve in Table 2, n_i is the number of data points on curve i, and N is the total number of data points in the entire data set. The value of m_2 thus calculated is 6.68 x 10^{-4}. g/(cm3 ·°C). The intercepts of the modified lines are calculated using m_2 and the midpoint of the original line between the measured data points. This yields curves of the form $\rho_{oil} = m_2 T + b_2$, and the fitting parameters are reported in Table 3.

% mass loss	Slope (m_2)	Intercept (b_2)
0	$-6.68 \cdot 10^{-4}$	0.9459
6.2	$-6.68 \cdot 10^{-4}$	0.9672
9.9	$-6.68 \cdot 10^{-4}$	0.9861
13.2	$-6.68 \cdot 10^{-4}$	0.9966
17.4	$-6.68 \cdot 10^{-4}$	1.0074

Table3: Parameters for the modified best fit curves for the density data using a single slope value

3.1.3 Comparison of Physical Properties with Previous Studies using Cold Lake Blend

General comparisons can be made with the previous findings of Belore (2010) and Environment Canada (2013) that were reported for Cold Lake Blend (CLB); the comparisons are not exact, as different values of temperature, states of weathering, and initial conditions were reported. The dilbit samples delivered to VTCHL were more similar to the samples analyzed by Belore (2010) than Environment Canada (2013). In the former study, the initial (unweathered) density at 15°C was 0.936 g/cm^3; in the latter study, the initial density at 20°C was 0.9216 g/cm^3, which suggests a higher percentage of diluent in the initial composition; (this would require some mass loss through weathering before reaching the same conditions as the initial condition in the current study). Pertinent comparative values are summarized in Tables 4 and 5 below:

Study	% mass loss	T(°C)	Dyn. Viscosity (mPa·s)
Belore (2010)	0	1	1363
Environment Canada (2013)	0	0	803
Current study	0	0	716
Belore (2010)	0	15	368
Environment Canada (2013)	0	15	285
Current study	0	21.4	402
Belore (2010)	16.99	1	98625
Environment Canada (2013)	16.9	0	129000
Current study	17.4	0	254000
Belore (2010)	16.99	15	14486
Environment Canada (2013)	16.9	15	18300
Current study	17.4	21.4	81614

Table 4: Comparison of CLB viscosity measurements between current study and past studies

Study	% mass loss	T(°C)	Density (g/cm3)
Belore (2010)	0	1	0.948
Environment Canada (2013)	0	0	0.9376
Current study	0	0	N/A
Belore (2010)	0	15	0.936
Environment Canada (2013)	0	20	0.9216
Current study	0	20.8	0.932
Belore (2010)	16.99	1	0.990
Environment Canada (2013)	16.9	0	0.9909
Current study	17.4	0	N/A
Belore (2010)	16.99	15	0.981
Environment Canada (2013)	16.9	15	0.9816
Current study	17.4	22.4	0.9926

Table 5: Comparison of CLB density measurements between current study and past studies

The results of Tables 4 and 5 reveal that the weathered CLB from the current study has somewhat higher viscosity and density than that of the previous studies, perhaps due to the different initial conditions and methods of weathering. Note that the viscosity is very sensitive to the degree of weathering, as an order of magnitude increase is typically associated with each ~3% increase in mass loss. The slope of the density versus temperature curves obtained in this study are similar to the values obtained in the earlier studies (-6.4 x 10^{-4} to -8.6 x 10^{-4} g/cm3·°C in Belore (2010) and -6.1 x 10^{-4} to -9.7 x 10^{-4} g/cm3·°C in Environment Canada (2013)). In the previous studies the slopes tended to decrease in steepness with increased degree of weathering. Only the Environment Canada (2013) study achieved density greater than 1.0 g/cm^3; this was obtained for the 25.3% mass loss condition, which was achieved using a rotary evaporator held at 80°C.

3.2 Evaluation of Oil-Particle Aggregate Characteristics at Bench Scale

3.2.1 Methods

Bench-scale experimental facilities were used to form the oil-particle aggregates. The primary techniques utilized included mixing baffled flasks containing water, oil, and sediment on an orbital shaker followed by ultraviolet (UV) epifluorescence microscopy analysis of the deposits.

The mixing was performed with a Fisher Scientific MaxQ 2000 orbital shaker (1.9-cm orbit diameter) with Wheaton model 38-430 trypsinizing flasks (150 mL). Detailed geometry of the trypsinizing flasks can be found in Kaku et al. (2006a, 2006b).

The conductivity and temperature of the water used was the same for all tests; (i.e., these were not experimental variables). Tap water was mixed with the biocide Sodium Azide at a mass concentration C_{NaN3} = 0.0002, which yields a specific conductance equal to 640 µS/cm, as measured with a YSI 6920. This conductance is at the upper end of the observed range in the Kalamazoo River. The water with Sodium Azide solution was maintained in a temperature-controlled room throughout the testing period. Temperature of the water was between 21°C and 22°C when added to the flask. 120 mL of the solution was used for all tests.

A specified mass of dry sediment was added to the flask after the water. (Sediment characteristics are described in a later subsection.) Surface tension effects commonly kept a portion of the sediment at the surface rather than sinking into the water, which was influenced by the sediment being dry when added. To ensure the sediment became saturated and was detached from the water surface before the oil was added, the water and sediment were shaken for 10 minutes at 200 RPM. The flask remained at rest for at least 15 minutes to allow sinking of sediment below the water surface prior to adding the oil.

Oil was dispensed into the flask using glass gas-tight 1 mL syringes graduated in 10 µL increments; the more viscous oil samples could not be drawn into the syringe body through suction and required the plunger be removed and the oil loaded into the top. During loading, the syringe body was filled in its entirety, such that when inserting the plunger, oil overflowed the syringe; this ensured no air was trapped in the syringe body which would potentially influence the ability to dispense specified volumes accurately. Unless otherwise specified, 100 µL of oil was dispensed into the flask.

The flask containing water, oil, and sediment was shaken for a specified time at a specified rate (in revolutions per minute) on the orbital shaker. After the shaking ceased, the suspension was allowed

to settle for at least 12 hours before removing the deposit from the baffled flask. The deposit removal process involved first removing as much as possible of the free oil forming the surface film. This was done by inserting a wooden dowel rod into the flask and just penetrating the surface film to capture any of the heavy film, which adhered to the rod. The rod was then removed. A second film removal process involved inserting a rolled heavy-duty paper towel into the flask and dipping just below the water surface; this was repeated numerous times by re-rolling and using clean portions of the paper towel. After this process, the heavy surface film and much of the sheen was eliminated, but it was generally not possible to eliminate all the sheen. The removal of the sediment was performed using a 25 mL transfer pipette with the inlet end tip cut off to increase the bore size to greater than 1 mm. A wash bottle with tap water was used to maintain at least 1 cm of water depth in the flask to prevent any remaining sheen from coming into direct contact with the sediment deposit and also to help concentrate the deposit into a single region of the flask to facilitate collection with the pipette. From the baffled flask, the removed deposit was placed in a 200 mL glass beaker. Additional sheen was removed from the beaker using a heavy-duty paper towel cut to size and laid onto the water surface. Although this procedure was found to be the most effective amongst the various procedures attempted, the presence of specks of sheen adhered to the glass dishes used for the microscopy analysis was not entirely eliminated.

After cleaning the pipette with dichloromethane (DCM) and rinsing with tap water and then distilled water, a sample of the deposit in the beaker was transferred to a Fluorodish (model FD35, manufactured by World Precision Instruments, Inc.) with the pipette. The Fluorodish had a 35-mm outside diameter with a 23-mm diameter glass-bottomed well. The glass bottom is 0.17 mm thick, equivalent to the most common type of glass cover slip used with microscope slides.

Deposits of OPA were evaluated with a Zeiss Axiovert 200M UV epifluorescence microscope with Zeiss Axiocam 506 camera at the UIUC Institute of Genomic Biology. The microscope has a motorized stage whose position can be monitored in the image acquisition software. UV light is provided by an XCite illuminator. The ultraviolet light source, filters, and objective lens are located below the stage. Visible light is provided from above the stage. The depth of focus varies between 4 and 7 µm for the UV channels using the 10X objective lens; and it varies between 1 and 2.5 µm when using the 20X objective lens. Images were recorded on four UV channels along with the visible light channel. The excitation and emission wavelengths established by the UV filters are specified as follows, with a separate image recorded for each channel:

- Blue channel: Excitation (335 to 383 nm); Emission (420 to 470 nm)
- Green channel: Excitation (450 to 490 nm); Emission (500 to 550 nm)
- Orange channel: Excitation (524 to 549 nm); Emission (562 to 658 nm)
- Red channel: Excitation (625 to 655 nm); Emission (665 to 715 nm)

The Axiocam 506 captures a separate 14-bit grayscale image on each channel with image size 2752 x 2208 pixels. When using the 10x objective, each pixel has edge dimensions of 0.4438 µm; therefore the imaged region has a size equal to 1221 µm x 980.0µm. When using the 20x objective, each pixel has edge dimensions of 0.2206 µm; therefore the imaged region has a size equal to 607.0 µm x 487.0 µm.

Sampling the Fluorodish to obtain a representative set of OPA to analyze was performed with the 10x objective to maximize the number of OPA captured in each image. To image the entire well region of each Fluorodish in its entirety would yield a data set that would require a very large time investment during both imaging and analysis; a subsample of the Fluorodish was therefore deemed most practicable. With the intent to prevent user bias regarding the OPA selected for imaging and to capture a reasonably large number of OPA, a sampling scheme was developed. The sampling pattern included 9 image locations at specified coordinates on the dish. The pattern is illustrated in Figure 5.

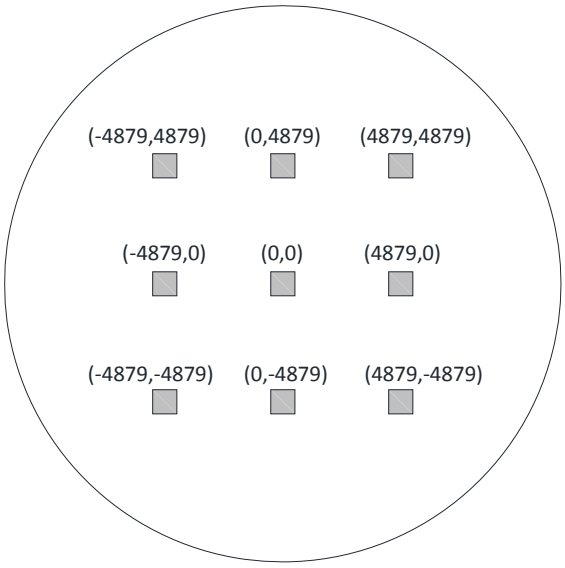

Figure 5: The sampling pattern used to image each Fluorodish. The (x,y) coordinates shown are in µm. The circular perimeter represents the edge of the glass-bottomed well of the dish.

The motorized microscope stage is controlled with a joystick, and the (x,y) coordinates of the center of the field of view can be viewed using the integrated imaging software. At each of the 9 positions,

an image was taken regardless of whether any OPA were present. The field of view was then moved downward (in the negative y-direction per the coordinate system used) to collect an additional image with approximately five percent overlap on the first image.

The microscope user has a great deal of control with respect to setting the depth of focus and the image exposure time. In general, the depth of focus was set to maximize the area of oil globules that were in focus within the field of view; this is a judgment made by the user. The software can be set such that the exposure time is automatically adjusted to minimize the number of pixels that are over-exposed and maximize the integrated histogram of the intensity range; this generally leads to different exposure times for each of the UV channels. When the images from the four UV channels are overlain, this generally yields a white appearance to fluorescing objects. After trial and error, it was determined that the best results were obtained in a different manner, by using an exposure time on each UV channel equal to 2.0 sec, unless such exposure time yielded significant over-exposure on a particular UV channel (i.e., when the initial automatic adjustment calculation yielded exposure times less than 2.0 seconds). In such case, only the exposure time for that UV channel was adjusted to the value calculated per the automatic adjustment procedure of the imaging software. Using this procedure, the oil globules generally had a characteristic color when images from the four UV channels were overlain. The orange channel generally fluoresced the strongest on the oil globules; the other channels were less intense but still altered the hue of the dominant orange color upon overlay. Having a clear color signature on the overlaid imagery allows distinction between actual oil globules and the strongly fluorescent specks of sheen that had become adhered to the Fluorodish glass (an undesirable artifact of removing the sediment deposit from the baffled flask).

3.2.2 Experimental Variables in the Orbital Shaker Tests

A number of variables are known to have significant influence on the formation of OPA, including but not limited to: (1) temperature, (2) conductivity, (3) weathered state of the oil, (4) mixing energy, (5) mixing time, (6) sediment type, (7) relative percentages of oil and sediment. Sufficient resources were not available for a rigorous experimental protocol followed by quantitative analysis of results to address the full matrix of variables. The values of the above variables used in the experiments are described herein.

The water temperature and oil temperature used in the mixing tests were maintained constant by storing the water / Sodium Azide solution and the weathered oil samples in the same temperature-controlled room. The temperature of each fluid was between 21°C and 22°C when added to the baffled flask. Temperature was not varied as an experimental variable.

Specific conductance of the water / Sodium Azide solution used as the disperse phase in all testing was 640 µS/cm. Specific conductance (conductivity) was not varied as an experimental variable.

Three weathered states of the dilbit were evaluated in the orbital shaker tests: 0% mass loss (unweathered); 10% mass loss (intermediately weathered) and 17.4% mass loss (heavily weathered).

The majority of the orbital shaker tests were performed at a constant mixing rate; the mixing energy was varied using shaking speeds in the range between 150 RPM and 250 RPM. Preliminary testing revealed that 150 RPM was sufficient to entrain only a small percentage of the oil film, and so limited tests were performed at that mixing level. Evaluation of measured turbulent kinetic energy dissipation rates (ε) levels reported in Kaku et al. (2006a,b) suggested that 200 RPM yields energy levels higher than what could be expected in most open-channel flow environments, and 250 RPM would be even more energetic; so limited tests were performed at 250 RPM. The majority of the testing was performed at 160 RPM, 180 RPM, and 200 RPM.

Mixing time for the constant mixing rate tests were fixed at 1 hour. Unconventional mixing techniques were also implemented that involved variable mixing rates. The unconventional mixing techniques involved shaking at 200 RPM for 5 minutes (during which time the oil was fully entrained), followed by stopping the shaker for 2 minutes (during which time the oil resurfaced as a film), followed by shaking at 135 to 150 RPM for 3 minutes (during which time the oil film rearranged and recoalesced at the surface); this three-step sequence was then repeated a number of times.

The sediment type was natural sediment from the Kalamazoo River. The river sediment used in the experiments was collected into six 5-gallon buckets using a shovel on August 21 and August 23, 2013. The sediment collection was performed by GRTusa staff. The sediment was collected from the bed of the Kalamazoo River in a depositional marginal backwater area located 0.25 miles upstream of the Talmadge Creek confluence and the oil-spill affected reach. The location was selected to be representative of similar depositional areas downstream of the oil spill with persistent submerged oil. The sediment used in the experiments was obtained from a single bucket. The grain size distribution of the sediment used for the analysis was determined using a LISST-ST laser diffraction instrument. Only two grain-size distributions were included in the experiments. The first was the un-sieved sample representing the full grain size distribution; the second was obtained from the same bucket of sediment, but was wet-sieved using a 53 µm sieve and only the portion passing was retained. The results are illustrated in Figure 6.

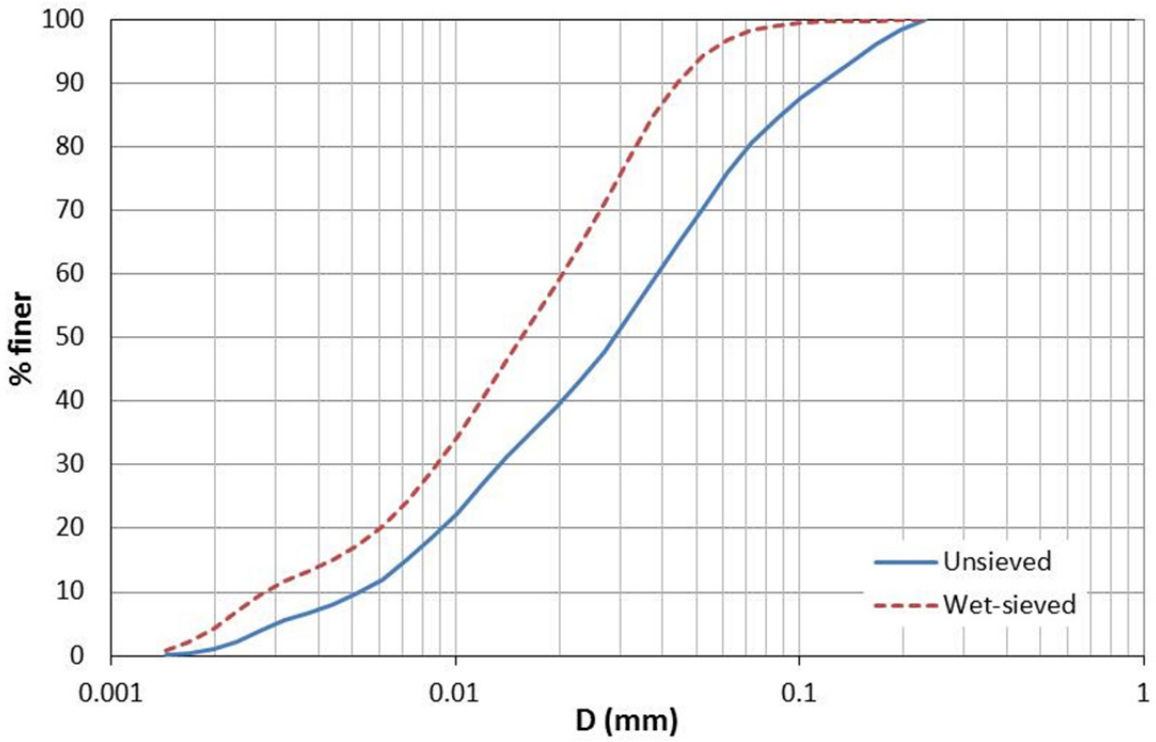

Figure 6: Grain size distribution of the Kalamazoo River sediment used in the orbital shaker experiments

Following are characteristic values illustrated on Figure 6:

- Un-sieved sediment: D_{16} = 7.6 µm, D_{50} = 29 µm, D_{84} = 84 µm
- Wet-sieved sediment: D_{16} = 4.7 µm, D_{50} = 16 µm, D_{84} = 37 µm

where D_{16}, D_{50}, D_{84} represent grain diameters with subscripts indicating the percent finer in the distribution.

In addition to the sediment whose composition is illustrated in Figure 6, a subsample of macroscopic organic detritus was obtained from a separate bucket that was found to contain abundant detritus. The organic detritus was separated by wet sieving using a 600 µm sieve and retaining only the portion that was retained on the sieve. The detritus consisted primarily of fragments of leaves, stems, twigs, and bark. The material was dried in an oven at 140°F and then crushed between the fingers such that size of organic particles was less than 3 mm. A photograph of the organic detritus is provided in Figure 7.

Figure 7: An image of the dried macroscopic organic detritus prior to being crushed into finer particles for use in the experiments. For scale, the rectangular indentation in the aluminum pan at the top right of the photo has a vertical dimension of 2.3 cm.

Regarding the relative amounts of oil and sediment used in the experiments, in general, 50 mg of dry sediment was used with 100 µL of oil. This was not systematically varied to determine its effect on OPA deposits.

3.2.3 Qualitative Observations of OPA Characteristics in the Experimental Deposits

As indicated previously, a rigorous experimental protocol involving the full matrix of variables described in 3.2.2 followed by quantitative analysis (mass of oil that submerged, size distribution of oil droplets in OPA, etc.) was not feasible within the scope of the current project. However, qualitative observations were used to guide the generation of OPA for use in the larger scale experiments, and the qualitative observations described herein may provide valuable insights that will guide future experimental work.

3.2.3.1 General Observations regarding OPA configurations

The primary OPA unit was found to be a single oil globule with fine sediment attached to its surface; this is the type of OPA referred to by Stoffyn-Egli and Lee (2002) as the droplet type. The droplet-type OPA is illustrated in Figure 8.

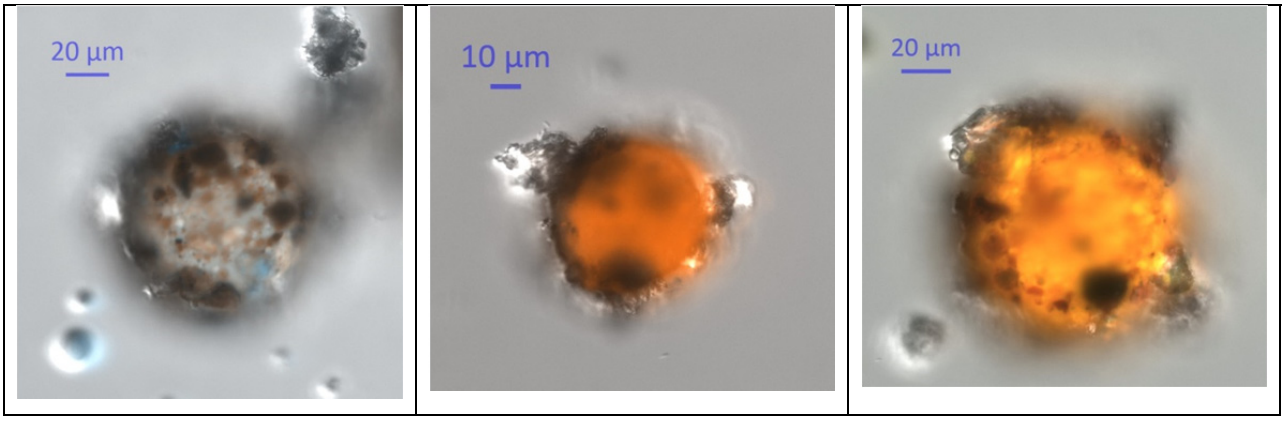

Figure 8: Several examples of droplet type OPA from the experimental deposits photo-micrographed using the 20x objective. The oil is the brightly-colored (fluorescent) circular feature; dark-colored (non-fluorescent) sediment is attached to the surface. The images are overlays of various combinations of the UV channels along with visible light.

The primary OPA units were commonly aggregated with other oil globules of various sizes, with each droplet having some sediment attached to its surface. The most common configurations were aggregates of 1 to 4 oil droplets along with attached sediment grains. Chain-like configurations were common. Smaller droplets were occasionally seen in densely-packed 3D structures. The chain-like configurations are illustrated in Figure 9.

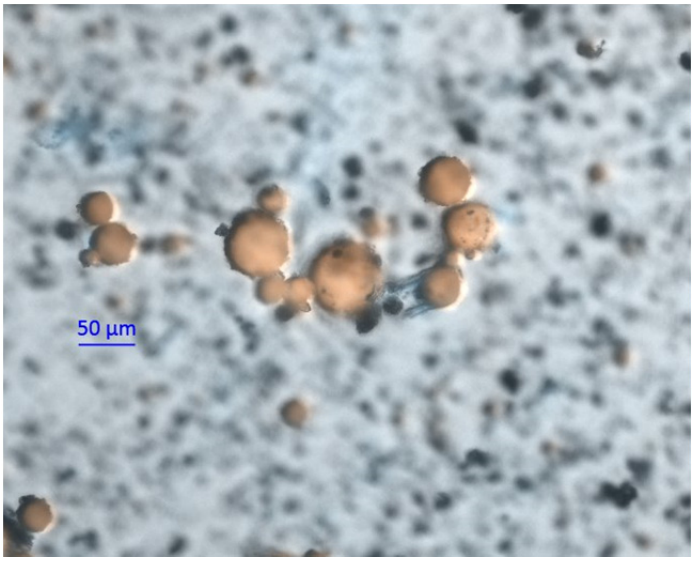

Figure 9: A chain-like configuration of oil globules.

Large globules having diameters well in excess of 1 mm were observable during the shaking experiments, but these were not represented in the deposit, always floating back to the surface when shaking ended. The most abundant globule size in the experimental deposits was on the order of 10 to 100 µm. Very few globules were observed in the deposit with diameters greater than 200 µm.

Although the un-sieved sediment sample illustrated in Figure 6 contains approximately 30% mass having diameter 50 µm and larger, very few sediment grains in that size class were found to be directly attached to oil globules in the deposit. The sediment grains attached to the globules were dominated by the low end of the distribution having grain-size less than approximately 10 µm.

After being moved to a Petri dish and settled in a closer arrangement, the simpler OPA configurations and oil-free sediment tended to be picked up in a pipette as large complex aggregates. Examples are shown in Figures 10 and 11.

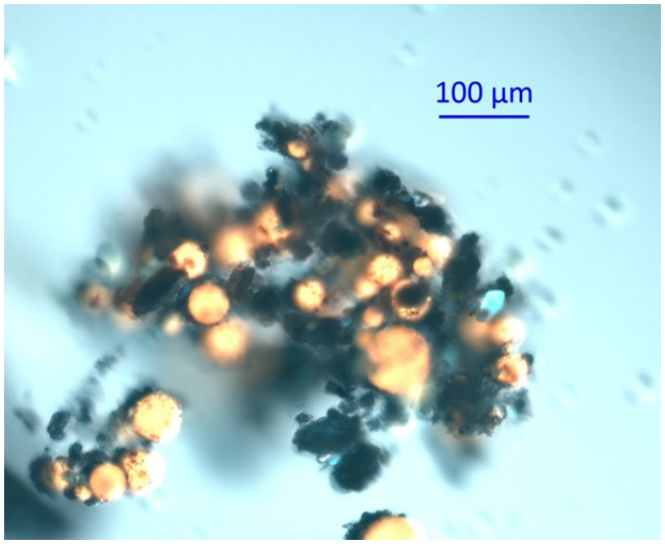

Figure 10: A complex aggregate with many globules and larger sediment grains adhered to its surface

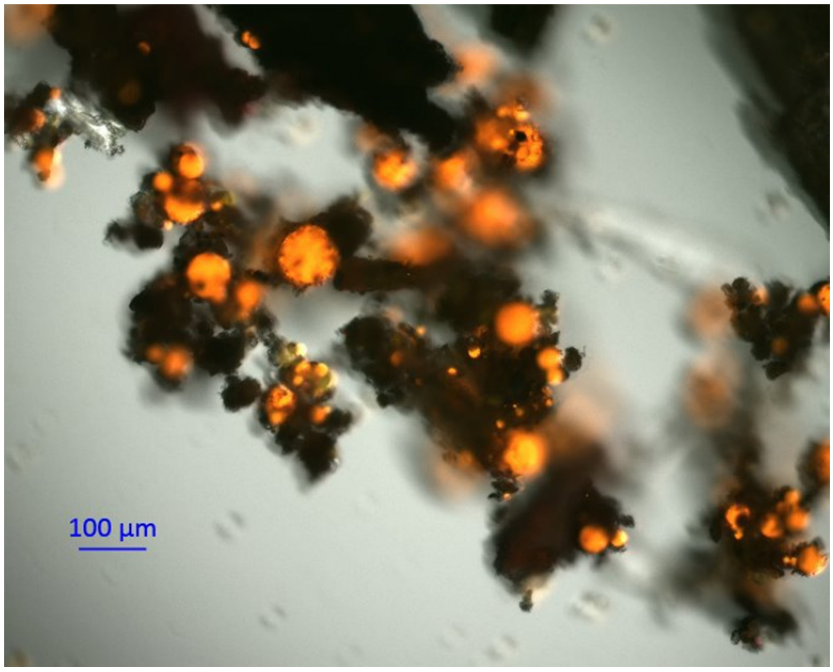

Figure 11: Another image of a complex aggregate

3.2.3.2 Observations regarding OPA formation in the presence of abundant organic detritus

Experiments using the organic detritus required the addition of sediment to prevent excess adherence of oil to the sides of the baffled flask; note that the sediment acts as a surfactant that tends to prevent excessive adherence. The mixture used for these experiments was 45 mg of wet-sieved sediment (Figure 6) and 50 mg of crushed organic detritus (Figure 7); 100 µL of oil was used in each flask. The tests revealed that oil globules did attach to suspended organic detritus. Globules do not show any preferential attachment to detritus relative to sediment grains, but do show some affinity for a common filamentous feature of presumably biological origin; the globules are commonly attached to the organic matter through intermediate grain(s) of sediment. The globules that attach to organic material tend to have smaller diameters than the bulk of the globules in the deposit that are attached to sediment grains. Examples showing the detritus are illustrated in Figures 12 through 15; examples showing the filamentous material are shown in Figures 16 and 17.

Figure 12: A view of oil globules attached to large organic detritus

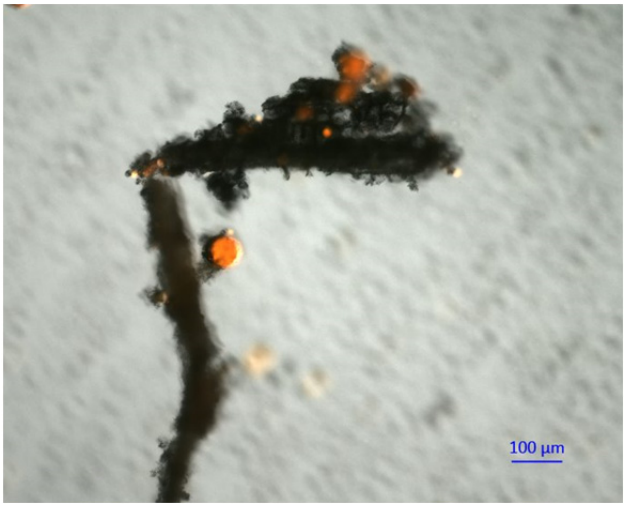

Figure 13: Another piece of large organic matter with globules attached.

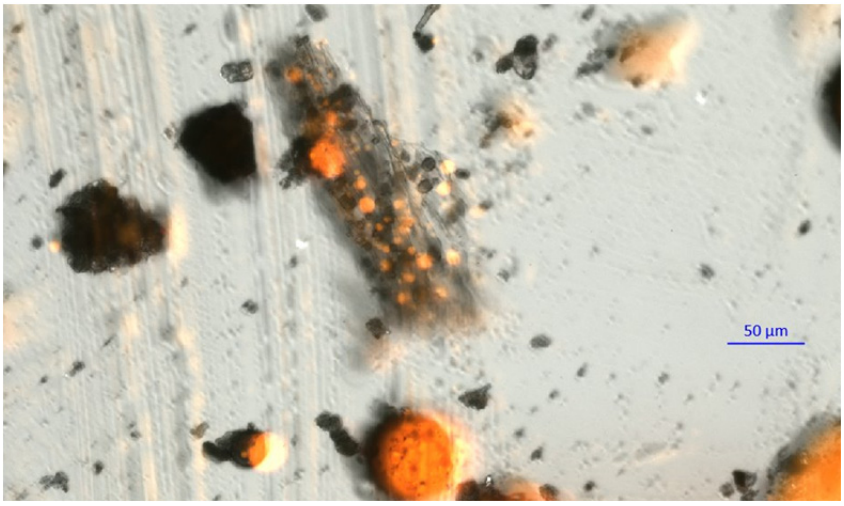

Figure 14: Fine globules attached to a thin piece of organic matter

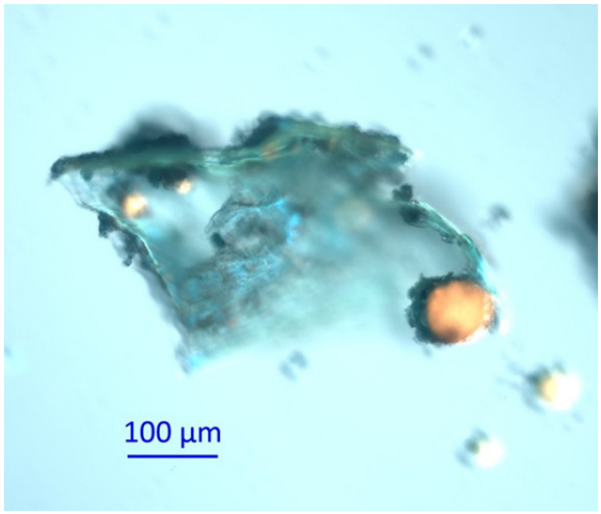

Figure 15: One large globule and two smaller globules attached to a flake of organic debris.

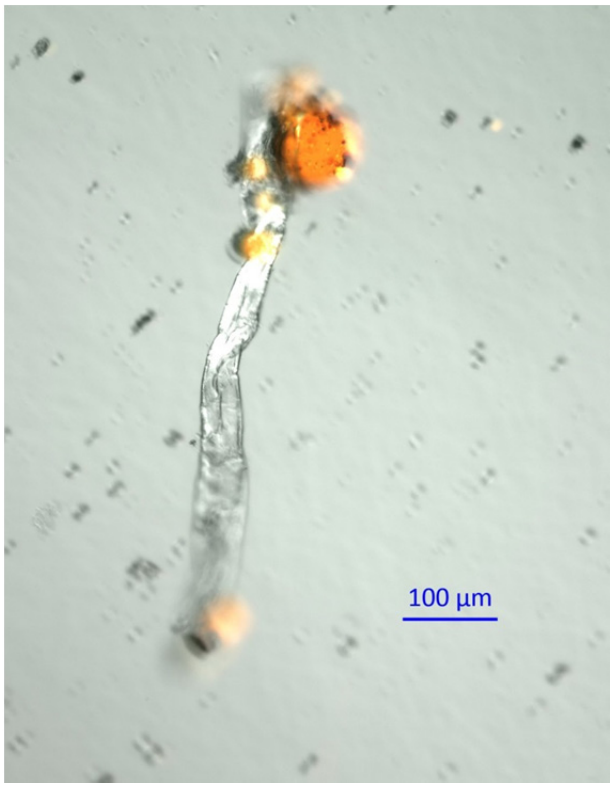

Figure 16: Filamentous material of presumably biological origin that is present in the sediment; several oil globules are attached.

Figure 17: Another view of OPA with the main particulate component being the filamentous material.

3.2.3.3 Observations regarding OPA formation at low mixing energies

At low mixing energy (150 RPM on shaker, ε on order of 10^{-2} m^2/s^3 per Kaku et al., (2006a)), little oil is entrained and C_{sed} >> C_{oil} in suspension. Oil globules are more likely to get trapped within aggregates of sediment. This is illustrated in Figures 18 and 19.

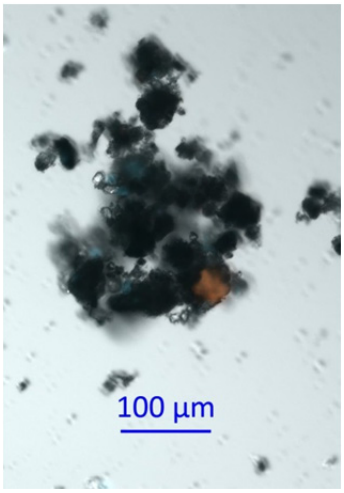

Figure 18: An oil globule within an aggregate of larger sediment grains

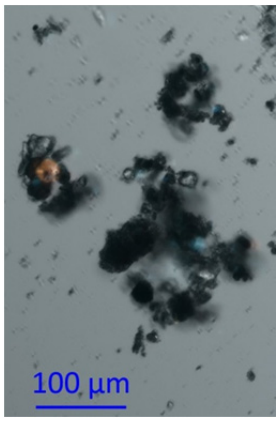

Figure 19: Another view of an oil globule within predominantly larger sediment grains; other aggregates of sediment alone are also shown.

3.2.3.4 Observations regarding solid-type OPA

After preliminary analysis of deposits using various mixing energies, weathered states of the oil, and sediment composition, it was found that the majority of globules were less than 100 µm; aggregates consisting of several large globules approached 500 µm characteristic dimension; the only particles that approached 1 mm in characteristic dimension were loose delicate aggregates similar to that shown in Figure 11 that tended to increase in size upon deposition and aggregation with other sediment on the bed. When resuspended during removal for microscopy analysis, none of these features had the appearance of what has been anecdotally described from field observations as oil "globs" as illustrated in Figure 20.

Figure 20: Large masses of sediment-laden tarry oil resuspended from the bed during fall 2014 dredging and captured from below the water surface with a sheen net. The large features were confirmed to consist predominantly of oil using UV epifluorescence microscopy. The samples were collected and photographed by Rex Johnson of GRT.

A prominent feature observed by site responders and field personnel is the presence of oil "globs" that emerge from the river bed under agitation (e.g., poling, dredging) and upon reaching the surface, degenerate into a sheen with a central core of gritty tar. These features have been described as generally being on the order of magnitude of several millimeters. Anecdotal evidence was provided by Ralph Dollhopf and Greg Powell of the U.S. Environmental Protection Agency (pers.

comm., 2013). In addition to the tarry globs that rise from the bed following agitation, Greg Powell referred to "flecks" of material suspended in the water column (approximately neutrally buoyant) during the early stages of the response. These appeared to be pieces of leaf litter, but when captured and rubbed between the fingers were found to be predominantly tarry oil. Such features were not readily observed during the preliminary analysis of deposits under various combinations of the relevant variables being experimentally controlled. The globs that lead to sheen are generally considered to be the primary nuisance that remains from the spill and are an aspect of Kalamazoo River oiled sediment that warrants greater understanding. An initial hypothesis regarding a potential means of incorporating sediment into the interior of an oil globule (in addition to that attached at the surface) was found to have some previous basis in the "solid" type OPA described by Stoffyn-Egli and Lee (2002). Their work indicated the importance of sediment attachment to one side of an oil surface, existing either on the surface as a film or attached to a solid surface such as a flask. The mechanism they described involved one side of an entrained unit of oil from such a surface being more hydrophobic due to the uneven distribution of sediment; this causes shapes other than spherical globules to be prevalent and can lead to folding of the non-spherical oil units. They also describe a process whereby the sediment may effectively sink into the body of the oil under the right conditions. The hypothesis formed during the current project involved a process whereby a sequence of multiple entrainment and resurfacing events may lead to incorporation of sediment into the globule through reconfiguration of globules. On the basis of the current hypothesis, an experimental procedure was conducted that did yield abundant larger-size OPA on the size order of 1 mm. This alternate hypothesis was not formulated to prove or disprove the mechanisms described by Stoffyn-Egli and Lee (2002). Rather, the hypothesis was formed in the attempt to generate the large sized-OPA known anecdotally as globs in the absence of the ability to do so using the previously described shaking techniques.

The experimental procedure for attempting to obtain large-size solid-type OPA was as follows:

- 50 to 100 mg of sediment was mixed with 120 mL of the water and Sodium Azide solution and allowed time to sink in the water column prior to adding the weathered oil (10% or 17.4% mass loss) at the ratio of 1 mg sediment to 2 µL of oil to the baffled flask.
- The shaker was run for 5 minutes at 200 RPM to fully entrain the oil and keep it entrained in the water column; this is referred to as the entrainment and mixing phase.

- After the 5 minutes was complete, the shaker was stopped and allowed to remain at rest for 1 to 2 minutes – until the readily visible oil droplets resurfaced; this is referred to as the resurfacing phase.
- The shaker was run for 3 minutes at 135 RPM, which is vigorous enough to promote recoalescence, yet not vigorous enough to yield entrainment; this is referred to as the recoalescence phase.
- The previous three steps were repeated from 6 to 12 times.

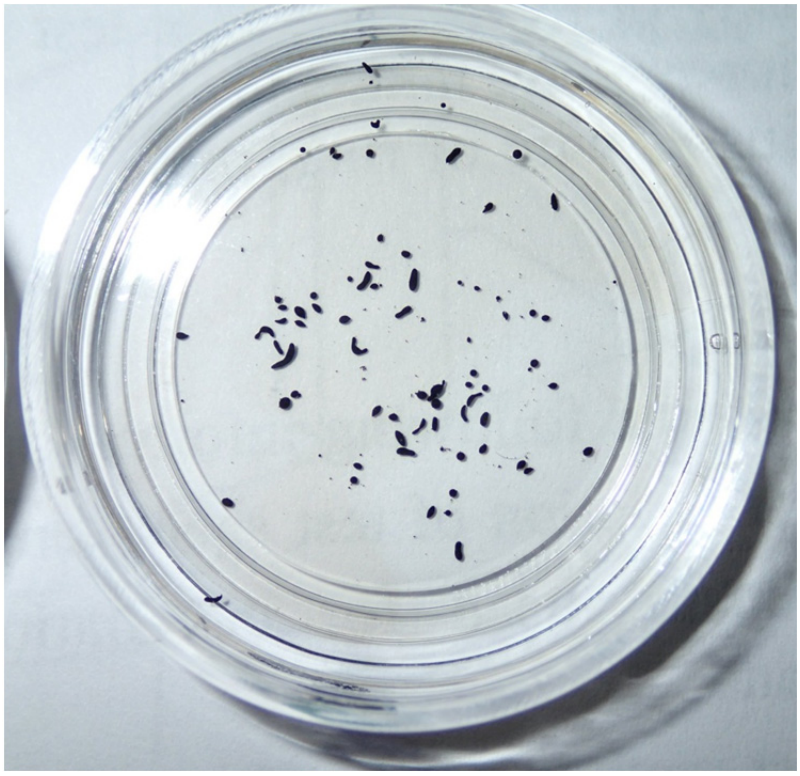

Figure 21: A view of the "solid"-type OPA generated through the above procedure in a 35-mm diameter Fluorodish.

A closer view obtained via UV epifluorescence microscopy of some of the individual OPA units from the Fluorodish (Fig. 21) are illustrated in Figures 22 through 24.

Figure 22: An elongated OPA with a pointed end.

Figure 23: A crescent shaped solid-type OPA

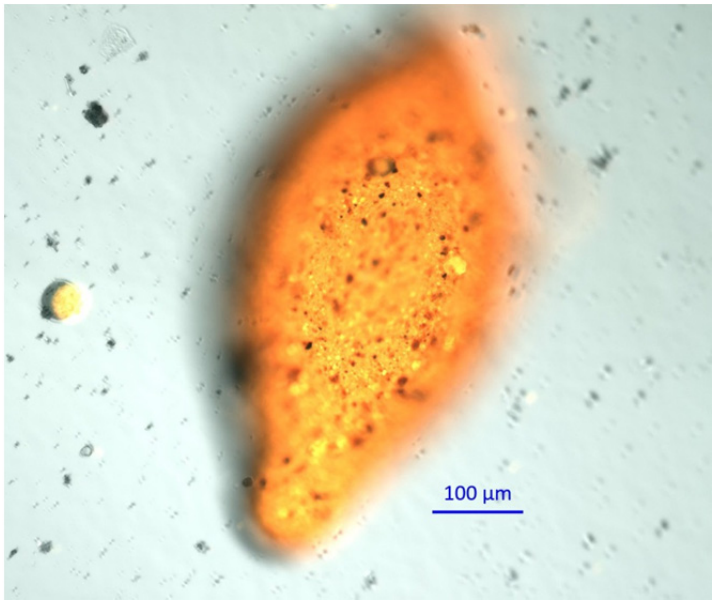

Figure 24: An intermediate non-spherical shaped solid-type OPA

Several notes are warranted regarding the above results. First is that the formation of the large solid-type OPA does not occur to the exclusion of the more common droplet-type OPA, which are also abundant in the deposit. Secondly, the mechanism described by Stoffyn-Egli and Lee (2002) pertaining to the folding of the entrained oil into irregular shapes is likely occurring in the generation of such OPA, evidence of which is provided in several of the images illustrated later from the settling velocity tests. The mechanism associated with sediment incorporation through reconfiguration of globules per the initial hypothesis cannot be discounted, but also cannot be definitively proven with the data obtained.

3.2.4 Quantitative Analysis of Oil Droplet Size Distribution

3.2.4.1 Oil Droplet Size Distribution in the Experimental Deposits

For the purposes of numerical modeling of resuspension, transport, and deposition of OPA, more detailed quantitative evaluation of the character of the OPA deposits is warranted. The first step in such an evaluation is to obtain the size of the OPA. The images obtained per the sampling plan illustrated on Figure 5 were analyzed to obtain oil globule size distributions. Tests were conducted at 160 RPM, 180 RPM, and 200 RPM on each of the oil types characterized by their weathered state: the unweathered oil (0% mass loss), the intermediately weathered oil (9.9% mass loss), and the heavily weathered oil (17.4% mass loss).

Evaluation of the images was first conducted to develop a procedure to automate the data analysis. Such a procedure requires edge detection of individual globules and the ability to discern individual globules in close proximity to each other. A number of difficulties were encountered. The first is that the two-dimensional images contain many globules that are stacked and overlain and the ability to discern and identify particles requires judgment on the part of the evaluator; oftentimes, it is necessary to consult different individual UV and visible light channels, different combinations of UV channels, and modify the intensity histogram of an individual UV channel in order to best distinguish individual globules. Another even more problematic issue is the ability to distinguish specks of sheen (an undesired artifact of the procedure in which deposits were removed) from globules without the aid of consulting different UV and visible light channels as described previously. In order to achieve a practicable means of automating the process, a procedure for deposit removal from the baffled flask would need to be developed that effectively eliminates the presence of sheen specks; and the amount of deposit added to the Fluorodish would need to be significantly reduced to minimize the occurrence of overlap and allow all individual OPA to effectively lay flat on the dish bottom. A third problematic issue is the presence of irregular edges owing to large regions of the globule perimeter being obscured by sediment particles (and thus making the region appear non-fluorescent). A fourth issue is edge blur. The microscope depth of focus is on the order of a few microns, while most globules are considerably larger than that. Thus, only a portion of the globules will be in focus in the 2-dimensional image. Globules that were in focus have crisp edges that can be accurately delineated; whereas the out-of-focus globules edges were not readily delineated.

Some brute-force manual trials were conducted to accurately identify globules and their diameters to determine if a systematic method behind the human judgments used in this process could potentially be discerned and then reproduced in automated code. While development of such a code is certainly possible, the level of sophistication required was determined to be beyond what could be practicably developed within the scope of the current project. The decision was made to proceed with the brute-force method of image analysis, requiring greater time investment per image, and fewer processed images. The method is described as follows. The .TIFF images were inserted into AutoCAD 2012 and then scaled such that the measured dimensions were in μm rather than pixels. A circle was drawn around each globule using the 2-point method, which requires only a small fraction of the circumference be discernible to accurately fit the circle that matches the discernible portion. In general, the orange channel provides the best image to use in drawing the circle; but as indicated previously, this process often involved evaluation of several UV and visible

light channels, and combinations thereof. Any properties of the circles (e.g., diameter, area, layer, coordinates, etc.) desired for evaluation can be output to a comma-delimited text file for quantitative analysis. A relatively simple image requiring minimal difficult judgments is provided to illustrate the evaluation procedure.

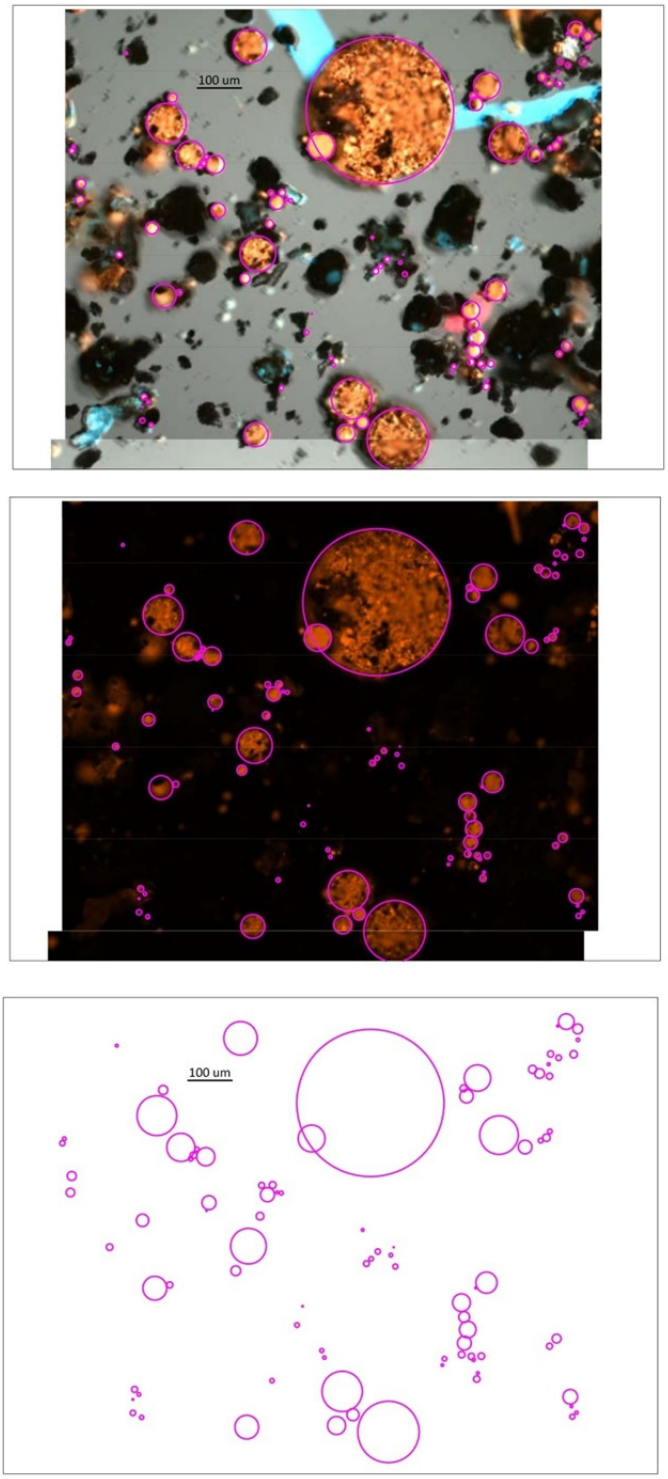

Figure 25: An example of establishing the globule diameters on a fairly straight-forward photomicrograph. The top panel is an overlay of all 4 UV channels and visible light; the middle panel is the orange channel, which was generally best to use in drawing the circles; the last image is the end result showing only the circles.

Autocad also can be used to create blocks with attributes; a number of globules within a single aggregate can be combined into a single block. The properties of the individual elements and attributes of the block can be output to a comma-delimited text file in the same manner. This effectively allows development of a database of OPA properties that can be queried. Relevant attributes can be defined by the user such as: number of globules in the OPA; whether the OPA is dominated by sediment or oil; largest visible sediment grain size attached to the globule. Some preliminary evaluation of such an approach was determined to be promising, but evaluating which globules comprised an aggregate and assigning the block attributes was found to be very time-consuming and was abandoned due to time limitations.

Each of the three weathered states of the oil (0% mass loss, 9.9% mass loss, 17.4% mass loss) was evaluated at three different orbital shaker speeds (160 RPM, 180 RPM, 200 RPM). In addition to these nine basic experimental cases, a sample from the experiment that developed the macroscopic solid-type OPA illustrated in Figures 21 – 24 was analyzed, yielding a tenth case; the experimental settings for this latter case were described in the previous subsection. Histograms of globule diameters were developed from the analyzed images; histogram bins were based on 32 log-spaced intervals between 1.25 µm and 250 µm, identical to the size bins used by the LISST-ST (for ultimate comparison with data obtained while mixing oil only). Four additional bins (Bins 33-36) extend the size range up to a maximum size of 485 µm based on the same log-spaced interval (factor 1.18) to incorporate the largest oil unit present in any of the images. The size range of each bin is provided in Table 6.

Bin #	Lower Bound (µm)	Upper Bound (µm)
1	1.25	1.48
2	1.48	1.74
3	1.74	2.06
4	2.06	2.43
5	2.43	2.87
6	2.87	3.38
7	3.38	3.99
8	3.99	4.71
9	4.71	5.55
10	5.55	6.55
11	6.55	7.73
12	7.73	9.13
13	9.13	10.77
14	10.77	12.71
15	12.71	14.99
16	14.99	17.69
17	17.69	20.88
18	20.88	24.64
19	24.64	29.07
20	29.07	34.30
21	34.30	40.48
22	40.48	47.77
23	47.77	56.36
24	56.36	66.51
25	66.51	78.48
26	78.48	92.61
27	92.61	109.28
28	109.28	128.95
29	128.95	152.16
30	152.16	179.55
31	179.55	211.86
32	211.86	250.00
33	250.00	295.02
34	295.02	348.14
35	348.14	410.83
36	410.83	484.81

Table 6: Bin size ranges used in the histograms

The histograms are presented according to the number of globules in each bin (p_{NUM}) and according to the volume of globules in the bin (p_{VOL}); the p values are normalized by the total number of globules and the total volume of globules, respectively, such that the sum of the p values yields 1.0 for each histogram. The volume calculation to establish p_{VOL} was based on the assumption that circular globules in the photomicrographs were spheres. For the few irregular-shaped masses of oil that were not circular, the feature was placed in a bin using the delineated area of the polygon to calculate an effective diameter of a circle with the same area. The volumes of the irregular polygons were calculated using the procedure of Stoffyn-Egli and Lee (2002), whereby the irregular shaped object was assumed to be cylindrical, with the height of the cylinder equal to the longest dimension of the polygon, and the diameter of the cylinder equal to the area of the polygon divided by the longest dimension. Histograms for a typical experiment are illustrated on Figures 26-27; note that all p_{VOL} histograms are heavily weighted to the bins containing the larger globule size. Histograms from each of the ten analyzed cases are included in Appendix A.

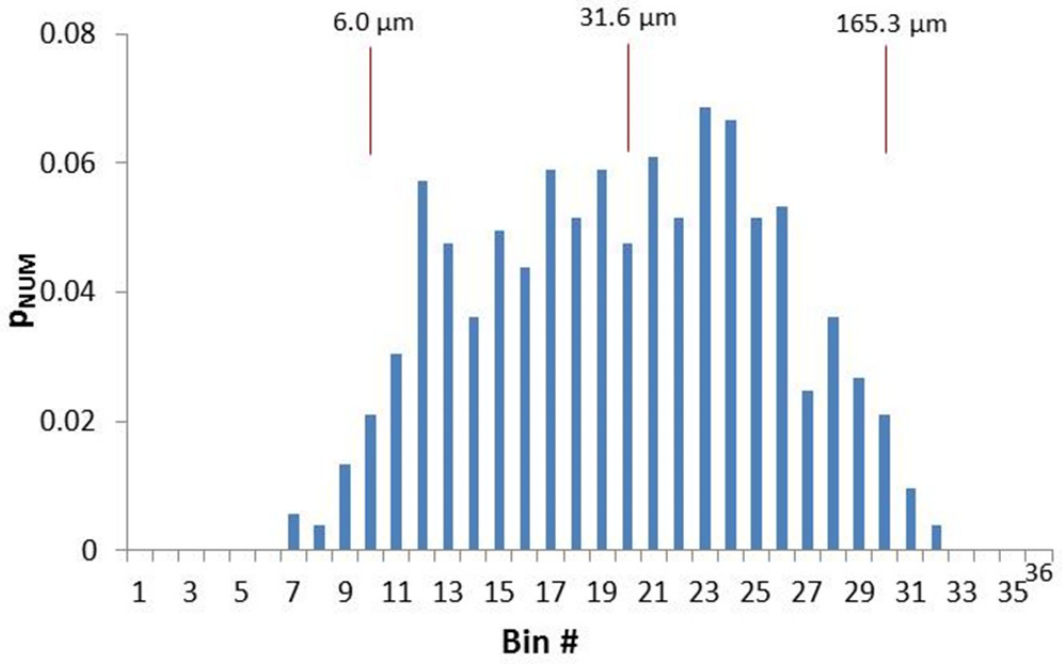

Figure 26: The histogram based on number of globules in each bin for the experiment using 0% mass loss oil shaken at 180 RPM (one hour).

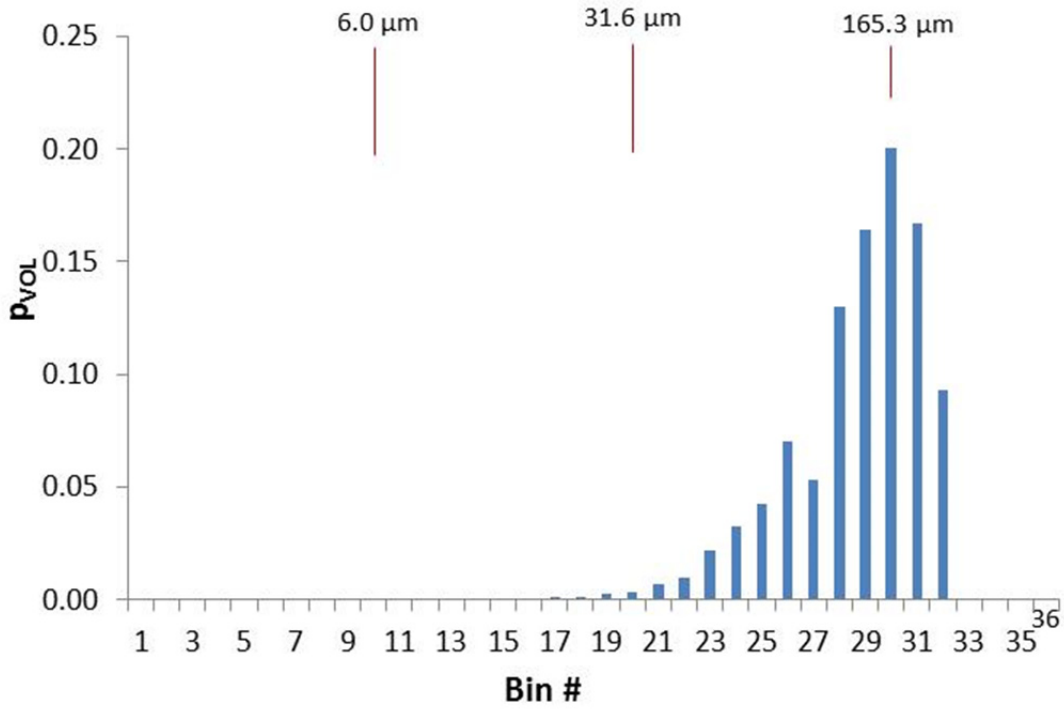

Figure 27: The histogram based on the volume of globules in each bin for the same experiment illustrated in Figure 26 (0% mass loss oil; 180 RPM). Note that the larger size classes dominate the volumetric distribution.

For the purpose of comparing globule size distributions between experiments to help ascertain the influence of experimental variables, overlaying histograms tends to yield cluttered plots. The more suitable method of illustration for comparison is to implement cumulative distributions; as with the histograms, the cumulative size distributions are presented with separate plots that contain the y-axis variable as: (a) percent finer by number; and (b) percent finer by volume. Plots are organized such that one of the experimental variables (weathered state of the oil and shaking speed) is constant and the other is varied.

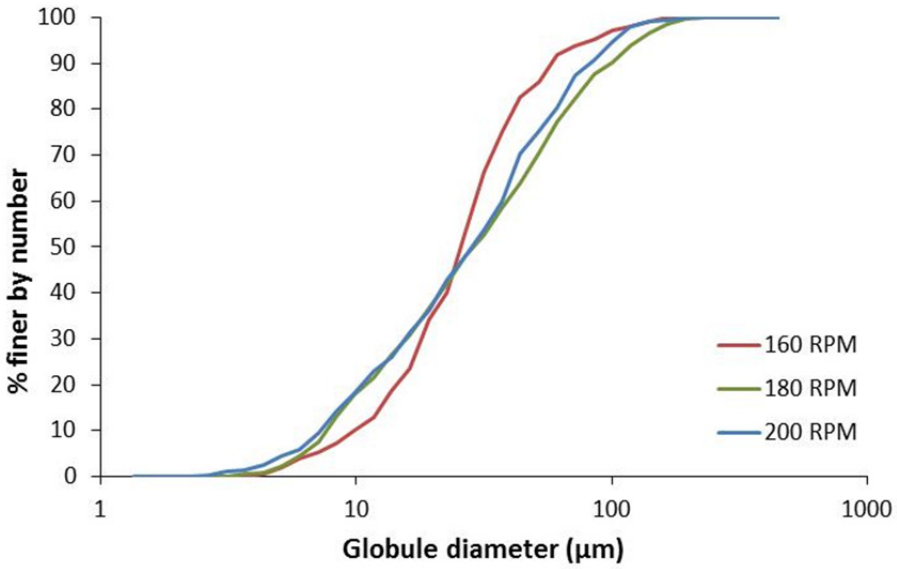

Figure 28: Cumulative globule size distribution from experimental deposits for the 0% mass loss oil at the three different shaking speeds.

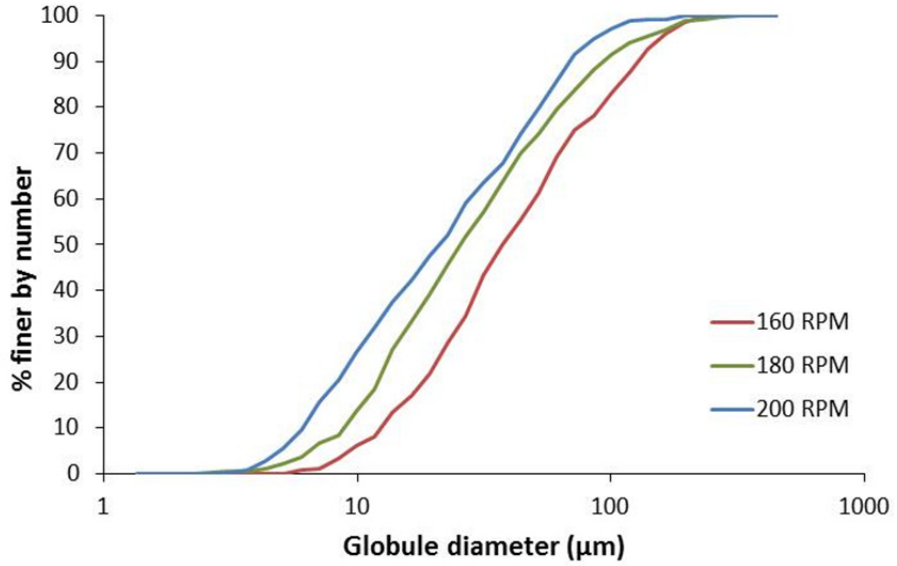

Figure 29: Cumulative globule size distribution from experimental deposits for the 9.9% mass loss oil at the three different shaking speeds.

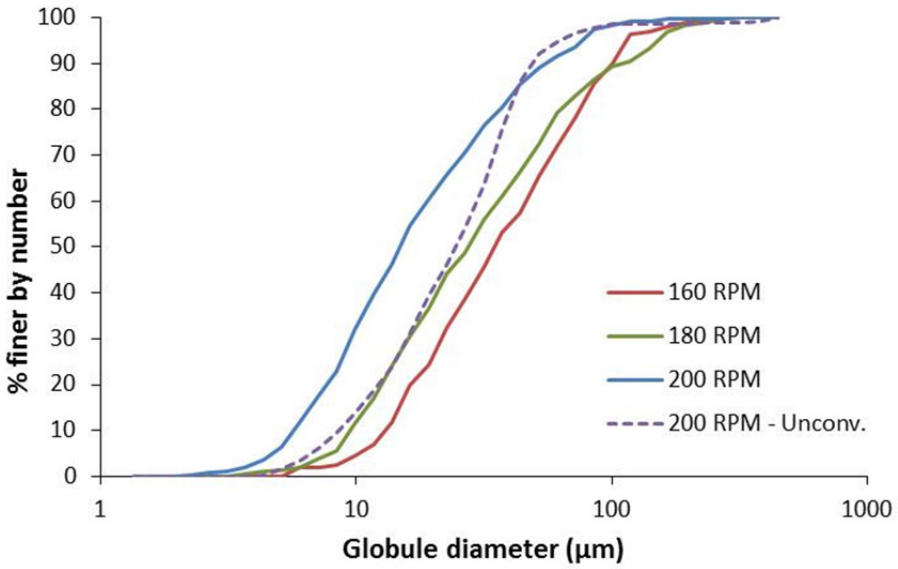

Figure 30: Cumulative globule size distribution from experimental deposits for the 17.4% mass loss oil at the three different shaking speeds. The dashed curve is the deposit analyzed from the unconventional shaking method that yielded the large solid-type OPA.

The following three plots show the same cumulative distributions as the previous three figures, but are organized according to common shaking speed with the different curves showing weathered states of the oil.

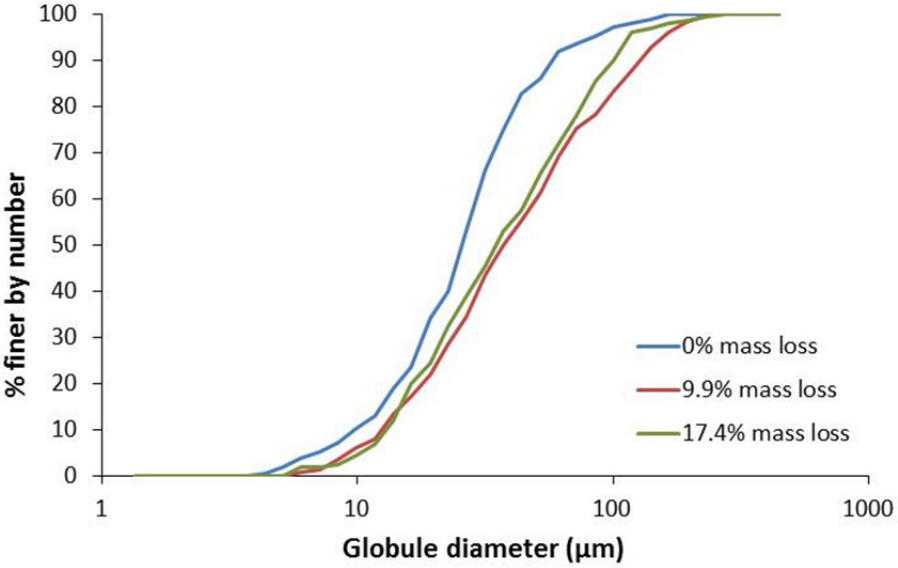

Figure 31: Cumulative globule size distribution from experimental deposits for three different weathered oil states shaken at 160 RPM. Note that the oil in the experimental deposit for the 17.4% mass loss case at this low shaking speed had abundant irregular-shaped features caused by oil adhering to the flask and only gradually breaking off into suspension.

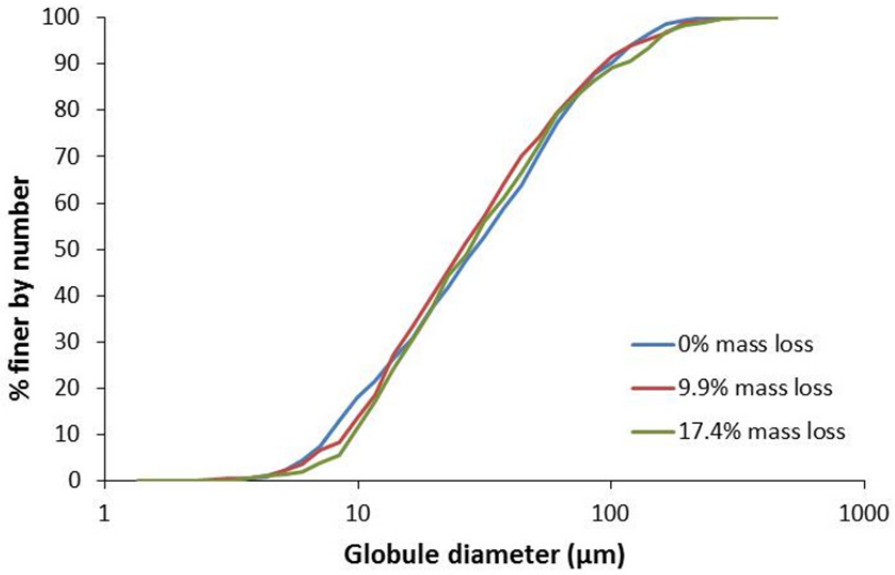

Figure 32: Cumulative globule size distribution from experimental deposits for three different weathered oil states shaken at 180 RPM.

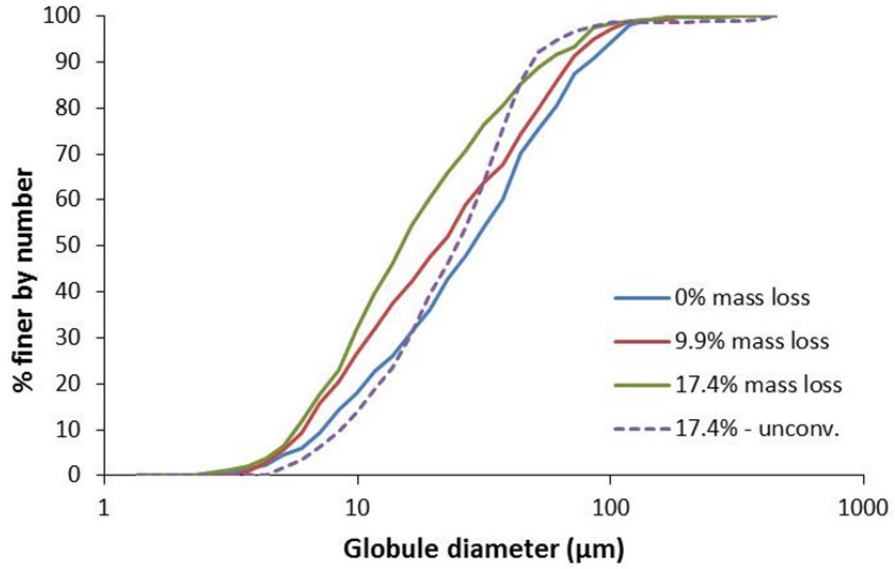

Figure 33: Cumulative globule size distribution from experimental deposits for three different weathered oil states shaken at 200 RPM. The dashed curve is the deposit analyzed from the unconventional shaking method that yielded the large solid-type OPA.

The following six plots follow the same sequence as Figures 28-33, but are based on the volume of oil in each bin rather than the number of globules. These curves are uniformly steeper, given the dominance of the distribution by the larger-sized globules. Globules less than 10 µm are included in the calculations, but yield negligible values and thus the plots do not extend to values less than 10 µm.

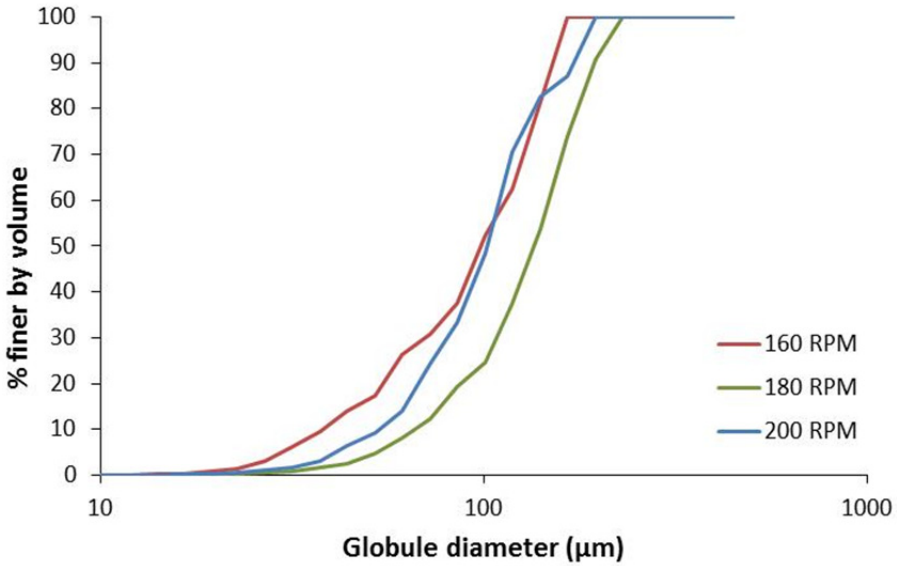

Figure 34: Cumulative globule size distribution (based on volume) from experimental deposits for the 0% mass loss oil at the three different shaking speeds.

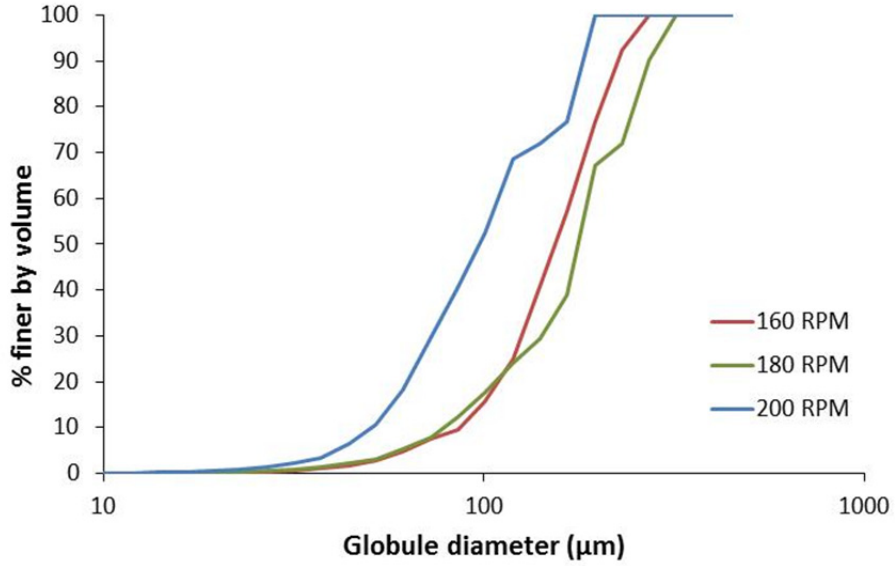

Figure 35: Cumulative globule size distribution (based on volume) from experimental deposits for the 9.9% mass loss oil at the three different shaking speeds.

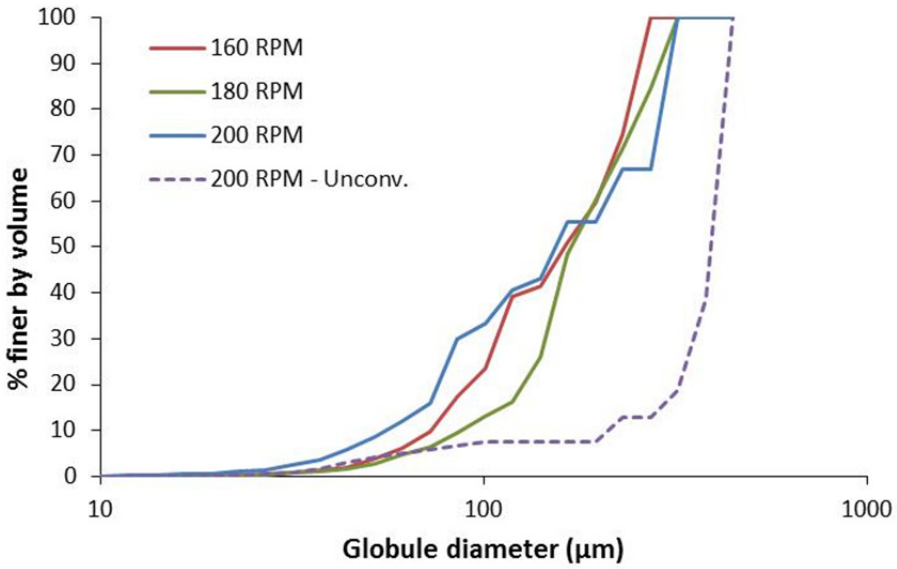

Figure 36: Cumulative globule size distribution (based on volume) from experimental deposits for the 17.4% mass loss oil at the three different shaking speeds. The dashed curve represents the experimental trial using the unconventional shaking method.

The following three plots again show the volume-based distributions, but the experimental variable that is held constant is changed to shaking speed.

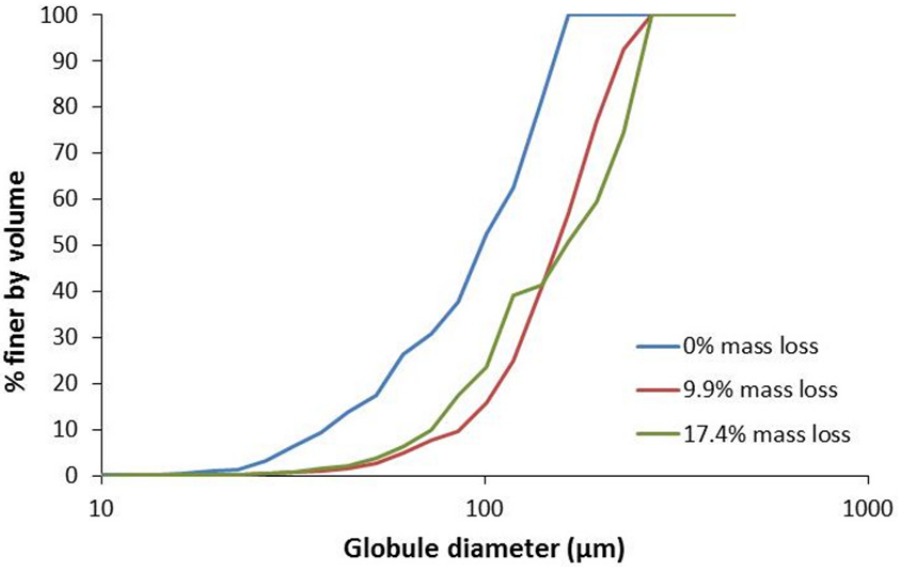

Figure 37: Cumulative globule size distribution (based on volume) from experimental deposits for three different weathered oil states shaken at 160 RPM. Note that the oil in the experimental deposit for the 17.4% mass loss case at this low shaking speed had an abundant amount of irregular-shaped features caused by oil adhering to the flask and only gradually breaking off into suspension.

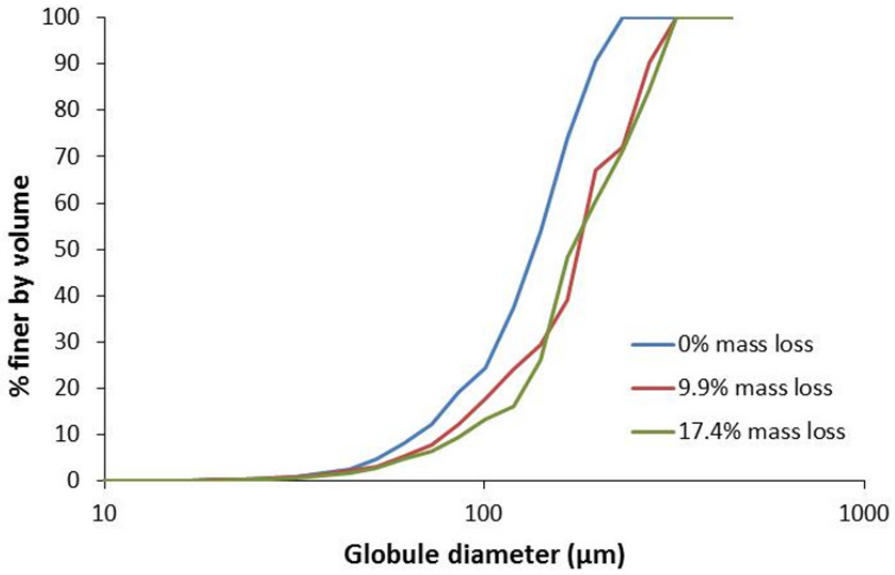

Figure 38: Cumulative globule size distribution (based on volume) from experimental deposits for three different weathered oil states shaken at 180 RPM.

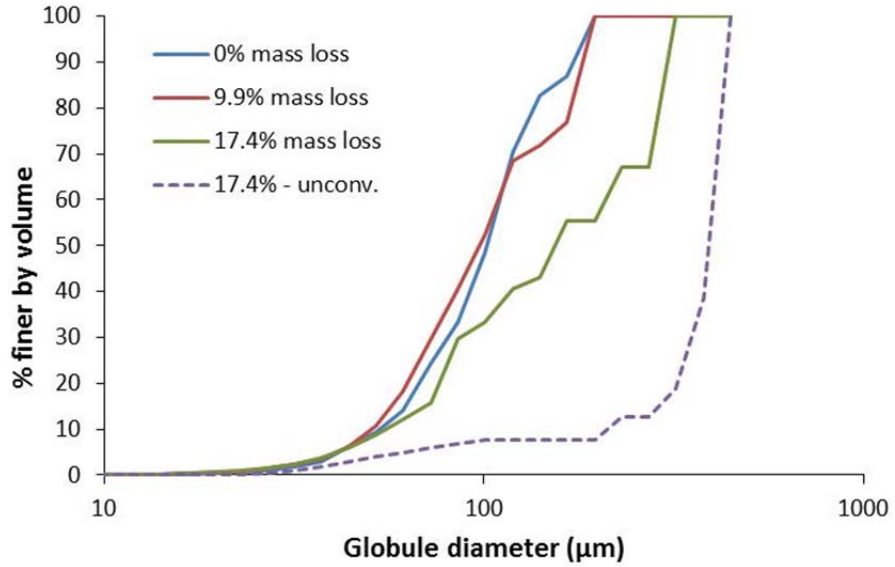

Figure 39: Cumulative globule size distribution (based on volume) from experimental deposits for three different weathered oil states shaken at 200 RPM. The dashed curve represents the experiment using the unconventional shaking method.

The size distributions of globules in the experimental deposits illustrated in Figures 28 - 39 reveal some expected and some unexpected results. When evaluating a single weathered state of oil, the distribution of globules tends to shift to smaller sizes at higher mixing energies. A qualitatively similar result would be expected if evaluating globules in suspension in the absence of sediment. However, when evaluating deposit compositions of a single mixing energy with respect to different

weathered states of oil, the relationship is more complex. The figures of constant shaking speed reveal that at low mixing energy (160 RPM) the unweathered oil tends to yield a smaller size distribution of globules in the deposit than the more heavily weathered oils, as would be expected on account of the oil viscosity effect, which increases the stability of large globules when the oil viscosity is higher. But as the mixing energy increases to 200 RPM, the trend reverses, with the more heavily weathered oils yielding a generally smaller size distribution than the unweathered oil. This occurs despite the result that the heavily weathered oil consistently yields maximum globule sizes larger than the less weathered oils at the same shaking speeds. This suggests a relative change in the interaction between sediment and the smaller-sized oil globules as the mixing energy increases when comparing different weathered states of the oil. The presence of the largest globules in the more highly weathered oils is more strongly revealed in the size distributions based on volume. It is important to note that the maximum size of spherical globule that can deposit has an upper limit based on the surface area to volume ratio of the globule, which largely controls the ratio of oil to sediment in a droplet-type OPA, and consequently the composite density. In all cases, the volume-based distributions are dominated by the globules in the large size classes, and the more heavily weathered oils more so than the unweathered oil.

3.2.4.2 Oil Droplet Size Distribution in Suspension

Data acquisition was also undertaken on the distribution of oil globules in suspension during the shaking experiments when the same volume of water and oil was used, but in the absence of sediment. This was undertaken to allow analysis of the distribution of the oil globules relative to that observed in deposited material. The size of globules less than 250 µm can be captured with the LISST-ST, provided that all size classes can be accurately sampled between the time that shaking ceases and the time the sample is collected; rapid resurfacing of the larger globules makes accurate sampling a challenge. The size of globules greater than 250 µm cannot practically be characterized through a standard sampling procedure due to the issue of rapid resurfacing. Photographic analysis was undertaken in an attempt to capture the larger sizes of globules. The setup for the photographic analysis is illustrated on Figure 40.

Figure 40: The setup for the photographic analysis; the baffled flask is mounted inside a small aquarium containing water to minimize optical distortion associated with the irregular flask geometry; the PIV camera rotates with the entire assembly. Lighting is provided from the rear.

In order to prevent the majority of the oil from adhering to the glass during the orbital shaker tests without sediment, a small amount of the additive poly-vinyl alcohol (PVA) was added. This compound is soluble in water. Because PVA acts as a surfactant that has some influence on the interfacial tension between oil and water, as little as possible was desired to be added. The optimum amount that prevented the majority of adherence, while minimizing the volume added for the heavily-weathered oil was 150 µL PVA per 120 mL of water. In order to maintain consistency between the tests, the same amount of PVA was added regardless of the weathered state of the oil. Many experimental challenges were encountered; the most difficult challenges pertained to obtaining representative samples of oil droplets in both the imagery (where only the central region of the baffled flask could be imaged without excessive distortion) and in the samples drawn from the flask after shaking for analyzing the small-sized droplets with the LISST. Within the time limitations of the project, these challenges were ultimately not successfully resolved.

3.3 OPA Settling Velocities

Settling velocity tests were conducted in a 1.6-m height Plexiglass settling column having a rectangular cross section with inside dimensions 20.2 cm x 10.5 cm. A vellum sheet graduated in 1 cm increments is affixed to the outside of the back wall of the column, which serves to identify the vertical position of the particles, to provide a uniform color background to aid in particle visualization, and to diffuse light from the light source that is present behind the settling column to improve photograph quality. A view of the settling column setup is illustrated in Figure 41.

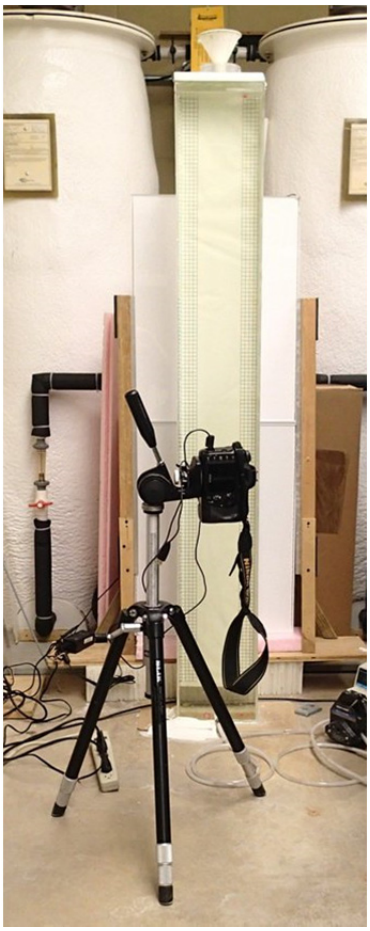

Figure 41: The settling column used for the settling velocity tests. The vertically mounted panels behind the column are LED light panels.

The water column is located in a temperature-controlled room. The column was filled with tap-water 24 hours prior to the beginning of the first set of settling velocity tests and the same water was used for all the tests. (Note that conductivity of water in settling column is not expected to be a variable that influences settling velocity of pre-existing OPA.) Several hours prior to each testing period, an air

bubbler line from a small aquarium pump was inserted with its outlet at the bottom center of the column to achieve light mixing due to a mild recirculation pattern in the water generated by air bubbles traveling vertically to the surface. The bubbler was removed from the water approximately 30 minutes before settling velocity tests were conducted. Immediately before testing began, water temperature throughout the depth of the water column was checked with a YSI 6920 probe to ensure no temperature gradients existed inside the column (and thus potential density differences and heat convection influences). During all tests the water temperature was uniform throughout the depth and in the range between 22 °C and 23 °C. The conductivity was 0.305 mS/cm.

Initial trials using the settling column with small particles less than approximately 100 µm revealed difficulty in tracking the particles with the camera setup or by naked eye due to the 10.5 cm depth of field of the settling column. Aggregates tend to follow an irregular path while reaching the configuration under which they achieve terminal settling velocity. The camera lens is required to be set close to the front of the column to capture high quality images of the particles; a high quality image also requires decreasing the depth of field through increasing the aperture size. Through a trial and error process, the greatest success was achieved in tracking particles visually; this required abandoning the use of the camera, as the viewer is also required to be in close proximity to the front of the column where the camera would otherwise be located. This limited the range of particle size evaluated to those greater than approximately 100 µm, as the human eye is also not adept at focusing at close proximity onto a relatively wide depth of field.

An objective of the settling velocity work was to ensure that the particles tested were indeed OPA rather than just grains of mineral sediment or organic matter. Deposits formed using the orbital shaker / baffled flask procedure include both OPA and particulate matter with no oil attached; except for the largest size class of OPA (the solid-type OPA), a distinction could not be made between OPA and particles with no oil attached without the use of microscopy. Therefore the decision was made to sacrifice statistical quality of the tests (i.e., testing large numbers of particles to obtain means and moments) for high-quality individual data points on a smaller data set. The procedure for selecting OPA involved separating individual particles from experimental deposits into Fluorodishes; in each dish, one to five particles were placed that were distinguishable from each other visually using a hand lens. Prior to performing the settling velocity tests, these individuals were imaged using the UV epifluorescence microscopy procedure described in Section 3.2. Many of the separated particles were found to not be OPA and were thus discarded from additional analysis. The approach of performing microscopic analysis

prior to performing the settling velocity tests has the advantage of ensuring the particles tested are OPA; it has the additional advantage that more detailed information pertaining to the OPA composition (e.g., relative percentage of sediment and oil, number of globules in the aggregate, etc.) can be related to the settling velocity. The disadvantage of the approach is that to obtain a more expansive data set on the order of 100 or more particles would require substantial time investment.

The OPA that remained were tested one at a time by drawing the OPA and a small amount of water from the Fluorodish into a 25 mL transfer pipette with the tip cut off to provide a wider bore. The OPA were then gently injected just below the settling column water surface. A stopwatch was used to record time. The experimenter visually tracked the particle; when it approached specified depths (e.g., 25 cm, 40 cm, 50 cm, 75 cm, 100 cm, 125 cm depth below the datum at the top of the water column) the experimenter adjusted viewing position such that their eye was at the level of the specified graduation mark and both the graduation marks and the aggregate were visible. The eye was focused on the graduation line; when the aggregate crossed the graduation line, the time on the stopwatch was noted and recorded. Note that the water surface was 13 cm below the top of the water column; (this was done to allow the YSI probe to be inserted before testing each day while providing a small amount of freeboard to prevent spillage). In general, the slope of the OPA vertical position versus time plot reached a constant slope (i.e., constant settling velocity) by the 40 cm graduation line (i.e., 27 cm below the water surface). The position of the particle in the (x,y) plane of the cross-section had also generally stabilized by the 40-cm mark. Plots of vertical position versus time were evaluated after tests were complete, and unless the slope changed after the 40-cm reading, the settling velocity was calculated using the time between the 50-cm reading and the 125 cm reading.

Results of the experiments are summarized in Table 7. The figures that follow illustrate the individual OPA tested. Any notes regarding the nature of the OPA and the behavior during settling are provided with the figures.

OPA ID	Settling velocity (mm/s)
3B	6.31
3F-1	2.00
3F-2	1.60
3G-1	2.80
3G-2	4.21
3G-3	2.62
3G-4	11.2
3K-1	6.46
3L-2	2.08
3M-1	1.51
3M-2	1.08
3N-2	1.36
3N-3	1.53
3O-1	4.03
3O-2	1.98
3P-1	2.35
3P-2	1.62
3P-3	2.61
3P-4	2.30
3S-1	2.64
3S-2	1.21

Table 7: OPA Settling Velocities

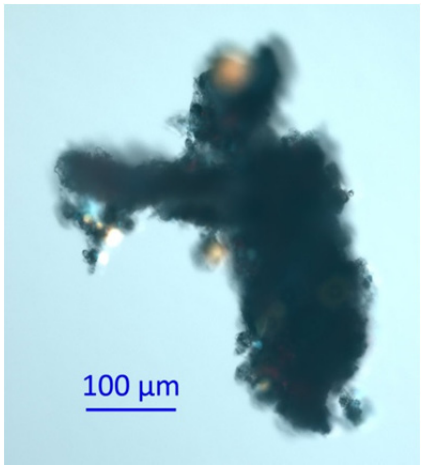

Figure 42: OPA ID 3B. This aggregate is comprised of a large piece of organic debris with fine sediment and small oil globules attached; the settling velocity character is not likely influenced greatly by the presence of the oil globules. Settling velocity = 6.31 mm/s.

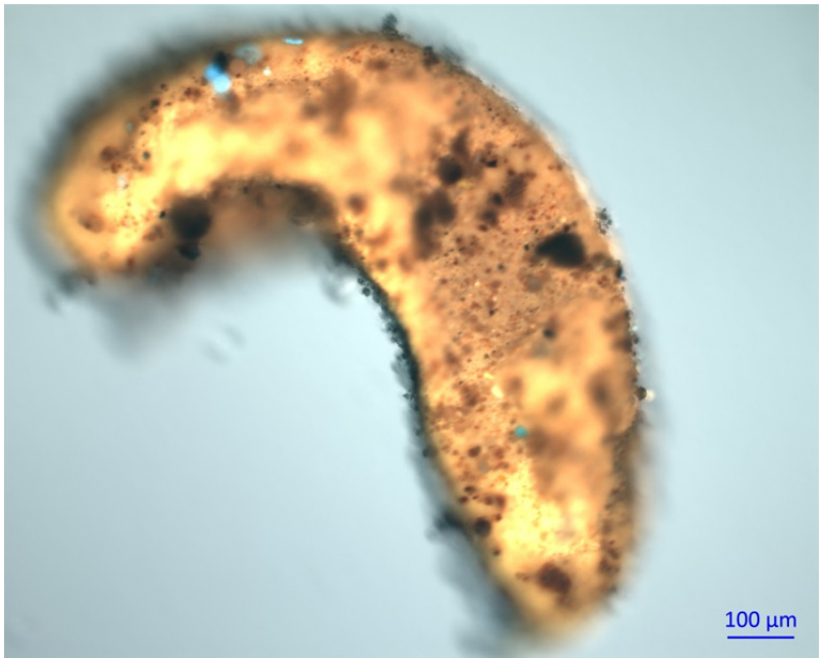

Figure 43: OPA ID 3F-1. This is the solid-type OPA. Settling velocity = 2.00 mm/s.

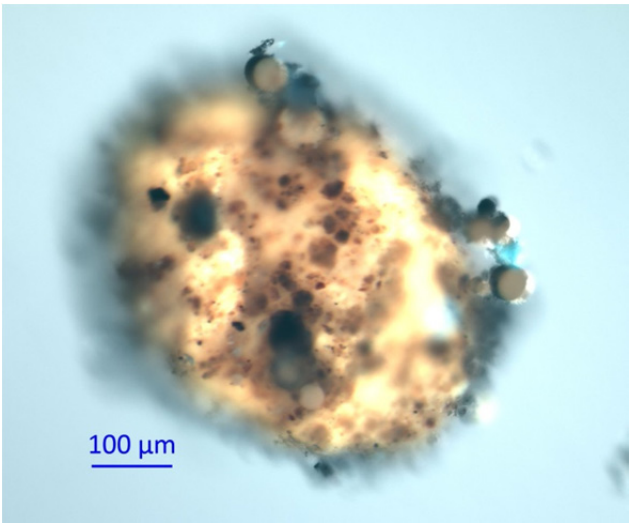

Figure 44: OPA ID 3F-2. Solid-type OPA with small droplet-type OPA units attached. Settling velocity = 1.60 mm/s.

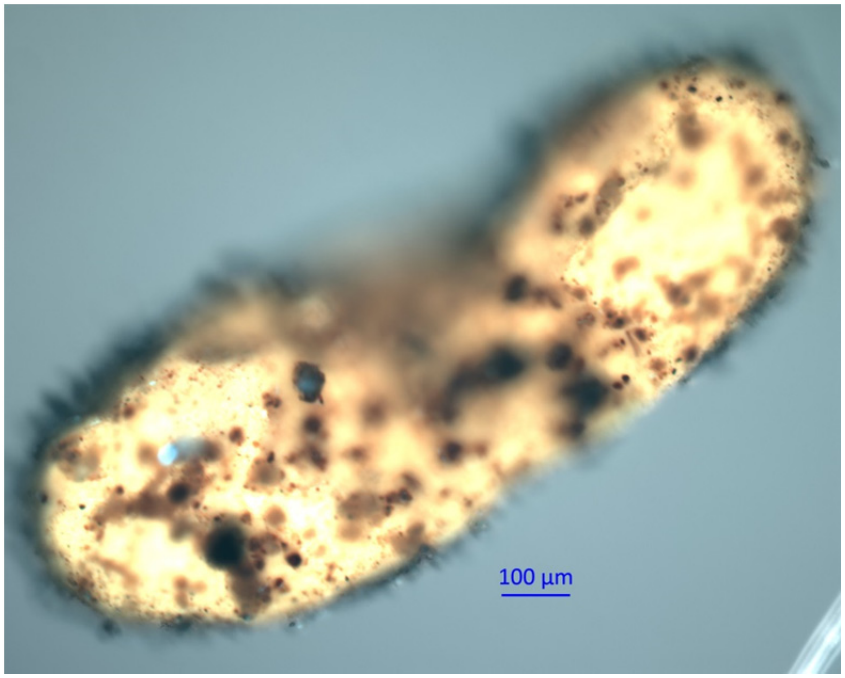

Figure 45: OPA ID 3G-1. Solid-type OPA. Settling velocity = 2.80 mm/s.

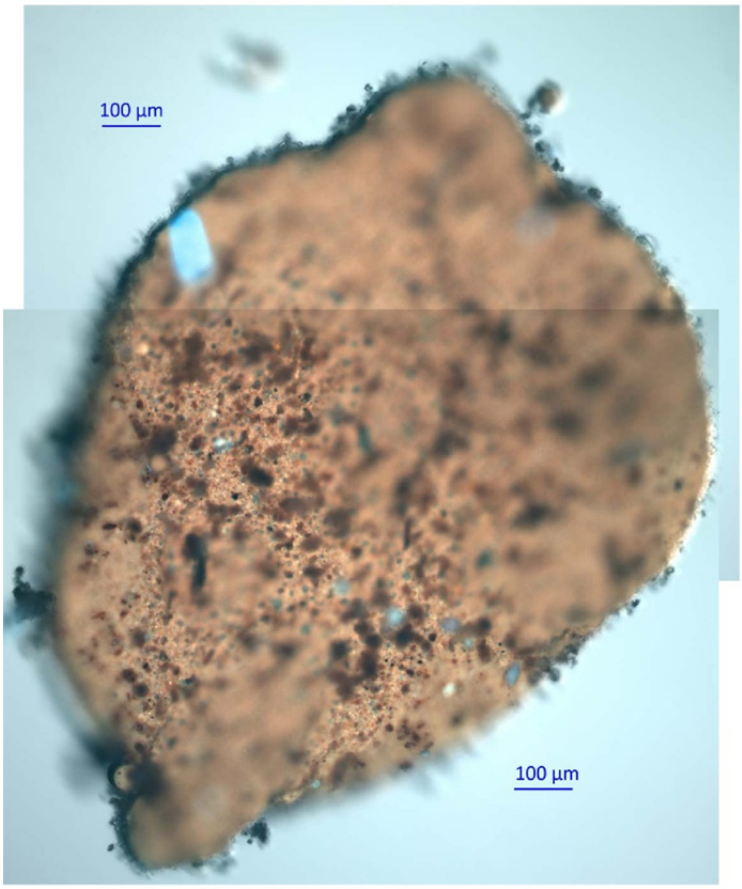

Figure 46: OPA ID 3G-2. Solid-type OPA. Settling velocity = 4.21 mm/s.

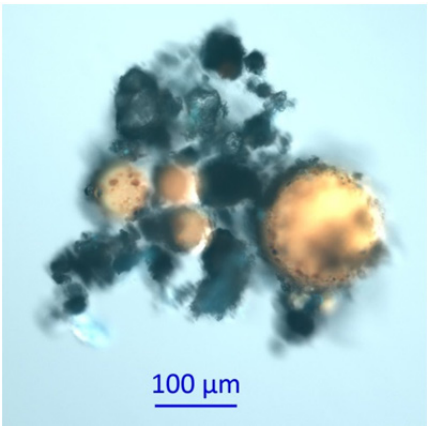

Figure 47: OPA ID 3G-3. This is a delicate aggregate that appears to be two depositional features (a 3-globule unit to the left and a 1-globule unit to the right) that bound loosely together with other sediment on the bed before being removed for analysis. It is configured in a plane. Despite its delicate configuration, it was quite stable while swirling in the Fluorodish and removal with the pipette. Settling velocity = 2.62 mm/s.

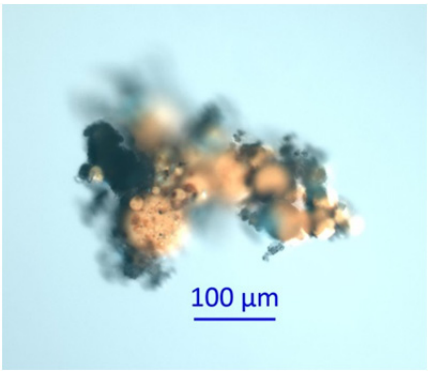

Figure 48: OPA ID 3G-4. This aggregate is anchored by a larger sediment grain on the end; during the settling experiment it aligned itself vertically, presumably with the heavy grain at the leading end and with the strand of oil globules trailing. Settling velocity = 11.2 mm/s.

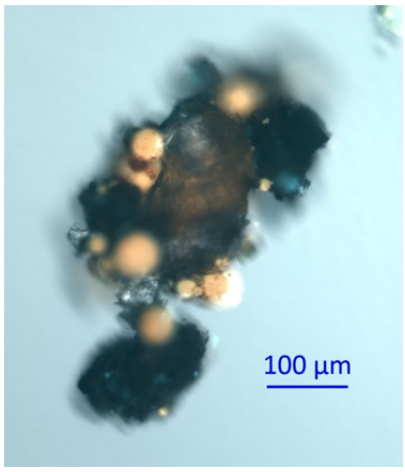

Figure 49: OPA ID 3K-1. This aggregate is similar in character to OPA 3B. The thin semi-transparent piece in the center appears to be a flake of vegetative matter or perhaps a flake of uncoated mineral sediment; the black pieces at the top and bottom are sediment grains with organic coating. Settling velocity = 6.46 mm/s.

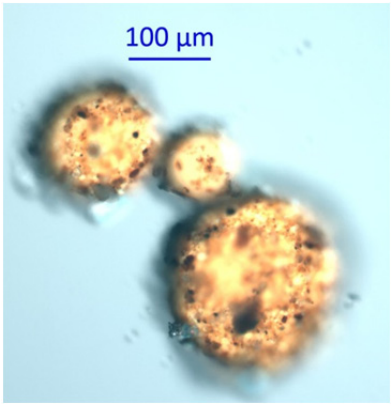

Figure 50: OPA ID 3L-2. A small chain of attached globules; this is a common configuration in the deposits. Settling velocity = 2.08 mm/s.

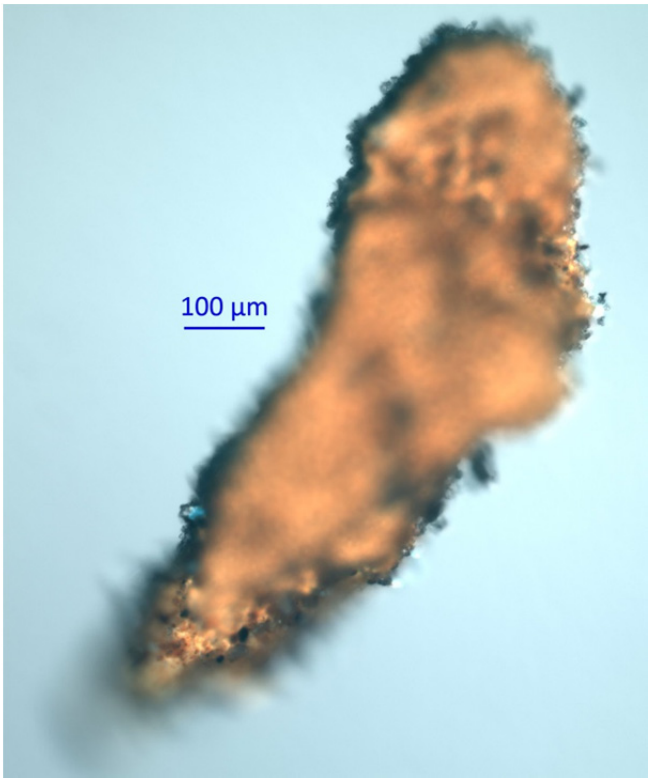

Figure 51: OPA ID 3M-1. Solid-type OPA.Settling velocity 1.51 mm/s.

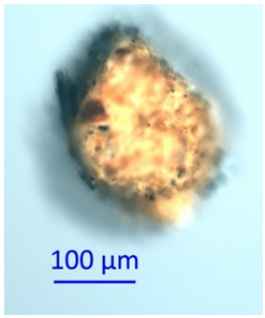

Figure 52: OPA ID 3M-2. Settling velocity = 1.08 mm/s.

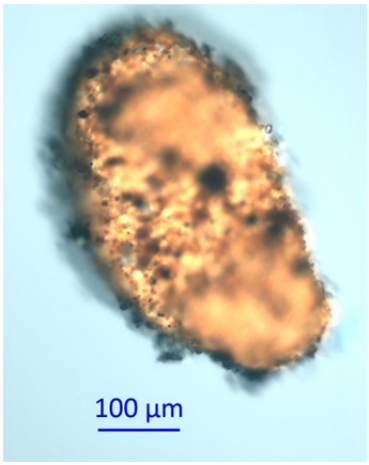

Figure 53: OPA ID 3N-2. Settling velocity = 1.36 mm/s.

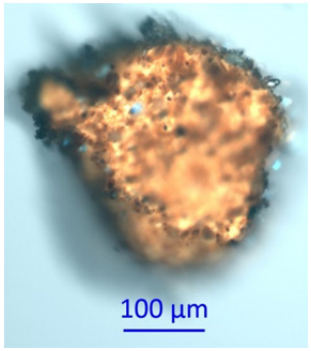

Figure 54: OPA ID 3N-3. Settling velocity = 1.53 mm/s.

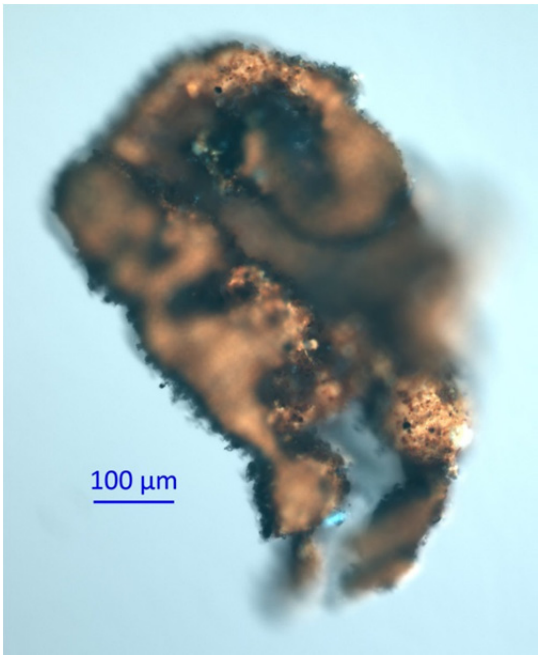

Figure 55: OPA ID 3O-1. This piece was discernibly planar. Notice the folded structure of the surface, which was observed in some of the solid-type OPA. Settling velocity = 4.03 mm/s.

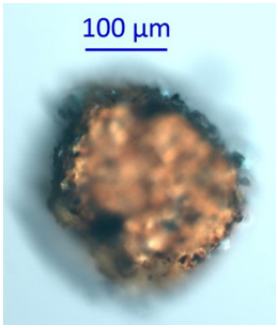

Figure 56: OPA ID 3O-2. Settling velocity = 1.98 mm/s.

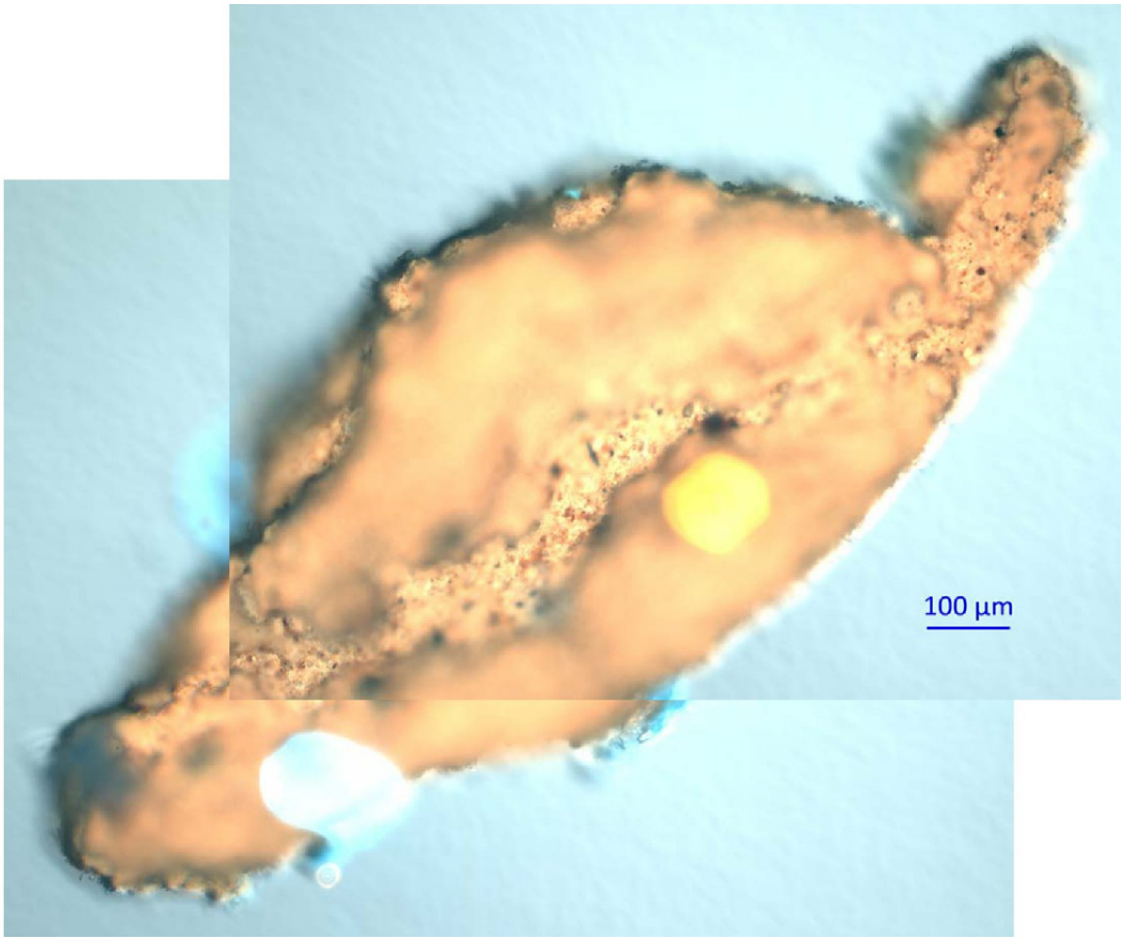

Figure 57: OPA ID 3P-1. A larger solid-type OPA with noticeable folding structure at the surface. Settling velocity = 2.35 mm/s.

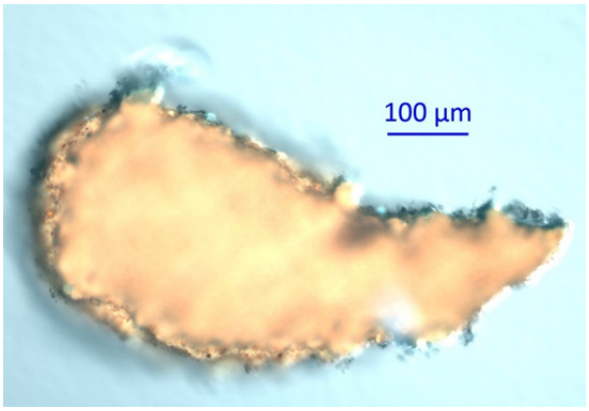

Figure 58: OPA ID 3P-2. Settling velocity = 1.62 mm/s.

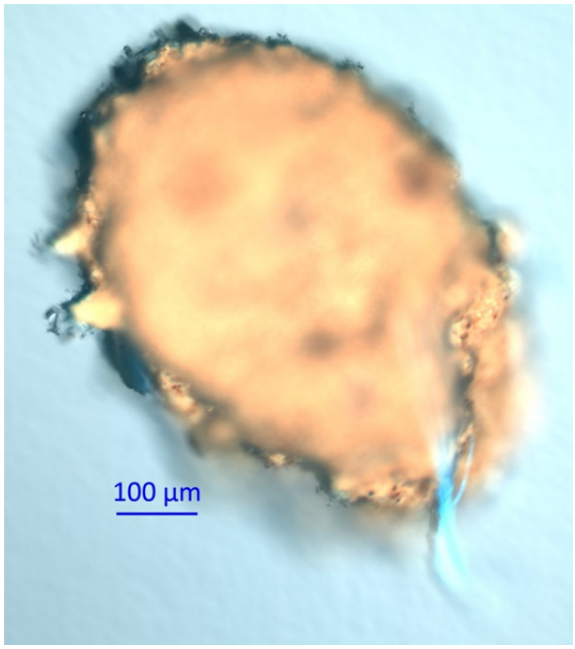

Figure 59: OPA ID 3P-3. Settling velocity = 2.61 mm/s.

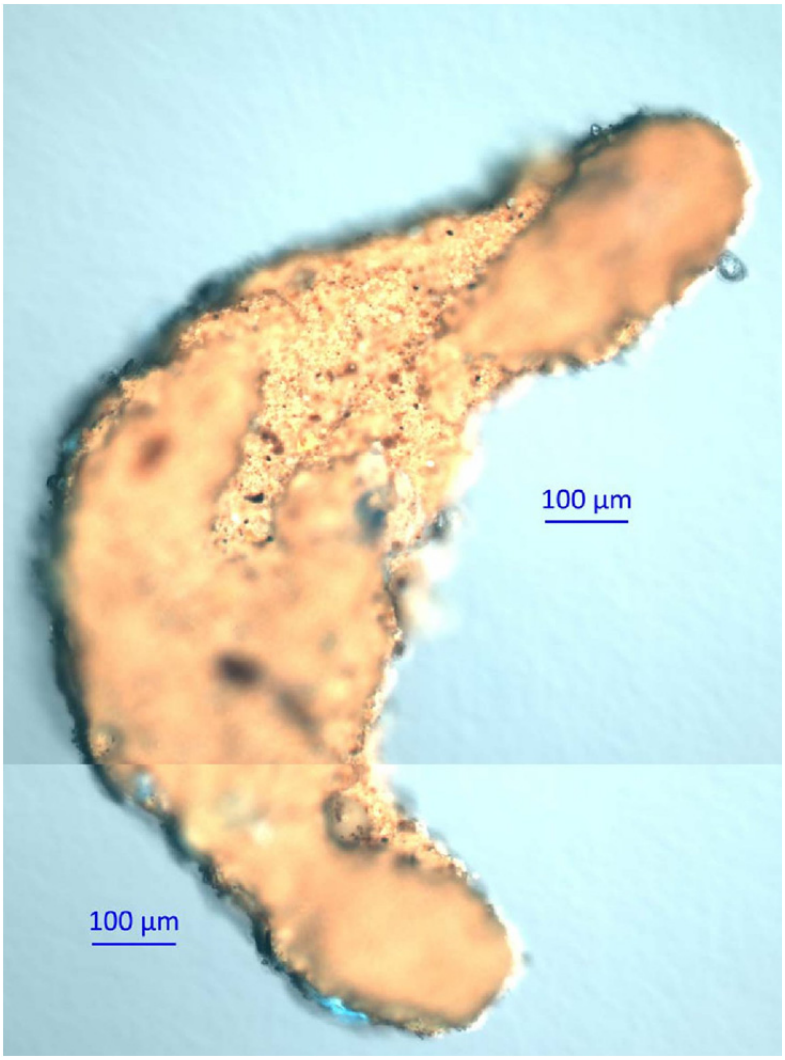

Figure 60: OPA ID 3P-3. A large solid-type OPA similar in character to 3P-1. Settling velocity =2.61 mm/s.

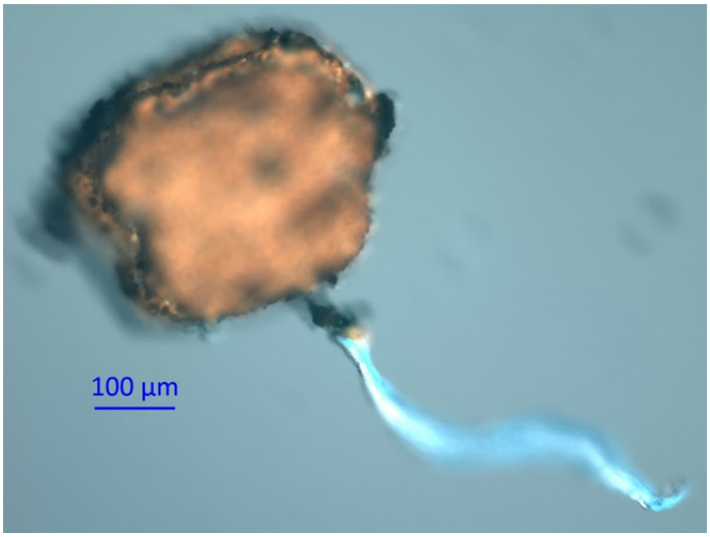

Figure 61: OPA ID 3S-1. A filamentous strand of presumably biological origin is embedded in this OPA. Settling velocity = 2.64 mm/s.

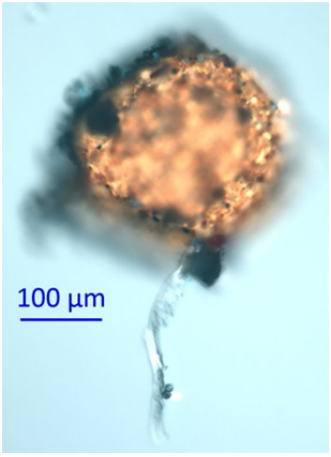

Figure 62: OPA ID 3S-2. Another filamentous strand embedded in the OPA. Settling velocity = 1.21 mm/s.

Brief Analysis of the Data

The limited results indicate general values for the settling velocity relevant to solid-type OPA and the aggregates dominated by the oil component tend to lie in the range between 1.0 and 3.0 mm/s for the full spectrum of sizes evaluated (order 100 µm to 1000 µm). Droplet-type OPA attached to large organic or mineral particulate matter can be expected to have somewhat higher settling velocities.

In order to provide a more robust quantitative analysis, either a physics-based approach or a statistical approach would be required. A physics-based approach would involve identifying percentages of oil, mineral sediment, and void space in the aggregates to quantify the submerged specific gravity; it would also involve ascertaining the drag coefficients associated with various shapes and sizes of OPA. In the statistical approach, a large quantity of particles would be analyzed having a range of physical properties to identify a range of settling velocities. A common practice is to plot aggregate size versus the settling velocity. The size is a relevant variable, but not necessarily the dominant variable that dictates settling velocity in OPA. Uncertainty exists in regards to defining a characteristic dimension to the aggregates; the photomicrographs only reveal a 2-dimensional view of the three-dimensional objects. Some of the OPA are clearly spherical or ellipsoidal and the third dimension can be reasonably inferred. But observations during settling suggest the more irregular-shaped solid-type OPA have a tendency to be thin and planar rather than having thickness with dimensions similar to photographed plane. Regarding variation in specific gravity, observations during the orbital shaker experiments reveal some large aggregates that are positively buoyant, neutrally buoyant, and negatively buoyant, which depends on the volume of the oil component and the amount of sediment attached or incorporated within the OPA. Therefore submerged specific gravities approaching 0 can certainly be expected in the environment; and consequently settling velocities approaching 0 could also be expected. A more robust statistical approach would be expected to yield a wider range of settling velocities owing primarily to the wide range of specific gravities that could be achieved with OPA.

3.4 Annular Flume Experiments

A primary objective of the laboratory tests was to quantify the hydraulic conditions that dictate the resuspension of OPA deposits on the river bed. While the bench scale facilities described in Section 3.3 can be used to achieve turbulence at the appropriate scale to represent open channel flow water column turbulence, it is not possible at bench scale to achieve the turbulence associated with a developed wall-bounded shear flow that represents conditions at the river bed responsible for entrainment of bed material. To achieve the wall-bounded shear flow at an appropriate scale, it was necessary to transition from bench-scale facilities to a larger scale flume. The ultimate objectives of the larger scale experiments are to determine the critical shear stress to achieve resuspension of OPA deposits and to determine entrainment rates.

The annular flume at the VTCHL was chosen for the resuspension experiments as it generates a developed boundary layer without the use of pumps that can disrupt the condition of entrained material. (Note that a pump in a recirculating linear flume would also have the potential to become fouled with oily material.) Dimensions and operating limits of the flume are reported in Table 8; the annular flume is illustrated in Figure 63.

Channel centerline radius	0.65 m
Maximum channel depth	0.4 m
Channel Width	0.2 m
Max. channel rpm	$\pm$10 rpm
Max. lid rpm	$\pm$16 rpm

Table 8: VTCHL Annular flume and operating limits

Figure 63: A view of the annular flume used for the current study.

The detailed specifications on the annular flume can be found in Pedocchi (2005). In brief, the annulus is filled with water and the lid is vertically adjusted such that the underside of the lid is in full contact with the water. Rotation of the lid is achieved by an electric motor; driving the flow by rotating the lid alone tends to create undesired secondary currents in the channel. To counteract this effect, the channel itself is rotated in the opposite direction as the lid via a separate motor. The channel and lid of the flume thus rotate independently and in opposite directions. Modifications to the system as described in Pedocchi (2005) included the addition of roughness elements to the underside of the lid to increase the roughness and enhance the turbulence generated by the lid. Those modifications remain in place. Using that setup, Pedocchi (2005) developed an operation curve for running at 20 cm flow depth that stipulated rotation of the lid and channel unit at the same magnitude, but in opposite directions; this minimized the transverse velocity components near the bed, an ideal condition for erosion experiments. The relation Pedocchi (2005) developed for bed shear stress as a function of lid and channel speed was as follows:

$$\tau_b = \rho f_b (U_L - U_C)^2 \quad (2)$$

Where τ_b is the bed shear stress; ρ is the fluid density; f_b is a dimensionless constant of proportionality representing a friction factor, U_L is the lid speed and U_C is the channel speed; note that U_L and U_C have opposite signs. The value of f_b determined through velocity measurements and log-law profile fits was f_b = 1.4 x 10^{-4}.

For the current experiments, the desired objective was to quantify OPA initiation of motion on a sediment bed and qualitatively assess the nature of transport. The smooth bottom of the channel was determined to be a poor surrogate for a natural bed, and so adhesive-backed sandpaper was applied to the flume channel bottom to allow the OPA to be in contact with granular material. Yellow-colored sandpaper was obtained to allow contrast with the black OPA; the sandpaper consisted of white sand (approximately 400 to 500 µm nearly uniform size as estimated using a hand lens and ruler graduated in mm) embedded in a plasticized yellow paint. The paint yielded a somewhat smoother surface than a uniform layer of sand spread on a solid surface; i.e., the maximum depth from the top of sand grains to the solid surface (top of the paint) was reduced relative to the former case. Underwater video was desired to observe conditions inside the flume more accurately than can be achieved by imaging through the curved acrylic window on the flume sidewall. A GoPro Hero 3+ Black Edition was used for

the video. In order to minimize the hydraulic influence of the camera setup on near-bed conditions, the camera was desired to be placed as high above the bed as possible and located downstream of the particles (thus pointing obliquely upstream). The decision was made to increase the flow depth from 20 cm to 30 cm in order to allow higher placement of the camera. The camera setup is illustrated in Figure 64.

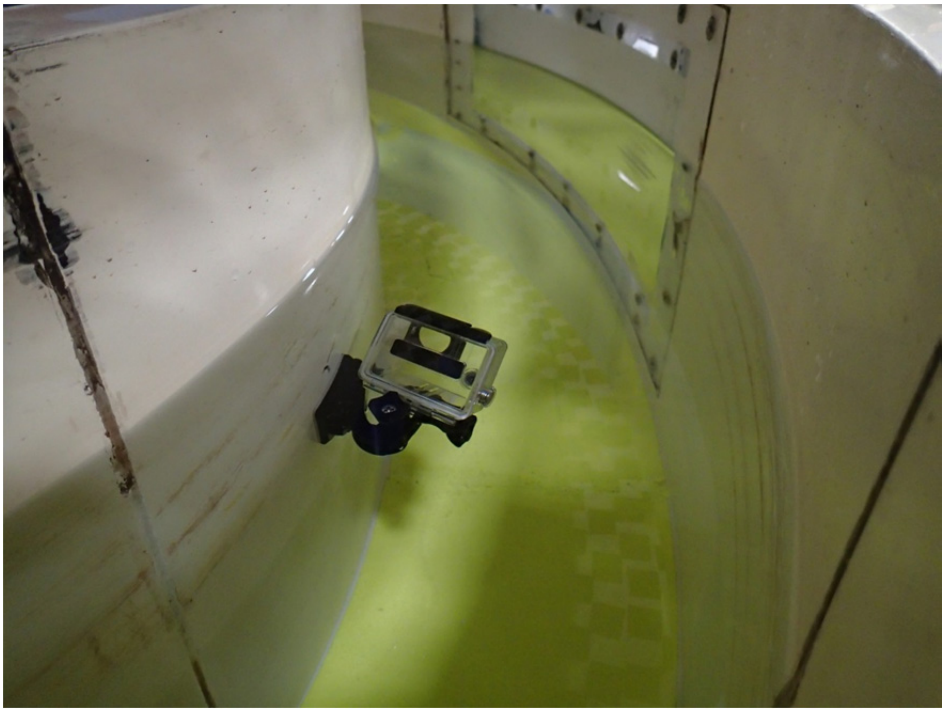

Figure 64: A view of the camera setup inside the flume; note that the camera is not inside the plastic case in this photo. The lid is raised and not engaged with the water surface to allow this photograph to be taken.

The lowest portion of the camera setup is the mount, whose bottom is 18.0 cm above the bed; the top corner of the camera case is the highest portion, which is 25.4 cm above the bed. The maximum protrusion into the flow in the radial direction is at the top right corner of the camera case at 8.3 cm from the inside wall.

The camera is pointed obliquely upstream and downward at an approximately 45-degree angle from a horizontal plane. The setup was located near the flume window, where a diffused lighting system consisting of a dense array of LED lights was mounted outside the window, with a sheet of bond paper covering the window to diffuse the light. The lighting system was attached to the flume such that it rotated with the channel.

Because of the modified hydraulics associated with the roughened bed and the greater flow depth, a new flume calibration was required to develop an operating curve for the experiments. To develop that curve, an arrangement of small irregular plastic sediment particles (diameters of order 1 mm) was placed over the central region of the bed. The goal was to obtain bedload transport that followed the centerline rather than being oriented with a strong transverse component toward either the inside wall (when the speed of the lid was too high relative to the channel) or toward the outside wall (when the rotation speed of the lid was too slow relative to the speed of the channel). This is the basic approach used by Partheniades and Mehta (1971) to develop the annular flume operating curves for experiments where uniform bed deposition was desired. The equal but opposite lid and channel rotation speed used by Pedocchi (2005) was not adequate under the new hydraulic condition; the lid rotation speed needed to increase relative to the bottom speed to maintain bedload transport in the central region of the bed. Furthermore, it was found that the ratio between lid speed and channel speed was not constant across a range of flows. The operational relation determined through the above experimental technique specified the following relation between the lid speed and the channel speed:

$$\frac{U_L}{U_C} = 2.4 - 0.06(U_L - U_C) \tag{3}$$

This equation can be readily solved to determine U_L and U_C for any desired value of ($U_L - U_C$). This equation was formulated from the experiments on plastic particles performed in the range of ($U_L - U_C$) between 5 RPM and 10 RPM. In the future, extrapolation of the relation much beyond that range should be verified.

Following development of the operational curve, the flume was calibrated to determine a relationship between the bed shear stress (τ_b) and ($U_L - U_C$). Five velocity profiles were measured that spanned the range of flows desired for running the OPA experiments. A Nortek Vectrino acoustic Doppler velocimeter (ADV) in the down-looking configuration was used for the measurements. The probe was mounted on a Lory point gage to allow accurate specification of the vertical position. As has been noted in previous studies (see Pedocchi (2005)), velocity profiles in annular flumes generally do not increase monotonically in the vertical direction as would be expected in an open channel flow. For the conditions used in this study, the mean velocity at a z-position increased from the bed up to an elevation only 6 to 8 cm above the bed before the mean velocity began decreasing. Seven points in the vertical profile were obtained in the elevation range between 1 cm and 6.15 cm at a log-spacing interval with factor 1.35. Good fits to the log-law were obtained in this region for each of the measured profiles, which allowed

calculation of the shear velocity (u^*) and subsequently the bed shear stress (τ_b). The results of the five profiles and the best fit to the form of Eq. (2) are provided in Figure 65.

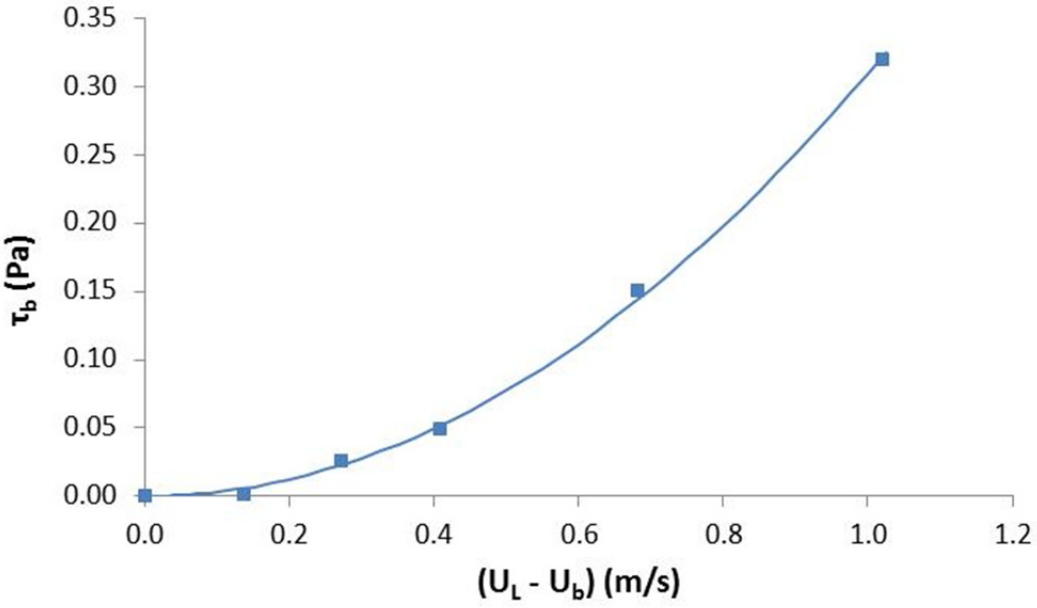

Figure 65: The results of flume calibration by measuring velocity profiles to allow calculation of the bed shear stress.

The relationship of Eq. (2) was found to yield a good fit, with f_b = 3.1 x 10^{-4}, which is somewhat higher than that found by Pedocchi (2005).

Oil-particle-aggregates were allowed to settle in the central region of the flume bottom in the portion of the flume near the window. The solid-type OPA used in the experiments were formed per the procedure described in Section 3.2.3.4. The only difference to the procedure was that instead of shaking at 200 RPM during the mixing phase, the heavily-weathered oil (17.4% mass loss) was entrained at 200 RPM and then the shaker speed was reduced to 160 RPM for the remainder of the mixing phase; the time in the mixing phase for each entrainment event was reduced to 2.0 minutes. This modified procedure was found to yield discernibly larger OPA; the large OPA were also observed to be more planar than OPA formed using 200 RPM for the mixing phase. The sample used in the annular flume experiment is illustrated in Figure 66.

Figure 66: A view of the solid-type OPA used in the annular flume experiment. The sample is in a 60-mm diameter Petri dish. The maximum dimension of the largest OPA shown is approximately 2.5 mm.

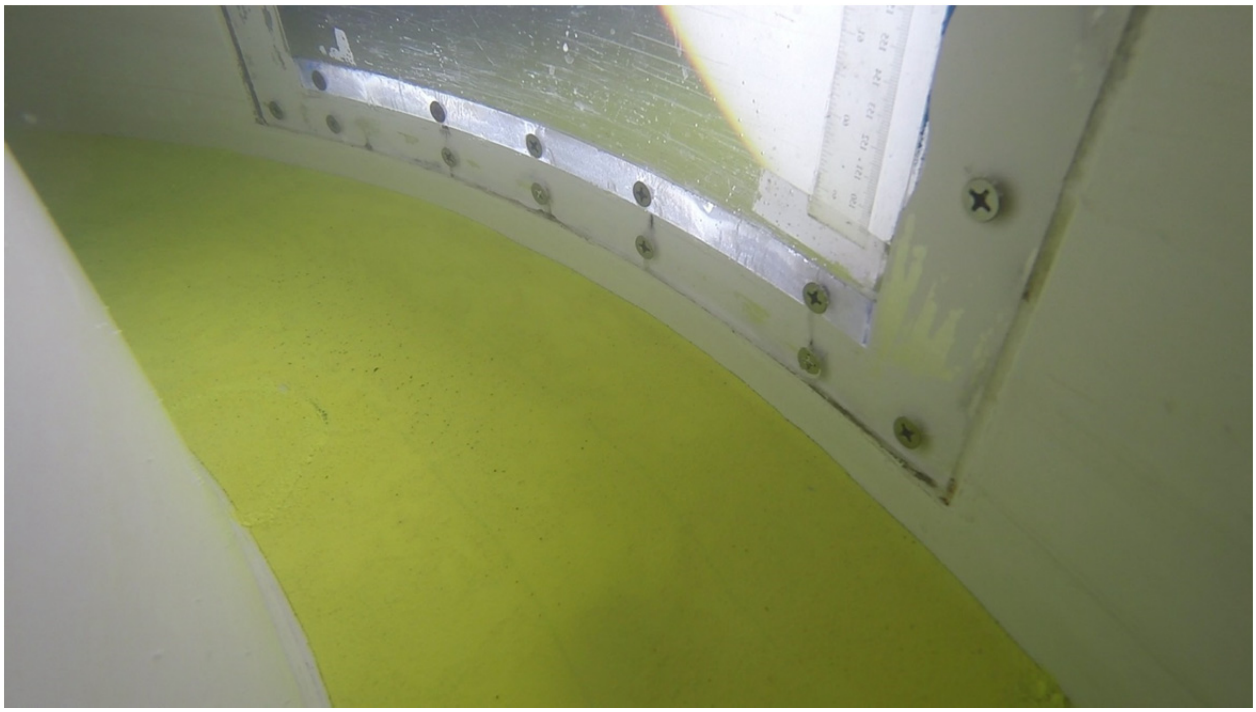

Figure 67: A frame captured from the video prior to the start of the experiment.

The experiment using OPA was begun at very low velocity conditions, with (U_L – U_C) equal to 2 RPM, which is equivalent to 0.136 m/s. Per the developed relation illustrated in Figure 65, this yields a very small shear stress equal to 0.0057 Pa. While most of the OPA particles were not mobilized, several of the smaller OPA were mobile as bedload, rolling or sliding along the bed. The (U_L – U_C) values were increased at 0.5 RPM increments and the velocity was maintained for 3 minutes at each increment. In general, several additional OPA were mobilized at each interval, gradually winnowing the deposit. The last OPA to be mobilized was one of the larger pieces from the sample; it began to roll on the bed as bedload at (U_L – U_C) equal to 10 RPM (or 0.68 m/s); this yields a bed shear stress equal to 0.14 Pa. At 6 RPM, fairly regular OPA were observed passing through the camera field of view in suspension; some transport continued to pass through the field of view as bedload through the maximum (U_L – U_C) value of 12 RPM (or 0.82 m/s), but a greater abundance of OPA were being transported in suspension.

The annular flume experiments suggest that in a heterogeneous deposit of solid-type OPA, the critical shear stress is highly variable, associated with an expected variety of specific gravity and size. Thus it is not practicable to assign a single value as the critical bed shear stress for solid-type OPA. While cohesive forces likely play a role in the force balance that determines the initiation of motion, the very low shear stresses that initiates motion in some of the particles suggest that the cohesive forces are weak (at least in this laboratory environment) and the predominant resistive force is the friction due to the particle mass, such that a Shields-type relation (e.g., Garcia, 2008) may be most appropriate to predict initiation of motion. The most important parameters in such a relation are the submerged specific gravity and the size, both of which are expected to be highly variable. Note that as the specific gravity approaches zero, a situation likely common for some portion of the solid-type OPA deposited on the bed, initiation of motion is predicted for any non-zero value of the bed shear stress, as the Shields parameter approaches infinity. The data set is limited and submerged specific gravity is not known for each individual OPA in the experiment; however, if additional data supports these findings, the most important parameterization in transport models pertaining to this type of OPA is probability distributions of the size and specific gravity of OPA deposits. However, adherence of the OPA to bed sediments through physicochemical processes that occur at the bed and potential reworking of the OPA into the bed sediments are not resolved in this experimental procedure.

Several additional notes regarding the analysis are warranted. OPA that are mobilized at bed shear stress values less than 0.0057 Pa on a flat bed most likely do not become stable under any flow condition until individual OPA become situated in sheltered positions amongst larger roughness

elements. In such a configuration, the OPA may be stable at considerably larger values of bed shear stress; therefore continuous bedload transport of small OPA under non-zero bed shear stress should not be presumed based on the results of the annular flume test. It is also important to note that an abundance of the OPAs deposited on the bed are expected to be in the standard droplet-type configuration rather than the solid-type configuration evaluated herein. The physics that dominate resuspension of that type of OPA are likely not clearly distinguishable from that of typical cohesive sediment deposits, where consolidation and a large number of site-specific factors (water chemistry, biological activity, etc.) play the most important role.

Chapter 4: SUMMARY

Laboratory tests were conducted on Cold Lake Blend diluted bitumen (dilbit) obtained in July 2013. The choice of dilbit type and the timing of the sample procurement were based on the Cold Lake Blend being reasonably similar in physical properties to the Enbridge Line 6B oil that spilled into the Kalamazoo River in July 2010. The primary objectives of the laboratory tests as outlined in the original work plan were to quantify important parameters regarding the resuspension, transport, and deposition of oil-particle aggregates (OPA) deposited on the Kalamazoo River bed. The primary objectives were to be achieved using an annular flume and settling column. However, because so little is known about the configuration of submerged oil among mineral sediment and organic matter comprising the bed, a secondary objective was formulated to ascertain the characteristics of OPA that deposited on the bed. The secondary objectives were achieved using bench-scale facilities for mixing and UV epifluorescence microscopy to analyze experimental deposits.

The Cold Lake Blend was weathered by bubbling pressurized air through the fluid. Characteristic states of weathering used in the bench scale mixing tests included unweathered (0% mass loss), intermediately weathered (9.9% mass loss) and heavily weathered (17.4% mass loss) dilbit; the maximum mass loss achieved was 17.4%. The density and dynamic viscosity values measured were similar to previously reported values in Belore (2010) and Environment Canada (2013); the most noticeable difference between the current study and the earlier studies was somewhat higher densities and viscosities under the more heavily weathered states, particularly that involving 17.4% mass loss. Across the full range of temperatures and weathered states tested, the density of the Cold Lake Blend used in the current study fell within a range between 0.922 g/cm3 and 0.993 g/cm3; and the dynamic viscosity varied across five orders of magnitude, between 5.2 x 10^1 and 2.5 x 10^5 mPa·s. Under the densest oil condition achieved (heavily weathered), although the oil density is close to that of fresh water, it maintains positive buoyancy under the temperatures used for the laboratory tests pertaining to OPA formation and behavior.

The bench scale mixing tests were performed at room temperature where the air, water, and oil temperatures were between 21°C and 22°C. Formation of OPA was achieved using Kalamazoo River sediment obtained from a depositional environment upstream of the spill-affected reach. The grain size distribution had a D_{16} of 7.6 µm, a D_{50} of 29 µm, and a D_{84} of 84 µm (where D_{XX} indicates the grain diameter such that XX percent of the cumulative distribution is finer-grained). The specific conductance

of the freshwater medium was 640 µS/cm, which is within the range of conductance observed in the Kalamazoo River.

Mixing was achieved using an orbital shaker with baffled flasks where the turbulent kinetic energy dissipation rates (ε) had characteristic values on the order of 10^{-1} to 10^{-3} m^2/s^3 based on previously reported values (Kaku et al., 2006a,b) from measurements using identical equipment. Knowledge of ε is important, as this variable is most commonly used to characterize the fluid turbulence responsible for the breakup of the oil. It thus provides a means to scale the bench-scale laboratory results up to the prototype scale of the river environment. Dilbit was added to the surface of a dilute mixture of suspended sediment and freshwater within the baffled flasks and mixed for specified time periods. Although a large number of variables are important in the mixing process, the experimentally controlled variables included in the current study were limited to the weathered state of the oil and the mixing energy (which is correlated to the speed of the orbital shaker). Deposits of sediment were removed for analysis using ultraviolet (UV) epifluorescent microscopy.

The predominant form of OPA observed in the experimental deposits was the droplet-type per Stoffyn-Egli and Lee (2002); the fundamental unit of the droplet-type OPA consists of a spherical oil globule with grains of particulate matter attached to the surface. Aggregates containing one to four oil droplets (globules) were the most common in the deposits. When loose sediment deposits were consolidated into smaller containers, larger more complex OPA were commonly observed. Although large droplets well in excess of 1 mm diameter were prevalent during mixing, such large droplets did not achieve sufficient sediment attachment during mixing under any of the experimental conditions to appear in the experimental deposits. The most common globule sizes observed in the deposits had diameters between 5 µm and 100 µm; when evaluated on the basis of volume of oil in the deposit, the larger-sized droplets greater than 60 µm dominated the distributions. Very few spherical droplets were identified in the OPA having diameter greater than 200 µm; the largest spherical droplet observed using constant mixing rates was 336 µm.

Abundant solid-type OPA (Stoffyn-Egli and Lee, 2002) were generated when implementing unconventional mixing techniques that involved varying the mixing rates to achieve repeated sequences of oil entrainment, resurfacing, and re-coalescence. The solid-type OPA have been found by Stoffyn-Egli and Lee (2002) to incorporate sediment inside the body of the oil mass. The solid-type OPA were observed to consist of irregularly shaped oil masses that are considerably larger than the spherical droplets observed in the droplet-type OPA; solid-type OPA commonly had a maximum length dimension

exceeding 1 mm. Although droplet-type OPA were abundant in the deposits formed using the unconventional mixing techniques, the volume of oil in the deposits formed using the unconventional mixing technique was dominated by the few large irregular-shaped solid-type OPA.

Settling velocity tests were performed on a number of OPA that had been photomicrographed using the UV epifluorescence microscope. The OPA consisted of both solid-type and droplet-type OPA, predominantly in the size range of 100 µm to 1000 µm. The OPA had settling velocities between 1.0 and 11.2 mm/s, with the majority being in the range between 1.0 and 3.0 mm/s. The settling velocities reported are based on a fairly limited data set, and the findings must be qualified based on the understanding of the processes of OPA formation. For those OPA that become negatively buoyant and deposit on the bed, during its previous history of mixing in the water column, an oil globule must transition from being positively buoyant to being negatively buoyant as more suspended particulate matter becomes attached. A range of submerged specific gravities, and thus settling velocities, would be expected even for OPA in a fairly narrow size range. Thus the settling velocity of OPA as a function of size must be understood as a statistical property in the absence of deterministic evaluation of the amount and type of sediment attached.

Annular flume tests were conducted on a sample of the solid-type OPA. When deposited on a uniform fixed granular bed, the critical shear stress to initiate motion was found to vary from a value less than 0.0057 Pa up to 0.14 Pa. Mobilized material was transported both as bedload and in full suspension. Heterogeneity in the size and submerged specific gravity of OPA formed under controlled experimental conditions suggest that critical shear stress can be expected to vary over several orders of magnitude. OPA that are mobilized at bed shear stress values less than 0.0057 Pa on a flat bed most likely do not become stable under any flow condition until individual OPA become situated in sheltered positions amongst larger roughness elements. In such a configuration, the OPA may be stable at considerably larger values of bed shear stress; therefore continuous bedload transport of small OPA under non-zero bed shear stress should not be presumed based on the results of the annular flume test. It is also important to note that an abundance of the OPA deposited on the bed are expected to be in the standard droplet-type configuration rather than the solid-type configuration evaluated herein. The physics that dominate resuspension of that type of OPA are likely not clearly distinguishable from that of typical cohesive sediment deposits, where consolidation and a large number of site-specific factors (water chemistry, biological activity, etc.) play the most important role.

ACKNOWLEDGMENTS

The staff at the University of Illinois VenTe Chow Hydrosystems Laboratory (VTCHL) would like to thank Jacob Hassan of the USEPA for project funding and support. Faith Fitzpatrick of the USGS Wisconsin Water Science Center is acknowledged for coordinating the many elements required of this project and making resources available to us. Michel Boufadel of the New Jersey Institute of Technology and Ken Lee of CSIRO are acknowledged for providing much guidance regarding the technical details of conducting the laboratory experiments along with general information pertaining to the physics of oil breakup and interaction with suspended particulates. Rex Johnson of GRT/START is acknowledged for assistance with data, providing sediment from the river, and providing useful discussions pertaining to site-specific knowledge of the Kalamazoo River and the observed character and behavior of oiled sediment.

The following staff and students of the Ven Te Chow Hydrosystems Laboratory provided substantial assistance during various phases of this project. Ian O'Leary was instrumental in the design and fabrication of the setup used for photographic analysis of oil globules used on the orbital shaker; he also conducted many of the trials required to get the system set up to its end condition; and he was responsible for developing the code used for image processing. Jorge San Juan Blanco assisted with the image analysis of OPA deposits. Nicholas Moller built the temperature sensor system used to measure oil temperatures and conducted the velocity measurements in the annular flume necessary for the calibration. Andrew Waratuke, lab manager of VTCHL, assisted with various logistical components of the lab work. Karissa Duarte provided assistance during setup of the annular flume experiments.

Shiv Sivaguru and Xudong Guan of the UIUC Institute for Genomic Biology are acknowledged for much assistance in using the UV epifluorescence microscopy equipment. Prof. William Buttlar of the UIUC Civil Engineering Department is acknowledged for allowing use of the asphalt lab and the equipment therein. The Illinois State Geological Survey is acknowledged for allowing use of their laboratory facilities and equipment for the density tests.

REFERENCES

Belore, R. (2010). Properties and fate of hydrocarbons associated with hypothetical spills at the marine terminal and in the confined channel assessment area. *Technical Data Report.* SL Ross, Calgary, Alberta.

Delvigne, G.A., van der Stel, J.A., Sweeney, C.E. (1987). Measurement of vertical turbulent dispersion and diffusion of oil droplets andoiled particles. *Final report: OCS Study MMS 87-111.* U.S. Department of the Interior, Minerals Management Service, Anchorage, Alaska. 501 p.

Dollhopf, R.H., Fitzpatrick, F.A., Kimble, J.W., Capone, D.M., Graan, T.P., Zelt, R.B., Johnson, R. (2014). Response to heavy, non-floating oil spilled in a Great Lakes river environment: a multiple-lines-of-evidence approach for submerged oil assessment and recovery: *Proceedings, 2014 International Oil Spill Conference*, Savannah, GA, May 7-9, 2014, p. 434-448. http://ioscproceedings.org/doi/pdf/10.7901/2169-3358-2014.1.434.

Environment Canada (2013).*Federal Government Technical Report: Properties, composition and marine spill behaviour, fate and transport of two diluted bitumen products from the Canadian oil sands*. pp. 1–85, ISBN 978-1-100-23004-7 Cat. No.: En84-96/2013E-PDF.

García, M.H. (2008). Sediment transport and morphodynamics, in M.H. García, ed., *ASCE manual of practice 110—Sedimentation engineering: Processes, measurements, modeling, and practice*, ASCE, Reston,VA, 21–163.

Kaku, V. J., Boufadel, M. C., and Venosa, A. D. (2006a).Evaluation of mixing energy in laboratory flasks used for dispersant effectiveness testing.*Journal of Environmental Engineering*, 132(1), 93-101.

Kaku, V. J., Boufadel, M. C., Venosa, A. D., and Weaver, J. (2006b). Flow dynamics in eccentrically rotating flasks used for dispersant effectiveness testing. *Environmental Fluid Mechanics*, 6(4), 385-406.

Khelifa, A., M. Fingas, and C. Brown, (2008). Effects of dispersants on Oil-SPM aggregation and fate in US coastal Waters, *NOAA/UNH Coastal Response Research Center, Final Report Grant Number: NA04NOS4190063*, 57 pages.

King, T. L., Robinson, B., Boufadel, M., & Lee, K. (2014). Flume tank studies to elucidate the fate and behavior of diluted bitumen spilled at sea,*Marine Pollution Bulletin*, 83, 32-37.

Lee, K. (2002). Oil–particle interactions in aquatic environments: influence on the transport, fate, effect and remediation of oil spills. *Spill Science & Technology Bulletin*, 8(1), 3-8.

Lee, K., Wong, C.S., Cretney, W.J., Whitney, F.A., Parsons, T.R., Lalli, C.M., Wu, J., 1985. Microbial response to crude oil and Corexit 9527: SEAFLUXES enclosure study. *Microbial Ecology*, 11, 337–351.

Lee, K., Stoffyn-Egli, P., and Owens, E.H. (2001). Natural dispersion of oil in a freshwater ecosystem: Desaguadero pipeline spill, Bolivia, in *Proceedings of the 2001 International Oil Spill Conference*, American Petroleum Institute, Washington DC, Publication no. I4710B, 1445-1448.

Lee, K., Bugden, J., Cobanli, S., King, T., McIntyre, C., Robinson, B., Ryan, S., and Wohlgeschaffen, G. (2012).*UV-Epifluorescence Microscopy Analysis of Sediments Recovered from the Kalamazoo River*,

Centre for Offshore Oil, Gas and Energy Research (COOGER) Technical Report dated October 24, 2012.

Ma, X., Cogswell, A., Li, Z., & Lee, K. (2008). Particle size analysis of dispersed oil and oil-mineral aggregates with an automated ultraviolet epi-fluorescence microscopy system. *Environmental Technology*, 29(7), 739-748.

Partheniades, E. and Mehta, A. (1971). Deposition of fine sediments in turbulent flows. *Water Pollution Control Research Series 16050 ERS 08/71*, Technical Report, U.S. Environmental Protection Agency, Washington D.C.

Pedocchi, F. (2005).*Evaluation of a laser difraction instrument and an annular flume for cohesive sediment studies*.M.Sc. Thesis, University of Illinois at Urbana-Champaign, Urbana, IL.

Stoffyn-Egli, P. and K. Lee, 2002, Formation and characterization of oil–mineral aggregates, *Spill Science & Technology Bulletin*, 8(1), 31-44.

APPENDIX A

Histograms of Oil Globule Distributions in Experimental Deposits

Bin #	Lower Bound (µm)	Upper Bound (µm)
1	1.25	1.48
2	1.48	1.74
3	1.74	2.06
4	2.06	2.43
5	2.43	2.87
6	2.87	3.38
7	3.38	3.99
8	3.99	4.71
9	4.71	5.55
10	5.55	6.55
11	6.55	7.73
12	7.73	9.13
13	9.13	10.77
14	10.77	12.71
15	12.71	14.99
16	14.99	17.69
17	17.69	20.88
18	20.88	24.64
19	24.64	29.07
20	29.07	34.30
21	34.30	40.48
22	40.48	47.77
23	47.77	56.36
24	56.36	66.51
25	66.51	78.48
26	78.48	92.61
27	92.61	109.28
28	109.28	128.95
29	128.95	152.16
30	152.16	179.55
31	179.55	211.86
32	211.86	250.00
33	250.00	295.02
34	295.02	348.14
35	348.14	410.83
36	410.83	484.81

Table A1: Bin size ranges used in the histograms

** Note: Table A1 is equivalent to Table 6 in the body of the report; provided here for reference

0% Mass Loss Oil; 160 RPM

- 206 globules in sample
- 2 irregular-shaped features

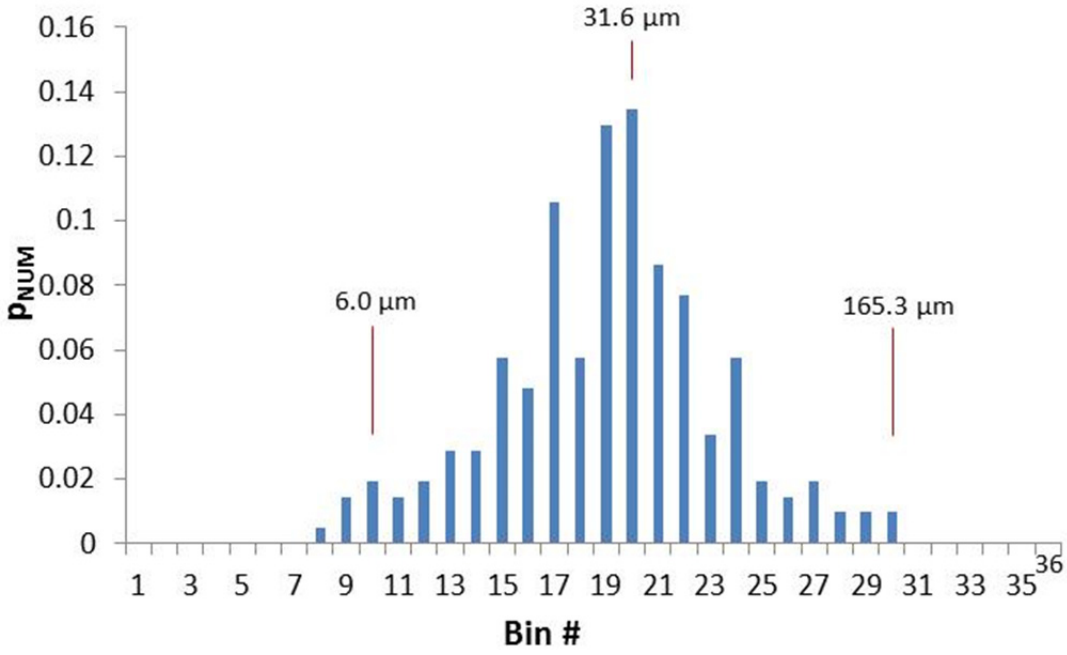

Figure A1: Histogram based on number of globules in each bin

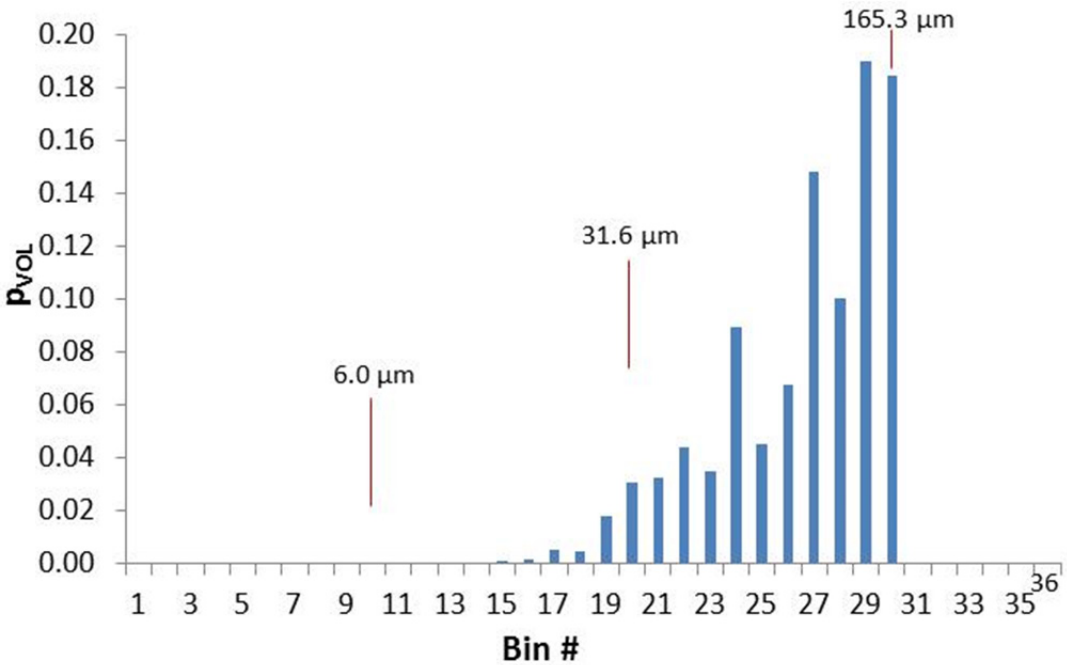

Figure A2: Histogram based on volume of globules in each bin

9.9% Mass Loss Oil; 160 RPM

- 262 globules in sample
- 0 irregular-shaped features

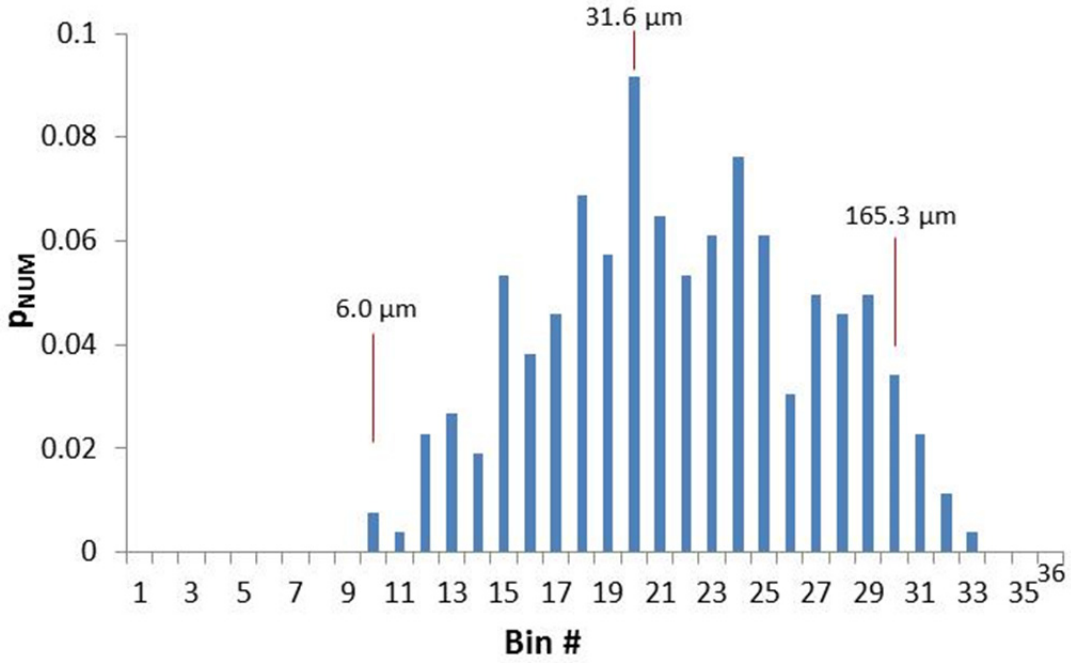

Figure A3: Histogram based on number of globules in each bin

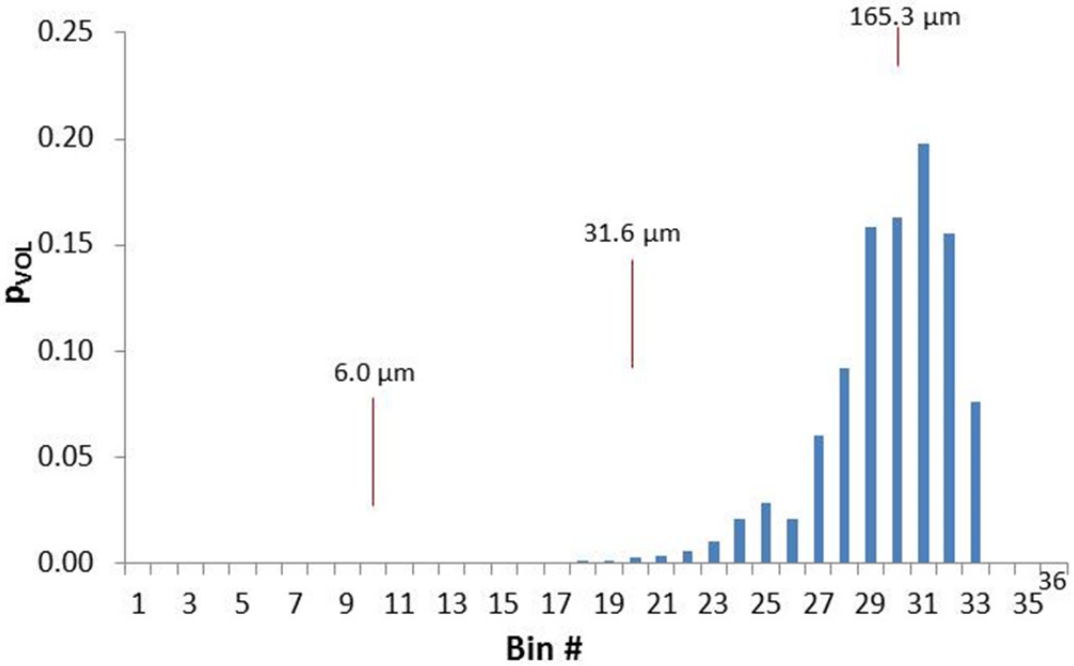

Figure A4: Histogram based on volume of globules in each bin

17.4% Mass Loss Oil; 160 RPM

- 116 globules in sample
- 44 irregular-shaped features

Note that the abundance of irregular-shaped features a byproduct of oil sticking on flask and only gradually breaking off into suspension

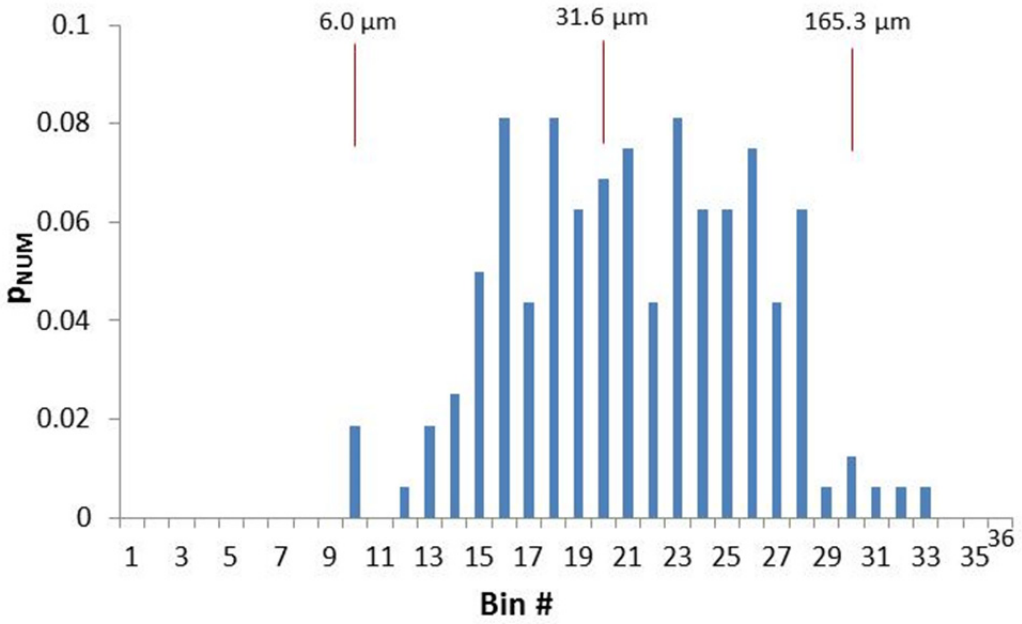

Figure A5: Histogram based on number of globules in each bin

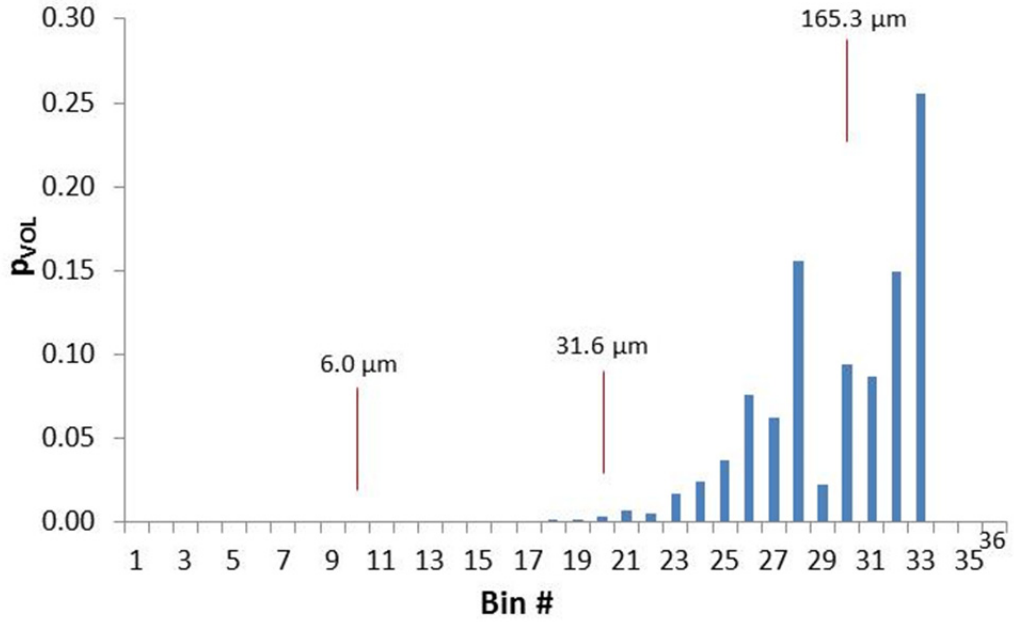

Figure A6: Histogram based on volume of globules in each bin

0% Mass Loss Oil; 180 RPM

- 525 globules in sample
- 0 irregular-shaped features

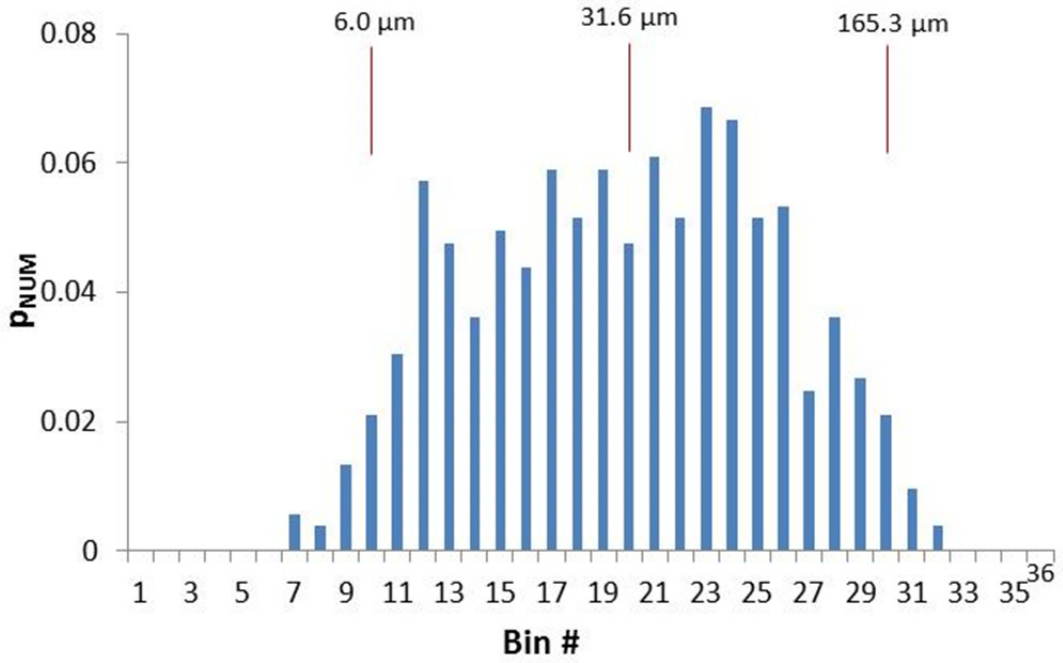

Figure A7: Histogram based on number of globules in each bin

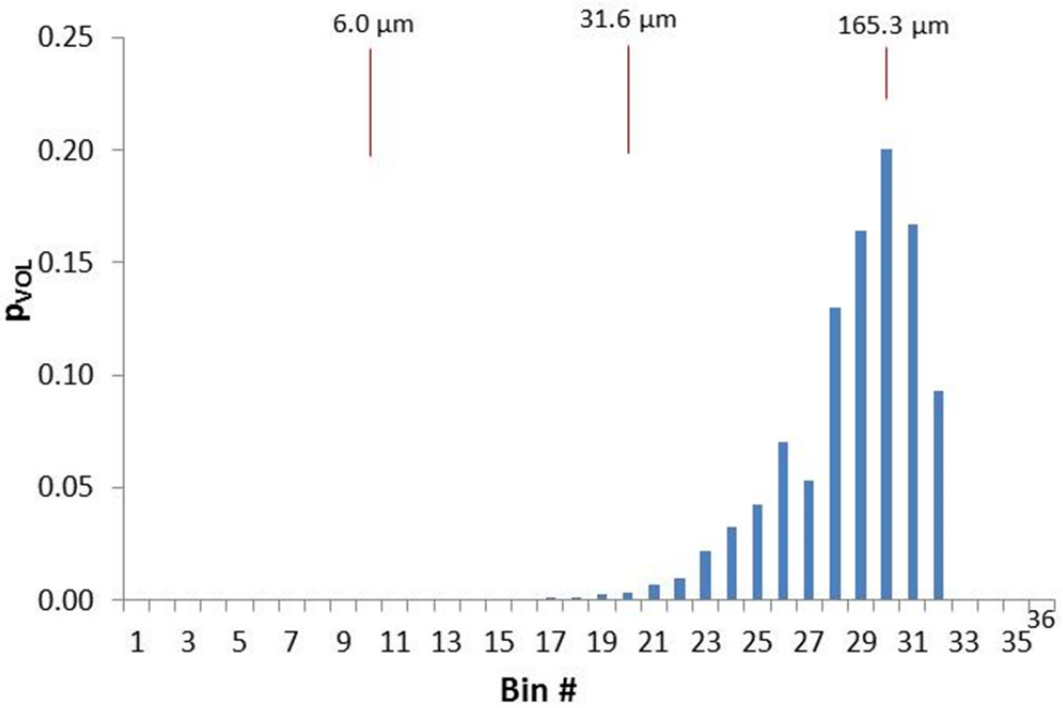

Figure A8: Histogram based on volume of globules in each bin

9.9% Mass Loss Oil; 180 RPM

- 507 globules in sample
- 0 irregular-shaped features

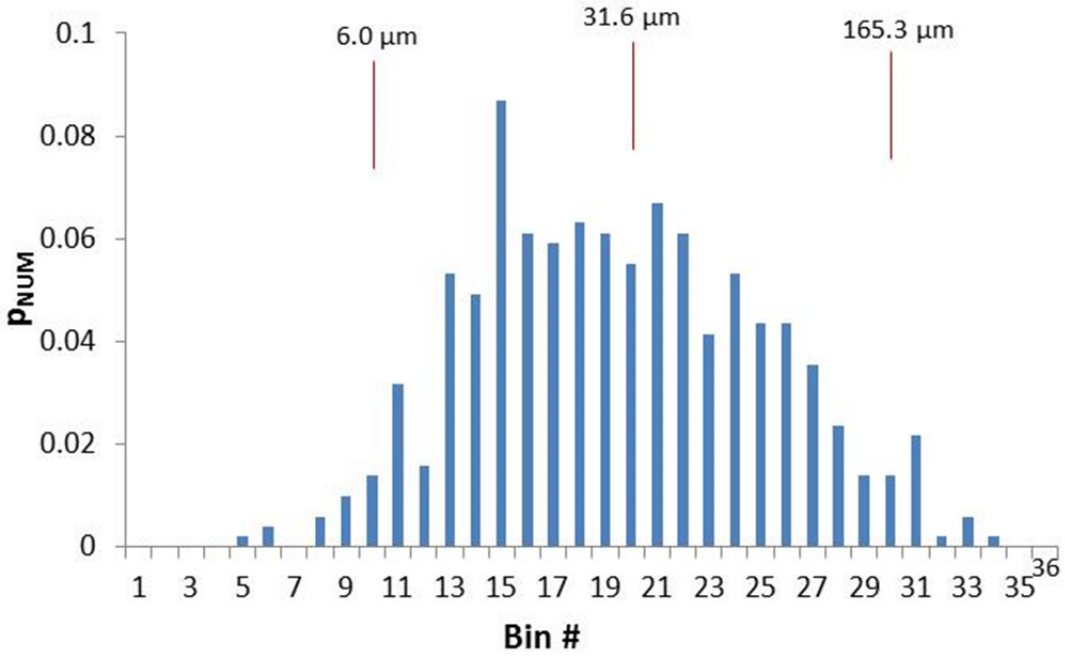

Figure A9: Histogram based on number of globules in each bin

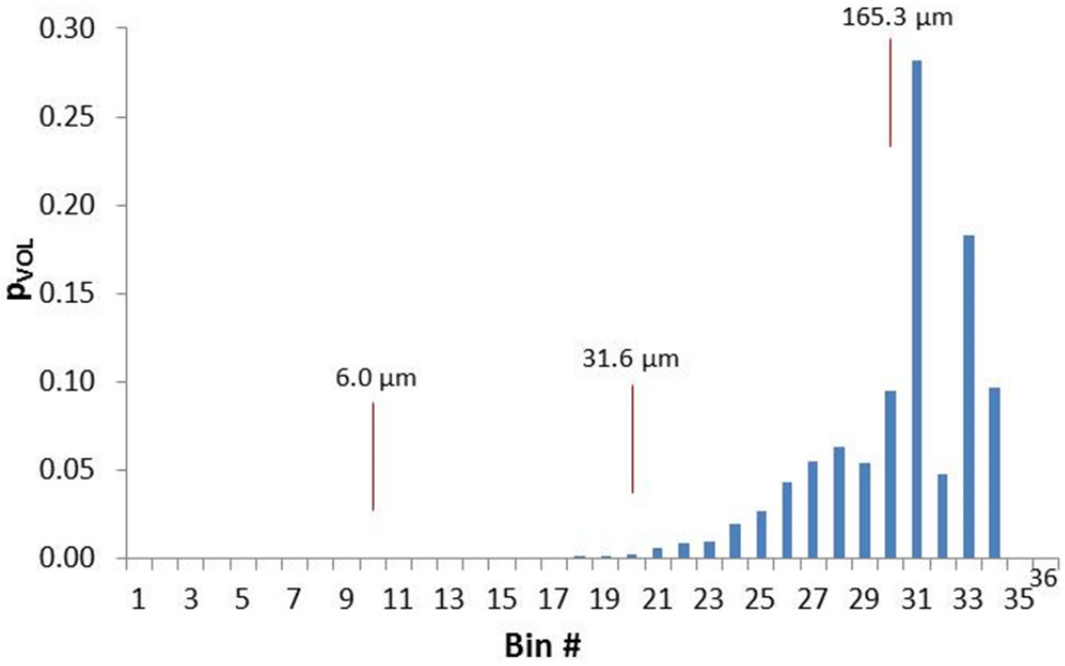

Figure A10: Histogram based on volume of globules in each bin

17.4% Mass Loss Oil; 180 RPM

- 296 globules in sample
- 2 irregular-shaped features

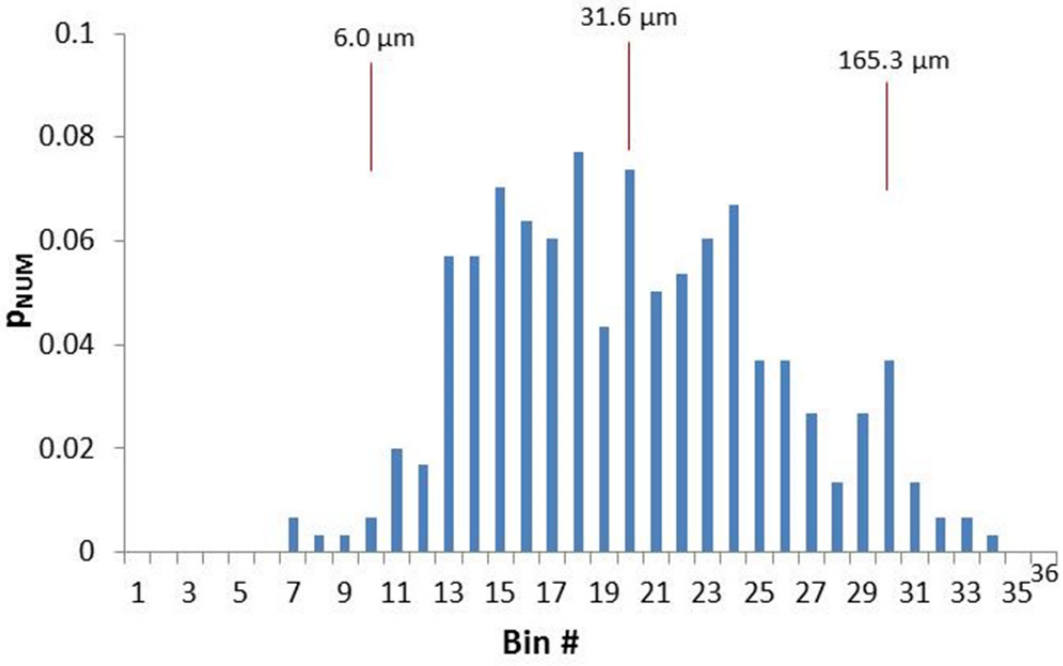

Figure A11: Histogram based on number of globules in each bin

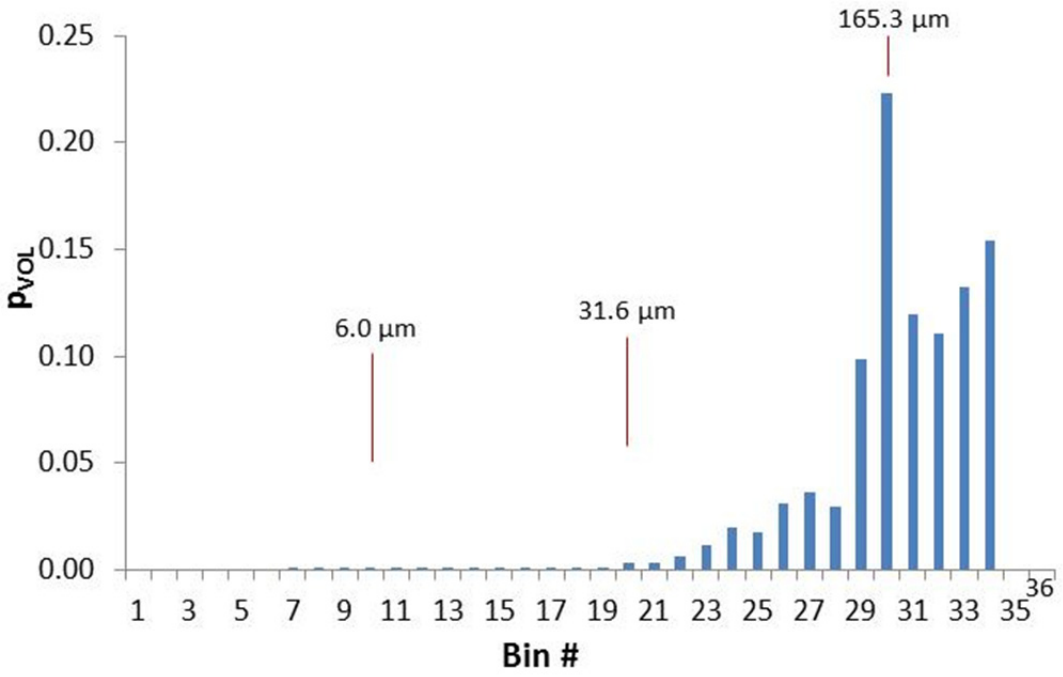

Figure A12: Histogram based on volume of globules in each bin

0% Mass Loss Oil; 200 RPM

- 403 globules in sample
- 0 irregular-shaped features

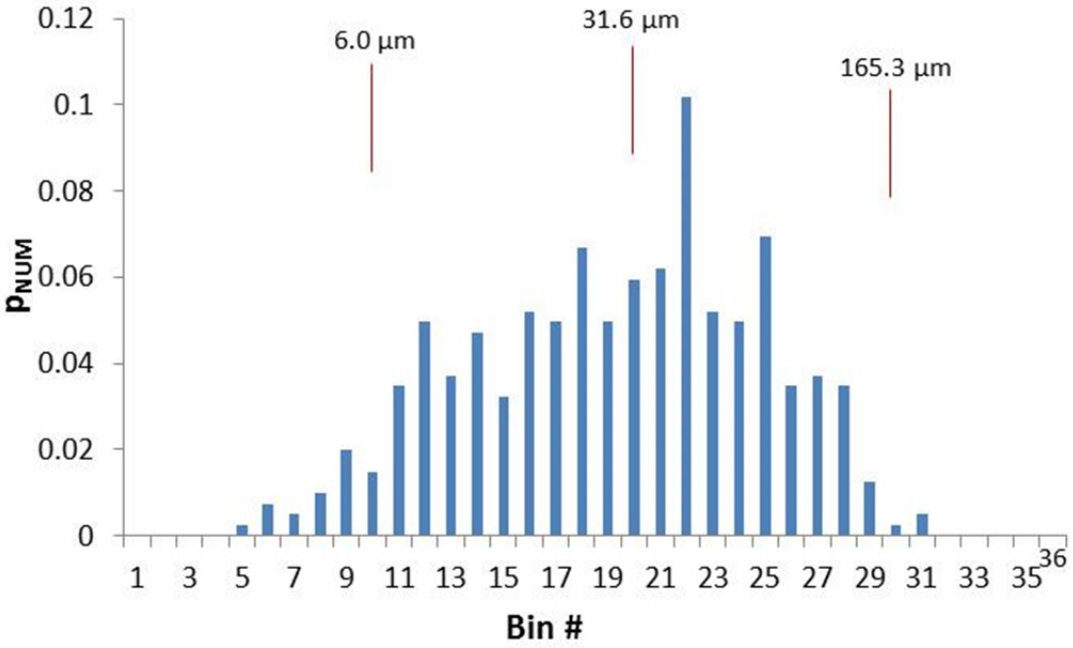

Figure A13: Histogram based on number of globules in each bin

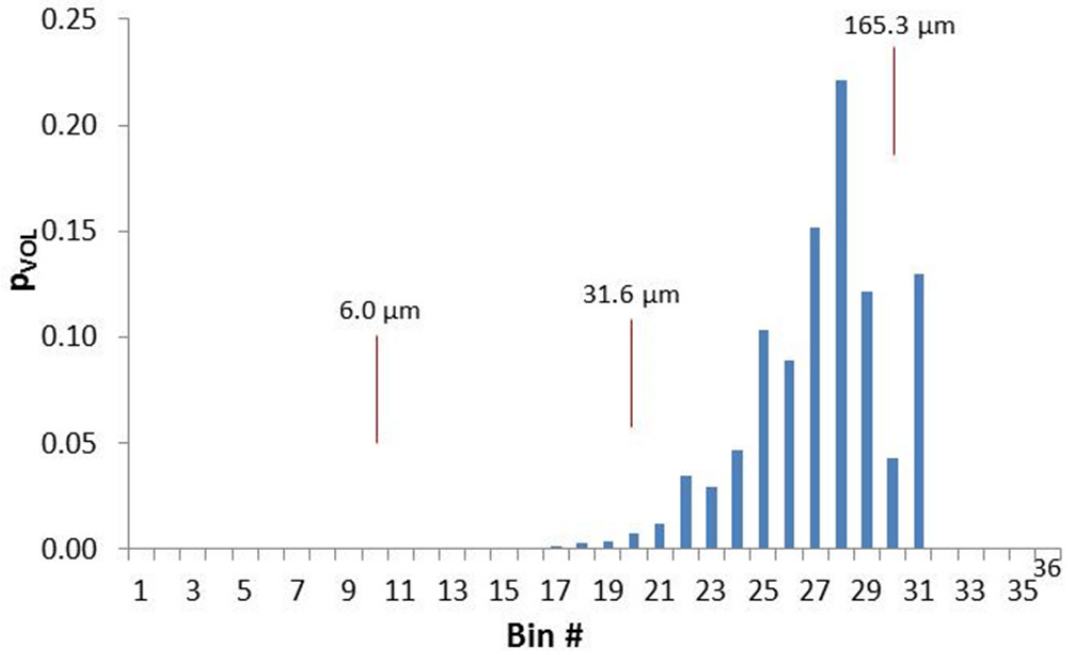

Figure A14: Histogram based on volume of globules in each bin

9.9% Mass Loss Oil; 200 RPM

- 424 globules in sample
- 1 irregular-shaped feature

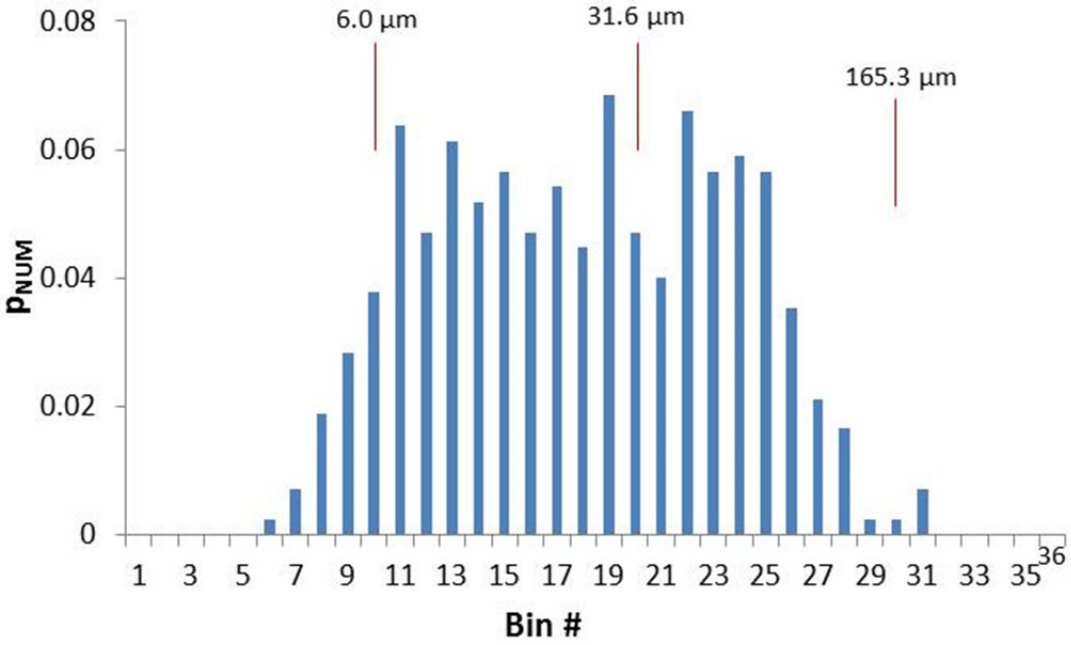

Figure A15: Histogram based on number of globules in each bin

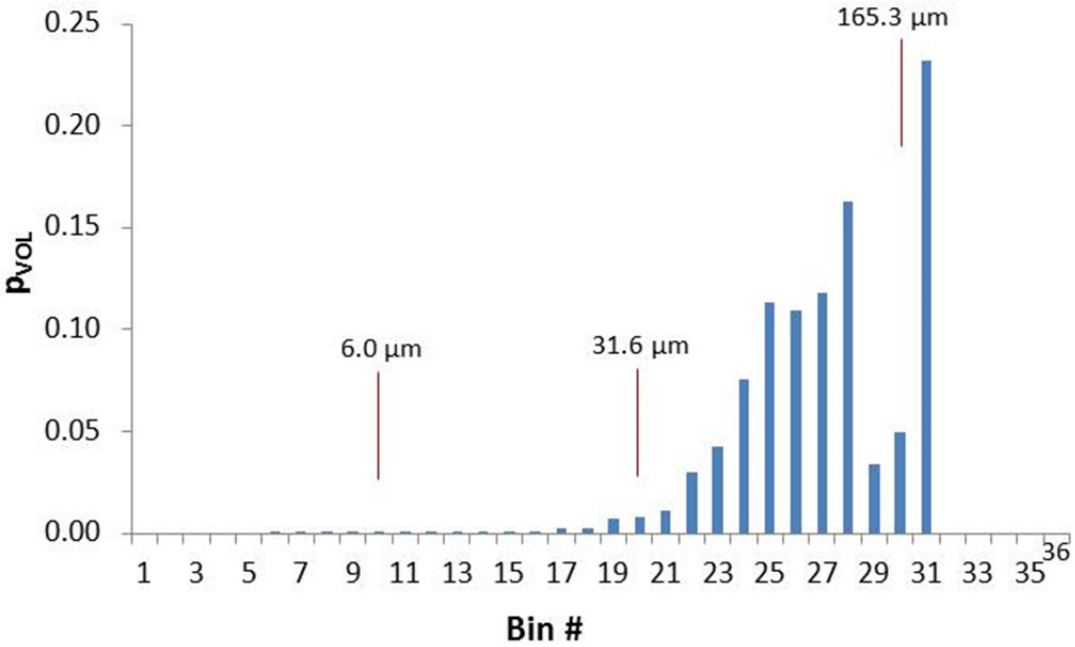

Figure A16: Histogram based on volume of globules in each bin

17.4% Mass Loss Oil; 200 RPM

- 627 globules in sample
- 1 irregular-shaped feature

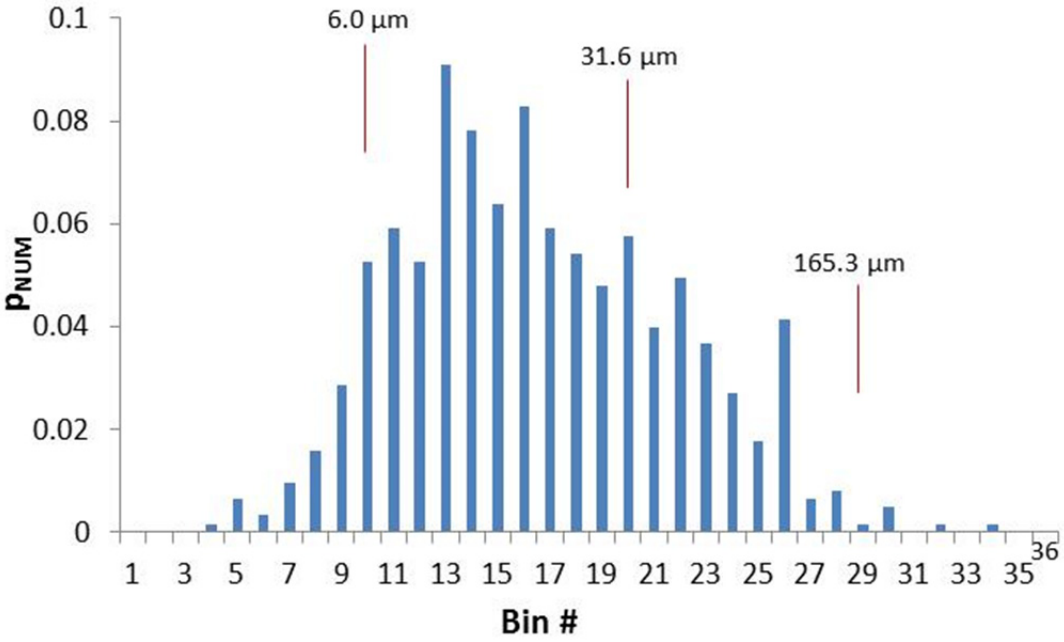

Figure A17: Histogram based on number of globules in each bin

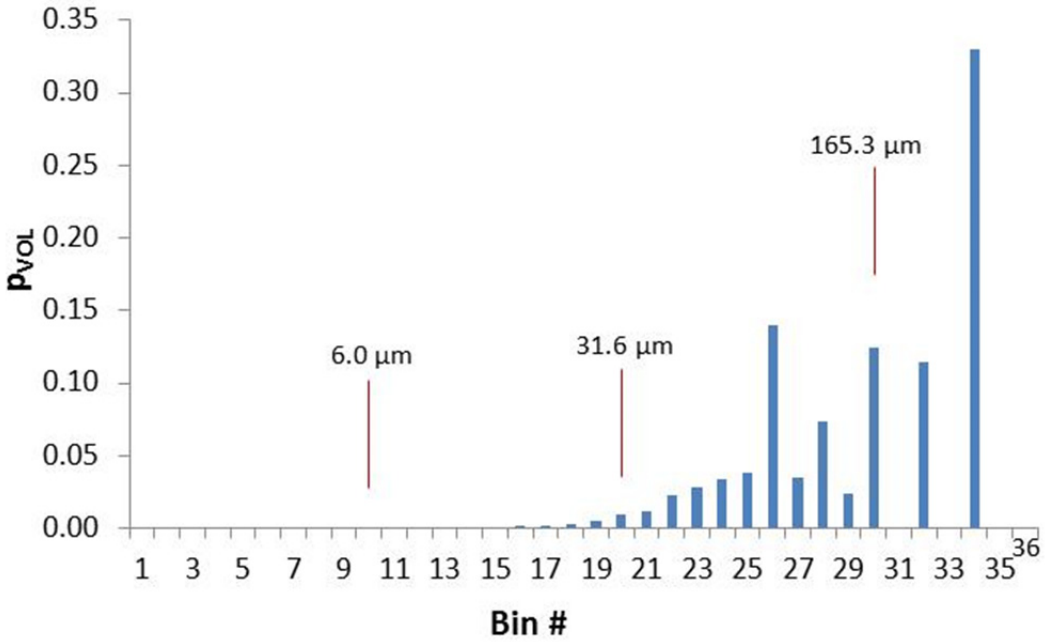

Figure A18: Histogram based on volume of globules in each bin

17.4% Mass Loss Oil; 200 RPM – **Unconventional Shaking Protocol**

- 405 globules in sample
- 4 irregular-shaped feature

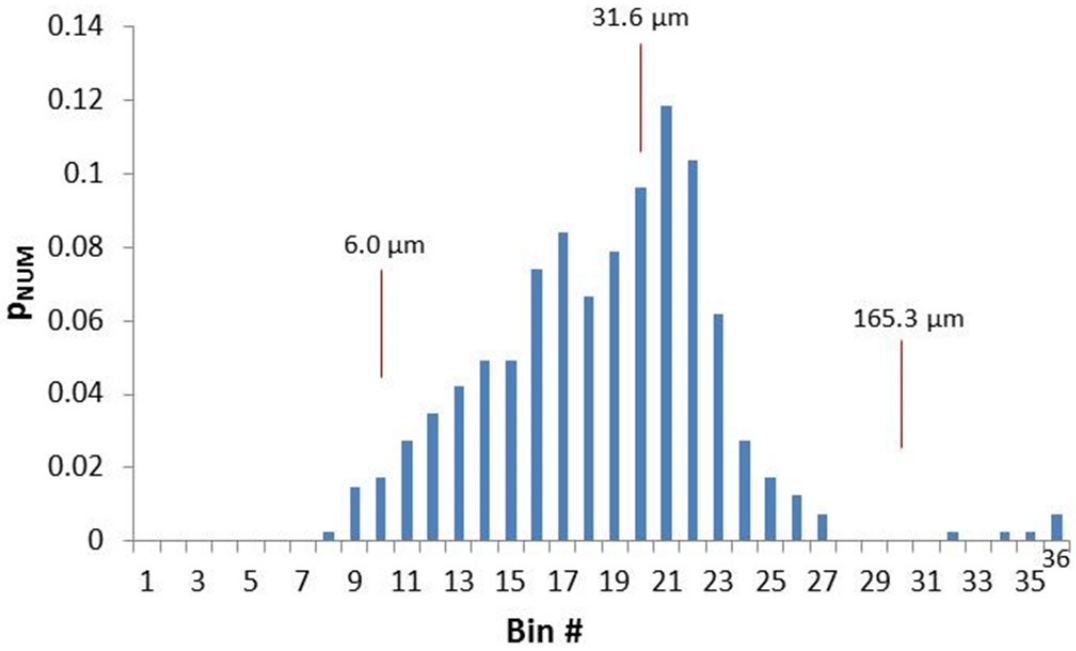

Figure A19: Histogram based on number of globules in each bin

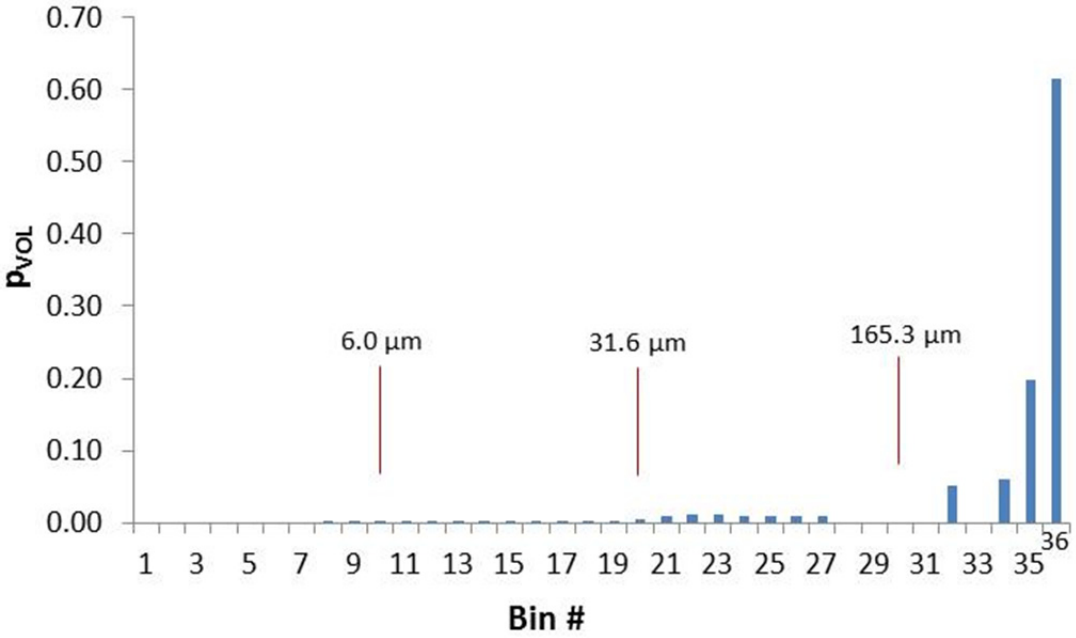

Figure A20: Histogram based on volume of globules in each bin